UNIVERSITÀ DEGLI STUDI DI MILANO

FACOLTÀ DI MEDICINA E CHIRURGIA

DIPARTIMENTO DI SCIENZE E TECNOLOGIE BIOMEDICHE

CORSO DI DOTTORATO DI RICERCA IN MEDICINA MOLECOLARE

CICLO XXIII

Indirizzo: Genomica, Proteomica e Tecnologie Correlate

TESI DI DOTTORATO DI RICERCA

In vivo imaging of stem cell mediated treatment in a mouse model of spinal cord injury

(MED/36)

TESI DI:

Dott.ssa Ramona LUI

TUTORE Chiar.mo Prof. Giovanni Lucignani

Firma……

CO-TUTORE Dott.ssa Luisa Ottobrini

COORDINATORE Chiar.ma Prof.ssa Maria Luisa Villa

Firma……

ANNO ACCADEMICO 2009/2010

Abstract

ABSTRACT

Introduction: *The use of adult stem cells in cell-mediated therapies is an area of considerable interest within tissue regeneration research. However, important variables such as the distribution of the injected cells, cell survival, target organ localisation cell proliferation and differentiation cannot be evaluated in vivo by using classical imaging approaches. This study propose multiple labelling protocols for in vivo visualisation by MRI, nuclear imaging and BLI of adult murine neural stem cell-mediated therapy, in spinal cord injury animal models.*

Methods: *Murine neural stem cells (mNSCs) were directly labelled with different amounts of SPIOs (0 - 100 - 200 - 400 µg Fe/ml) in the culture medium and incubated with iron labelled medium for 24, 48 or 72 h in presence of carriers such as poly-L-Lysine (PLL), polybrene (PB) and protamine sulphate (PS). PLL and PS were tested at different ratio (Fe/PLL 1:0,03, 1:0,06 and 1:0,09 and Fe/PS 1:0,025 and 1:0,05). Labelled cells were analysed for viability, iron content (Perl's Staining and spectrophotometer analysis), morphology, staminality and differentiation capability. After the labelling protocol set up, the loaded cells were injected into the tail vein of a spinal cord injury murine model and their distribution was followed by MRI for two months. Initial cell distribution was also followed by nuclear imaging after cell labelling with ^{111}In-oxine (60 µCi/10^6 cells). Cells localization, distribution e viability, over time, were analysed in vivo by BLI after injection of mNCS infected with a viral vector expressing Luciferase under a PGK constitutive promoter (PLW vector).*

Results: *the iron content/cell increased in proportion to the incubation time and to the iron concentration in the medium and in relation to different carriers (PLL, PB and PS) i**n** labelled mNSCs. Longer incubation time (48 and 72h) and higher iron concentration (400 µg Fe/ml) resulted in marked toxicity and lower cell viability. The use of PB and PLL, as carriers, didn't produce any increase of the labelling efficiency. The incubation for 24h with 200 µg Fe/ml in presence of different amount of PS didn't influence significantly the cell viability and the proliferation rate. Furthermore, the percentage of iron-positive cells and the iron content/cell increased in proportion to the PS content in the medium even if higher amount of PS (Fe/PS 1:0.05 ratio) resulted in an aberrant morphology. For this reason, 200 µg Fe/ml incubated with Fe/PS 1:0.025 ratio for 24h, has been chosen as the best labelling condition.*

Labelled cells were able to form new neurospheres and maintained the nestin expression demonstrating the maintenance of self-renewal capability and stem cell features and were also able to differentiate, as confirmed by β-tubulin III and GFAP expression analysis.

Nuclear imaging confirmed initial distribution to filter organs while MRI allowed to detect the presence of an iron signal due to stem cell localization into the lesion site since 7 days after injection. BLI permitted to demonstrate the viability of PLW infected mNSCs migrated at the lesion site and supported the MRI data.

Conclusions: *These results permitted to conclude that NSCs can be efficiently labelled with different molecules without significantly perturbing physiological stem cell features and self-renewal capability. These labelling protocols can be applied for the in vivo visualisation by MRI, nuclear imaging, and BLI of the distribution of stem cells after their transplantation into murine model of disease.*

RIASSUNTO

Introduzione: *L'utilizzo delle cellule staminali adulte nella terapia cellulo-mediata è di grande interesse nella ricerca sul trattamento e la ricostituzione dei tessuti danneggiati da traumi e malattie degenerative ed infiammatorie.*
Tuttavia, importanti variabili come la distribuzione delle cellule iniettate, la sopravvivenza cellulare, la localizzazione all'organo target, la proliferazione ed il differenziamento cellulare non possono essere valutate in vivo. Lo scopo di questo studio è quello di mettere a punto diversi protocolli di marcatura per la visualizzazione in vivo, tramite MRI, imaging nucleare e BLI, di cellule staminali neurali murine adulte (mNSCs) utilizzate nel trattamento del trauma spinale in modelli animali.
Metodi: *Le mNSCs sono state marcate in modo diretto con differenti concentrazioni di SPIOs (0 - 100 - 200 - 400 µg Fe/ml) nel terreno di coltura e incubate con il terreno marcato per 24, 48 e 72 ore in presenza di agenti trasfettanti come poli-L-Lisina (PLL), polibrene (PB) e protamina solfato (PS). PLL e PS sono state testate a differenti rapporti (Fe/PLL 1:0,03, 1:0,06 e 1:0,09 e Fe/PS 1:0,025 e 1:0,05). Le cellule marcate sono state analizzate per quanto riguarda la vitalità cellulare, il contenuto di ferro (colorazione di Perl e analisi spettrofotometrica), la morfologia ed il mantenimento della staminalità e delle capacità differenziative. Dopo la messa a punto dei protocolli di marcatura, le cellule marcate sono state iniettate nella vena caudale di un modello murino di trauma spinale e la loro distribuzione è stata seguita per due mesi tramite MRI. La distribuzione iniziale delle cellule è stata anche seguita tramite scintigrafia dopo la marcatura cellulare con ^{111}In-oxina (60 µCi/10^6 cellule). La localizzazione, la distribuzione e la vitalità cellulare nel tempo sono state analizzate in vivo anche tramite BLI dopo il trapianto delle mNSCs infettate con un vettore lentivirale esprimente il gene Luciferasi sono il controllo del promotore costitutivo PGK (vettore PLW).*
Risultati: *L'accumulo intracellulare di Ferro nelle mNSCs è risultato proporzionale al tempo di incubazione e alla concentrazione di ferro nel terreno di coltura e ai differenti agenti trasfettanti (PLL, PB e PS).*
Al contrario, tempi di incubazione più lunghi (48 e 72 ore) e concentrazioni maggiori di ferro (400 µg Fe/ml) hanno determinato un evidente aumento della tossicità e in una minore vitalità. L'utilizzo di PB e PLL non ha prodotto aumenti statisticamente significativi del contenuto di ferro intracellulare.
L'incubazione per 24 ore con 200 µg Fe/ml marcate, in presenza di differenti concentrazioni di PS, non ha influenzato in modo significativo né la vitalità né la capacità proliferativa delle cellule. Inoltre, la percentuale di cellule ferro-positive è aumentata in proporzione al contenuto di PS nel terreno di coltura anche se alte concentrazioni di PS (ratio Fe/PS pari a 1:0.05) hanno avuto come conseguenza una morfologia aberrante. Per questo motivo 200 µg Fe/ml in presenza di PS (1:0.025 Fe/PS) per 24 ore di incubazione è risultata essere la migliore condizione di marcatura.
Come dimostrato dal mantenimento dell'espressione della nestina e della capacità di dare origine a nuove neurosfere, la marcatura non ha condizionato né la staminalità e né la capacità di autorinnovamento. Inoltre la marcatura non ha influenzato la capacità differenziativa delle mNSCs come confermato dall'analisi dell'espressione della β-tubulina III e della GFAP. Questi dati hanno permesso di dimostrare che le

condizioni di marcatura cellulare non influenzano le caratteristiche fenotipiche e funzionali delle cellule staminali.
L' imaging nucleare ha confermato la distribuzione iniziale agli organi filtro mentre l'MRI ha permesso di rilevare la presenza delle cellule marcate con il ferro nel sito di iniezione sin dal settimo giorno dopo la somministrazione.
Il BLI ha permesso di dimostrare la vitalità delle mNSCs infettate con PLW migrate al sito di lesione ed ha confermato i dati di MRI.
Conclusioni: *Questi risultati hanno permesso di dimostrare che le mNSCs possono essere efficientemente marcate con molecole differenti senza perturbare in modo significativo la loro fisiologia e morfologia cellulare e la capacità di auto-rinnovamento. Questi protocolli di marcatura possono essere applicati per la visualizzazione in vivo tramite MRI, imaging nucleare e BLI, della distribuzione delle cellule staminali dopo il trapianto nel modello murino lesionato.*

Index

INDEX

LIST OF ABBREVIATIONS

Ab: Anti-body
CCD: Charge-coupled device
DC: dendritic cell
^{18}F -FDG: ^{18}F-FluoroDeoxyGlucose
fSC: fetal spinal cord
FDA: Food and Drug Administration
FLASH: Gradient Echo sequence
FLASH 3D: Gradient Echo 3 dimensional sequence
FLI: FLuorescence Imaging
FOV: Field Of View
GFP: Green Fluorescent Protein
IL: InterLeukine
^{111}In-oxine: Indium-111-oxine
INFγ: INterFeron gamma
i.s.: intraspinal
i.v.: intravenous
mNSC: murine neural stem cell
MSC: Mesenchimal Stem Cell
MSME: Spin Echo sequence
NMR: Nuclear Magnetic Resonance
NSC: neural stem cell
OB: Olfactory bulb
o.m.: original magnification
PB: PolyBrene
PET: Positron Emission Tomography
PLL: Poly-L-Lysine
PS: Protamine Sulphate
QD: Quantum Dot
RARE: fast Spin Echo sequence
RMI: resonance magnetic imaging
SCI: spinal cord injury
SPET: Single Photon Emission Tomography
SPECT: Single Photon Emission Computed Tomography
SPIO: SuperParamagnetic Iron Oxide
SVZ: subventricular zone
T2: time of loss of transversal magnetization
TAAs: Tumour Associated Antigens
TNFα: Tumour Necrosis Factor alpha

TSCI: traumatic spinal cord injury
TU/ml: Trasducing Unit per milliliter
UBC: Umbilical Cord Blood
US: UltraSound
VCN: vector copy number

Introduction

1. SPINAL CORD INJURY

A spinal cord injury (SCI) is a damage or trauma to the spinal cord that results in a loss or impaired function causing reduced mobility or feeling in the regions downstream the lesion. Common causes of damage are traumas (car accident, gunshot, falls, sports injury, etc.) or diseases (Transverse mieliti, Polio, Spina Bifida, Friedreich's atassia, etc.).
In SCI, the traumatic destruction of nerve fibres that carry motor signals from the cortex to the torso and limbs leads to muscle paralysis. In addition, destruction of nerve fibres can lead to loss of sensation, such as touch, pressure and temperature.
The traumatic spinal cord injury (TSCI) affects many people (15-40 cases every million people), most often of young age; the prospects of recovery are very small and the disability is permanent. The emotional and economic costs of spinal cord injury are great, especially for the long-term nursing care needed by serious disability. Despite multiple therapeutic approaches that target different aspects of the pathophysiologic cascade contributing to SCI, there have been no significant advances in clinical care that reliably attenuate injury or restore function.
From a pathophysiological perspective, SCI has been divided into two distinct phases [1].
Primary injury is an immediate response resulting from the direct action of mechanical force on the spinal cord. The strong inflammation initiated as a response to primary injury successively causes tissue edema, extensive demyelination, and cell death [2]. Secondary injury consists of all pathological events initiated by the original mechanical insult. The secondary injury following SCI is the result of a stroke-like ischemic insult; the biochemical and metabolic events associated to the vascular disregulation are numerous, and lead to the progressive degeneration that may exceed the early mechanical damage.
The pathophysiology of the spinal cord after the injury is mediated by a complex interplay of pro-inflammatory molecules and cytokines (MIP-2, TNFα, IL-1β, and IL-6), anti-inflammatory molecules and migratory cells.
Within the first 12 h, neutrophils first appear. MIP-2 overproduction associated to neutrophil infiltration suggests that this mediator plays a key role in inflammatory cell recruitment induced by SCI [3][4]. Within the 24-48h also lymphocytes and microglia mobilize to the injury site. Primary and secondary degeneration events together determine the extent of tissue damage even much farther than the limits of the mechanical impact. The attenuation of cellular and molecular abnormalities derived from the secondary injury may improve the recovery from SCI-derived disability.
Some pharmacological treatments, have, as goals, the attenuation of secondary ischemia-derived degeneration responsible for the worsening of initial conditions and the prevention of the neutrophilic and macrophagical infiltration into the site of injury [5].

1.1. Spinal cord injury therapy

Although, recently, the progresses in the field of spinal cord injury treatment have significantly improved the conditions and life expectancy of patients, nowadays

there are no real solutions for the recovery from a spinal cord injury. The surgical intervention aims to stabilize the spine in case of instability, cancels the risk of further spinal cord damage going to remove bone fragments and eventual discs occupying the spine canal and compressing it to maximize the chances of functional recovery of spinal affected by trauma.
However, recently, research has achieved encouraging results regarding the modulation of the inflammatory process but failed to induce regeneration of neurons lost with the trauma.
A decade ago, researchers demonstrated a small but significant neuroprotective and anti-inflammatory effect from an adrenal corticosteroid drug (methylprednisolone). It is the only treatment currently available to limit the extent of spinal cord injury and its risks are relatively low. Several studies continue to search for additional anti-inflammatory treatments that might prove even more effective.
Preliminary clinical trials of another compound, *GM-1 ganglioside*, indicate that it could be useful in preventing secondary damage in acute spinal cord injury. A large randomized clinical trial, suggested that it might also improve neurological recovery from spinal cord injury during rehabilitation.
These observations and others, have led to optimism that recovery can be improved by altering cellular responses immediately after injury.
Additional neuroprotective therapies, to prevent the spread of post-injury damage and preserve surrounding tissue, have been studied and tested thanks to the acquired knowledge about the mechanisms that cause secondary damage, such as excitotoxicity, inflammation and apoptosis.

The goals of research studies in the spinal cord injury treatment are the following:

- **Stopping excitotoxicity**
  When neurons die, they release excessive amounts of glutamate which floods the cellular environment and pushes cells into apoptosis. Several studies are investigating compounds that could keep nerve cells from responding to glutamate, potentially minimizing the extent of secondary damage.
- **Controlling inflammation**
  Within the first 12 hours after injury, the first wave of immune cells infiltrates the damaged spinal cord to protect it from infection and eliminate dead neuronal cells. The immune cells act and release cytokines, the hallmark of inflammation.
  Although cytokines can be toxic to neuronal cells because they stimulate the production of free radicals, nitric oxide, and other inflammatory substances that cause cell death, they also stimulate the production of *neurotrophic factors*, which are beneficial to cell repair.
  The aim of the research, currently, is to control the immune system cells and correlated molecules by encouraging their potential for neuroprotection and reducing their neurotoxic effects.
- **Preventing apoptosis**
  Several days after the initial injury, apoptosis spreads in damaged and nearby tissue. The exact biochemical events regulating apoptosis are not yet completely known.

Further studies are aimed at understanding these cellular mechanisms more fully. These studies will provide an opportunity to develop neural protective strategies to combat apoptotic cell death.

- **Stimulating regrowth of axons**

  Stimulating the regeneration of axons is a key component of spinal cord repair. The reconnection of axons injured during the spinal cord trauma could increase the chances for recovery of function.

  However, to get the axons growth after injury is a complicated matter. Central nervous system (CNS) neurons have the capacity to regenerate, but the environment in the adult spinal cord does not encourage growth. In adult CNS lacks all the cytokines and growth factors responsible of the early development of CNS and it also contains molecules that actively inhibit axon extension. For a successful transplant the environment has to be changed.

  At the present time, several studies are focusing their attention on neurotrophic factors and *guidance molecules* such as ephrins, semaphorins and netrins.

  During the development of CNS, in fact, axons grow following the *axonal growth cone*, an active tip only a few thousandths of a millimeter in diameter, which interacts with chemical signals that stimulate growth and direct movement.

  In the adult CNS, the myelin, which contains growth-inhibiting proteins, creates an hostile environment to axon growth.

  These proteins appear to preserve neural circuits in the healthy spinal cord and keep intact axons from growing inappropriately but in injured spinal cord, prevent regeneration.

  At least three growth-inhibitory proteins operating within the axonal tract have been identified: Myelin-associated glycoprotein (MAG), Nogo and oligodendrocyte myelin glycoprotein (OMgp). They are expressed by oligodendrocytes and bind to Nogo receptor (NgR) on neurons. These interactions result in inhibition of neurite outgrowth. The aim of research is to understand how these inhibitory proteins act, and then discover ways to remove or block them, or change how the growth cone responds to them. Axonal growth and neuronal cell survival are promoted by some regulatory proteins called Neurotrophic factors (or neurotrophins) which, however, in the injured spinal cord are downregulated instead of increased. Several studies have tested infusion pumps and gene therapy techniques to rise their levels post-injury and enhance regeneration.

  Once growth, the axons have to re-establish functioning synapses. Guidance molecules, proteins present on the surface of neurons and glia or secreted by these cells, act as chemical road signs, guiding axons growth in some directions rather than others.

  The supply of guidance molecules might encourage regeneration. The combination of these strategies could encourage growth, clear away debris, and target axon connections becoming a powerful treatment for spinal cord injury.

- **Promoting regeneration**

  The new frontier in treatment of spinal cord trauma is represented by cell transplantation. Cell grafts transplanted into the injured spinal cord act as bridges across injured areas to reconnect cut axons. Several fetal spinal cord

(fSC) transplantation experiments, performed in animal models of TSCI, permitted to demonstrate that fSC grafts grew well in the host spinal cord, fill the cavity and fuse with the host spinal cord [6] creating a bridge that would span the injured area [7][8][9]. Fetal spinal cord tissue implants give rise to new neurons, which, when stimulated by growth-promoting factors (neurotrophins), extend axons in the spinal cord producing also an encouraging functional outcomes. Indeed the transplants improved locomotor recovery and were able to modulate the excitability of lumbar motor neurons [10][11][12]. The promoting action of fSC transplants was preserved if the time interval between injury and grafting did not exceed 3–4 months [13].

Recently, the attention is focusing on stem cells and in particular in neural stem cells. Stem cells are capable of dividing and yielding almost all the cell types of the body, including those of the spinal cord. They have a big potential even if their biology is not yet completely understood such as the function of different kind of chemical signals emitted by the cells and used for cell-cell communication. Some of these signals will have to be recreated in the region of the transplant to stimulate proper growth and differentiation.

2. CELL- MEDIATED THERAPY

The Food and Drug Administration (FDA) provides the following definition of cell therapy: “The prevention, treatment, cure or mitigation of diseases or injuries in humans by the administration of autologous, allogeneic or xenogeneic cells that have been manipulated or altered *ex vivo*” [14].
The cell-mediated treatments, can be mainly divided into two classes: Immunotherapy, based on the administration of immune cells previously activated *ex vivo* and regenerative therapy based on the use of stem cells.
The goal of stem cell mediated treatments, within the regenerative medicine, is repairing, replacing or restoring damaged tissues or organs (figure 1).
There are different forms of cell therapy:

- stem cells transplantation;
- transplantation of mature and functional cells;
- transplantation of modified cells used to produce a needed substances;
- transplantation of cells extracted from a patient with a genetic aberration and opportunely modified to correct the genetic defect.
- transplantation of trans-differentiated cells derived from the patient's own differentiated cells (for example insulin producing beta cells transdifferentiated from isolated hepatocytes as a treatment for diabetes).

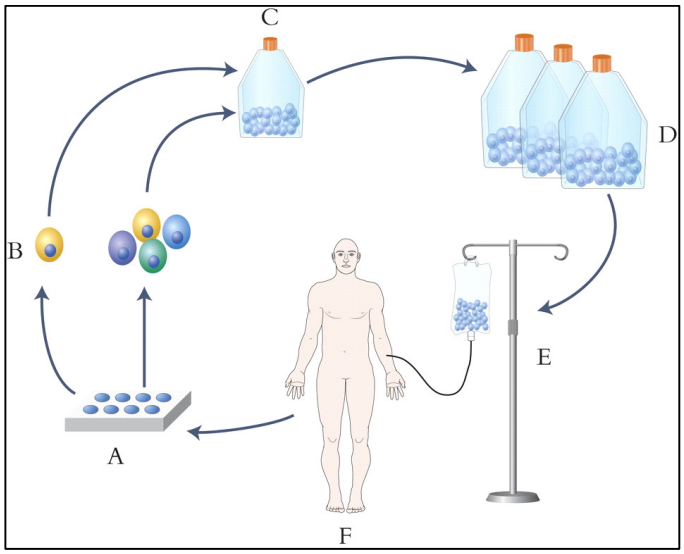

Figure 1: *Procedures for cell therapy: A) precursor of stem cells are harvested from the patient itself or from a donor; B) in vitro selection or analysis, C) in vitro expansion, D) large in vitro expansion, E) administration to patient, F) monitoring of homing/migration, differentiation, surviving, effect of cell-therapy.*

For what concerns stem cell therapy, bone marrow transplants have been used for the past 40 years to regenerate the blood and immune systems of patients with leukemia, lymphoma, severe aplastic anemia or inherited metabolic diseases. Unfortunately, the major limitation of allogeneic bone marrow transplants is the availability of matched donors.
Stem cells from Umbilical Cord Blood (UCB) have emerged as an alternative to bone marrow transplants, providing an easily obtainable and readily available cell source for treatment. Until recently, UCB transplants were limited to paediatric patients due to the low amount of stem cells obtained. However, in 2004 was demonstrated that the combination of stem cells from two UCB units could increase the cell dose, making it possible to extend this lifesaving haematopoietic treatment to adult patients.

Several studies have demonstrated that, in addition to regenerating the blood and immune systems, stem cells would also be used to replace damaged or diseased tissues and organs (cells for skin, muscle, liver, pancreatic islet cells, spinal cord injury, neurons).
An example of cell mediated therapy consists of the use of stem cells for regenerative treatments in degenerative and inflammatory diseases or traumatic injuries. Many cell types have been used depending on the tissue to be treated: neural stem cells, muscle stem cells, bone marrow cells, or not yet committed cells have been used to induce transdifferentiation for different applications.
Harnessing stem cells for using them as drug delivery systems is another goal for research; in fact stem cells may be able to bring chemotherapeutic agents directly to the target cancerous cells. They can also be used for the generation of liver cells or other tissues in order to screen new drug candidates for a safer pharmaceutical drug development process. The use of human cells or tissues may provide a better toxicology testing model than the traditional animal models currently in use.
Stem cell-mediated therapies finds different applications also in the treatment of inflammatory disease such as inflammatory myopathies, degenerative disease (Parkinson's, Alzheimer's, Multiple Sclerosis, Huntington, ALS, etc.) and in the treatment of traumatic injuries, such as spinal cord injury. In this scenario, a cell-mediated therapy could be useful in restoring the damaged tissue.
One of the most promising field of study regards the use of neural stem cells (NSCs) and their application in the regenerative medicine. The therapeutic perspectives related to the use of NSCs are based on two important properties: their ability to proliferate indefinitely and their plasticity. In all situations in which neuronal loss occurs, the NSCs, previously isolated and expanded in vitro can restore the lost functions when implanted into damaged tissue or administered by intravenous injection. These cells can be directly transplanted or manipulated *in vitro* inducing their differentiation toward the neuronal phenotype of interest before infusion.
Until now, several animal models of neurodegenerative diseases have been treated and at least partially cured by NSCs administration [15][16][17][18].
Recently, during the course of the trials, new and unexpected properties associated with these cells have emerged.

The NSCs, injected intravenously or directly into the damaged tissue in animal models of neurological diseases, are able to migrate to tumour cells in brain tumours, some of which are resistant to chemotherapy and radiation.
Starting from these findings, researchers over the years have engineered stem cells and neural precursors from adult or embryonic brain samples, and these cells have been used in studies of gene delivery to target genes or cytotoxic molecules in areas of interest. Unexpectedly, the same not manipulated NSCs, was demonstrated having cytotoxic properties against cancer cells in brain tumours. The mechanisms governing the tropism of NSCs in a specific way are not yet understood.
The first intuitions are based on prior knowledge of the molecular mechanisms that regulate cell migration during inflammatory processes. It has been observed that ischemia induces upregulation of chemokine SDF-1a (stromal cell-derived factor), whose receptor CXCR4 (CX-C motif receptor 4) is expressed on NSCs; blocking CXCR4, NSCs migration is substantially reduced [19].
Moreover, the NSCs tropism for injuries is a very important feature for the treatment of multifocal diseases such as multiple sclerosis or inherited metabolic diseases affecting the CNS such as phenylketonuria, mucopolysaccharidosis, Niemann-Pick disease, Fabry disease, Tay-Sachs and Gaucher disease. In these cases, the treatment of multiple damaged areas can be performed by a single injection of NSCs or NSCs lines, as demonstrated by Snyders' pioneering experiments in 1995 [20][21][22].
The NSCs ability to migrate toward the sides of injury in the adult brain has been confirmed in many experimental animal models of human diseases such as stroke, multiple sclerosis and experimental autoimmune encephalitis (EAE) [23][24]. Multiple sclerosis and EAE are demyelinating immune diseases that affects the CNS.
From these animal models observation emerged that the undifferentiated NSCs could also have important regenerative properties, on the contrary to what was believed until then. The EAE animal models showed a visible recovery, although most of the infused NSCs do not differentiate into oligodendrocytes. It seems that these cells will make their therapeutic action, not replacing the damaged oligodendrocytes, but acting as suppressors of cerebral autoimmunity [25].
Another phenomenon associated with NSCs, common to other stem cells of adult tissue, is the transdifferentiation, a cellular adaptation in response to stimuli of growth: a reprogramming process by which a stem cell of a specific adult tissue, comes to generate a particular cell of another tissue. It has been shownthat cells derived from mouse bone marrow infused into the blood circulation are able to reach the brain and differentiate into neural cells [26].
As in rodents, also human hematopoietic stem cells can cross the blood-brain barrier, reach the brain and differentiate into neural cells. In post-mortem autopsy samples of female patients who underwent bone marrow transplantation from male donors were found neurons of hematopoietic origin identified by the presence of Y chromosome [27]. At the same time, murine NSCs are capable of generating blood cells [28]. It remains to determine whether, in some cases, transdifferentiation may be due to cell fusion [29][30].

Regardless of the disease treated with a cellular therapy, the conception of the therapeutic products may require several complex procedures aimed at obtaining and/or modifying the cells. The steps may include:

- Cell Harvesting
- Cell Propagation
- Cell Expansion
- Cell Selection
- Pharmacological treatment of cells
- Alteration of the biological characteristics of cells

Before the clinical application of cell-mediated therapies, the research should overcome several technical obstacles.
The new goals for stem cell research should be:

- To understand and control the mechanism of turning undifferentiated cells into specialized cells. This will involve the identification of the complex signals needed to turn on and off the cell differentiation process.
- To identify, isolate and purify adult stem cell for safe and effective treatments.
- To control the differentiation of stem cells into the cell types needed to treat disease, in order to make it possible the generation of the sufficient quantity of correct stem cells or differentiated cells suitable for the treatment.
- To learn how to make patient-compatible the stem cell transplants, to avoid any rejection by the immune system.
- To demonstrate the clinical improvement and normal cell development and function after stem cells have been transplanted or administered into the patient's body. Cells have to integrate with patient's own tissues and function as patient's natural body cells.

To overcome these problems, molecular and cellular imaging techniques could provide information about the homing, viability and differentiation of stem cells once injected during the therapy permitting an early evaluation of cell-mediated treatment efficacy potential.
Specific cell populations can indeed be labelled and visualised *in vivo* through widely used methods such as magnetic resonance imaging, emission tomography and, only for animal models, bioluminescence and fluorescence imaging (see next paragraph).
Through cellular imaging we may achieve an in-depth understanding of the fundamental aspects stem cell therapy in order to refine the therapeutic strategies for humans. In the protocols based on the use of stem cells, *in vivo* imaging can provide new methods for studying *in vivo* stem cell homing and their differentiation into the tissue of interest, as well as the value of the possible use of adjuvant pharmacological treatments over time.

2.1. Cell therapies in the spinal cord injury

One of the most promising field of application of regenerative medicine is the traumatic spinal cord injury treatment.
Several types of cells have been studied for their potential to promote regeneration and repair, including *Schwann cells, olfactory ensheathing glia, fetal spinal cord cells,* and *embryonic stem cells*. In one group of experiments, investigators have

implanted tubes packed with Schwann cells into the damaged spinal cords of rodents and observed axons growing into the tubes.
One of the limitations of cell transplants, however, is that the growth environment within the transplant is so favourable that most axons don't leave and extend into the spinal cord. Olfactory ensheathing glia cells, instead, natural migrators, are able to extend out axons of the initial transplant region and into the spinal cord but it's not yet sure whether growth axons are completely functional.
Recent discoveries describe the possibility to use neural stem cells (NSCs), progenitors of neuronal cells, in cell-mediated therapeutic protocols, for the regeneration and reconstitution of damaged tissues.
Fetal neural stem cells (NSCs) transplantation was demonstrated to be very promising in the promotion of functional recovery after spinal cord trauma, and was associated with the differentiation of the stem cells injected into the cord [31][32].
Since the use of embryonic stem cells may raise ethical issues and practical problems such as the fate of the embryonic cells in adult environment and the required immunosuppression, the researchers have focused their attention on the adult neural stem cells [33].
Adult stem cells have been isolated from several adult tissues and other non-embryonic sources, and have been demonstrated a surprising ability for transformation into other tissue or cell types and for repair of damaged tissues [34][35].
The regenerative medicine and the stem cell research have as primary goal the regeneration and the replacement of dead or damaged cells.
Several studies demonstrated the capability of NSCs to participate in repair of damage and their utility in the treatment of degenerative brain conditions [36]. For example, in Parkinson's disease models, NSCs have been observed to integrate and survive for extended periods of time [37], and to rescue and prevent the degeneration of endogenous dopaminergic neurons [38].
Transplanted embryonic SCs and fetal NSCs survive and improve functional recovery after SCI [31][39][32].
Bottai et al. [40] have showed that adult NSCs, applied intraspinally or intravenously within 18 h after SCI, is able to counteract secondary degeneration and promote the recovery of function after acute SCI, as reported previously by Gorio et al. [41][1].
Exogenous NSCs could be recovered live and regrown *in vitro* up to 7 d after administration; in addition, NSCs modified the lesion environment by promoting the expression of neurotrophic factors, and also produced the main enhancement of the rate of recovery during this initial period. Later, NSCs were phagocytated by macrophages, but the extent of functional recovery was maintained [32].
One of the big limit of NSCs transplantation is the inaccessibility of the cell source, that is located deeply in the brain, therefore the identification of a readily accessible source of neural progenitors (NPs) obtainable without invasive procedures could be of a great benefit. Several non-neuronal tissues can be used as source of adult stem cells capable of neuronal differentiation [42][43][44][45]. Recently it has been demonstrated that a multipotent stem cell population (dermis stem cell [DSC]) is present in the dermis of mammalian skin, and if grown *in vitro* it preferentially forms floating spheres made of cells positive for fibronectin and nestin [39].

3. LOCATION OF STEM CELLS IN THE CNS

During the development of the CNS, stem cells localize within niches that are discrete anatomic zones. They have been identified in the dentate gyrus of hippocampus (SGZ) and in the subventricular zone (SVZ) along the lateral ventricles. Stem cells have also been found around the ependyma of the central canal and around the fourth ventricle. Other CNS niches include the hypothalamus, the optic nerves and the substantia nigra.
During postnatal development, these mitogenic regions decrease in size and eventually disappear. The only remaining structure, that persists even after the development, is the SVZ, which, however, is reduced to a thin layer.
Neural stem cells found in the CNS niches can proliferate along neuronal or glial lineage. Stem cell based repair occurs through the phases of multiplication, differentiation, migration and neo-synaptogenensis emerging form these sites.
Cell proliferation is triggered by growth factors like FGF-2 (fibroblast growth factor) and EGF-1 (epidermal growth factor). During the CNS development, differentiation along neuronal lines occurs under the influence of Shh (Sonic hedgehog), while notch pathway guides proliferation towards a glial lineage. Shh, a secreted glycoprotein is involved in anterior motor neuron induction in the spinal cord. In adult rats too, Shh increases the proliferation of neuronal progenitors [46].

In the adult CNS, besides the action of FGF-2 and EGF-1, already useful during the CNS development, other mechanisms are involved in controlling cell fate towards the self-renewal capability or NSC differentiation. The CNTF (ciliary neurotrophic factor) cytokine, supports embryonic stem cell self-renewal capability and pluripotency [47], and, as recently observed, also supports NSC self-renewal capability triggering the Notch signaling pathway (figure 2) [48][49]. The transient activation of Notch, however, causes the rapid and irreversible loss of neurogenic capacity [50]. Moreover, most of the SVZ neural stem cells infected with Notch, eventually become periventricular astrocytes, suggesting the possibility that radial glia and astrocytes of the SVZ are of the same lineage [51][52]. and demonstrating that Notch signaling is instructive for the gliogenesis and the maintenance of neural stem cells in an undifferentiated state. Furthermore, the neurogenic development of SVZ was partly attributed to the mutual action of local antagonists such as Noggin and BMPs (bone morphogenetic proteins) [53]. The BMPs are a negative regulators of neuronal differentiation, while Noggin reverts this effect through its binding to BMPs, preventing the activation of their signal [54][55]. The BMPs are expressed by SVZ cells, whereas Noggin is expressed by the ependymal cells [53]. These interactions between ependymal and adiacent SVZ cells might provide for the neurogenesis and gliogenesis regulation in the adult brain.

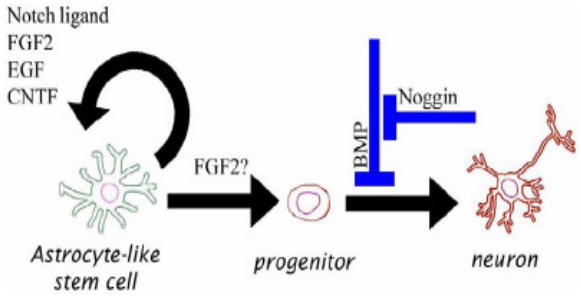

Figure 2: *Notch pathway and regulation of neuronal differentiation.*

So, in the CNS there are stem cells which have a potential to proliferate and there are factors which can induce their proliferation and guide the multiplying cells along various lineage.

3.1. SVZ neural stem cells (NSCs)

In the murine SVZ, there are three types of precursor cells: type B representing the GFAP (Glial fibrillary acidic protein) positive progenitors, type C (TAP transit amplifying progenitors) and finally the type A composed of migrating neuroblasts.
The type B GFAP positive neural progenitors are less susceptible to antimitotic treatment and are relatively quiescent cells.
The potential of SVZ progenitor cells appear to be limited, and the fate of their progeny is determined by positional information established in the early stages of CNS development [56].
More in particular, in the SVZ there are two subtypes of mitotically active cells: neural stem cells (NSCs), which represent a relatively quiescent cell population with a cell cycle length of 28 hours [57][58] and TAP (transit amplifying precursors) progenitors with a cell cycle length approximately of 12 hours. The neural stem cells (NSCs) present in the SVZ, are responsive to epidermal growth factor (EGF-1) or fibroblast growth factor (FGF-2) for the maintenance of staminality and self-renewal capability [59][60].
These growth factors are responsible of cell cycle length regulation: EGF-1 induced a faster cell proliferation than FGF-2 [61]. EGF-1 and FGF-2 may preferentially target one of these two different cell types [60][62]. Doetsch et al. have demonstrated that, intracerebroventricular infusion of FGF-2 into the lateral ventricle results in an increased number of new neurons in the olfactory bulb (OB), while the EGF-1 infusion reduces the number of neurons in the OB with a substantial increase in generation of astrocytes in the OB and striatum [62] even if other researchers have observed an equal increase in neurogenesis following FGF-2 or EGF-1 administration.
The human SVZ is anatomically different from murine SVZ. It's organized in four layers, where ependymal cells are separated by a ribbon of astrocytes because of a hypocellular gap [63]. In addition to ependymal cells, in the human SVZ are present three different types of GFAP positive astrocytes, and a very low number of

neuroblasts [64]. It's interesting to note that no type C cells were identified in this region in humans.

4. LIMITATIONS OF STEM CELL THERAPY

The use of stem cells in cell-mediated therapy is of considerable interest in research for the regeneration and reconstitution of tissues damaged by trauma and degenerative and inflammatory diseases. Numerous protocols include extraction of stem cells from healthy animals and implantation in diseased models.
However, the evaluation of treatment efficacy, at the moment is based only on functional recovery that is possible just several months after the transplant.
Furthermore, important variables such as the distribution of the injected cells, cell survival, target organ localization, cell proliferation and differentiation cannot be evaluated *in vivo*. All these variables are normally evaluated *ex vivo,* by means of immunohistochemistry, on bioptic samples and tissues from transplanted animals.
The development of molecular imaging technologies (nuclear medicine, investigational radiology and optic imaging) permits to overcome these limitations providing refined methods for the *in vivo* visualization, in real-time, of specific molecular processes for *in vivo* study of biological processes associated with the use of cell-mediated therapies.

5. *IN VIVO* IMAGING

In vivo imaging is a rapidly emerging biomedical research discipline that extends such observations in living subjects to a more meaningful dimension [65].
The field of *in vivo* imaging offers the opportunity to define the morphological size and location of organs and diseased tissue and provides patient-specific information, for example, the tumour localization, staging and treatment follow-up response. Furthermore, the imaging techniques permit to couple these morphological datasets with functional biological pathways in an attempt to better understand the properties of specific organs.
In medical research, *in vivo* imaging can be separated in molecular and cellular imaging depending on the object in study. These non-invasive techniques permit the characterization and quantification of targeted macromolecules and cells respectively, and of biological and cellular processes, at cellular and sub-cellular levels, in living organisms [65][66]. It is a novel multidisciplinary field, in which the images produced reflect cellular and molecular pathways and *in vivo* mechanisms of disease present within the context of physiologically authentic environments. The term “molecular imaging” implies the convergence of multiple image-capture techniques, basic cell/molecular biology, chemistry, medicine, pharmacology, medical physics, biomathematics, and bioinformatics into a new imaging paradigm [65].
In vivo imaging technologies are based on computerized tomography (CT), magnetic resonance imaging (MRI), positron emission tomography (PET), single photon emission computed tomography (SPECT), scintigraphy and ultrasound (US) imaging. These techniques, previously used in human studies, have recently been redesigned for studies in small animals, whereas other techniques initially used for *in vitro* assays, including nuclear magnetic resonance (NMR), bioluminescence (BL) and fluorescence (FL) methods, have been refined for *in vivo* studies [67] (figure 3).

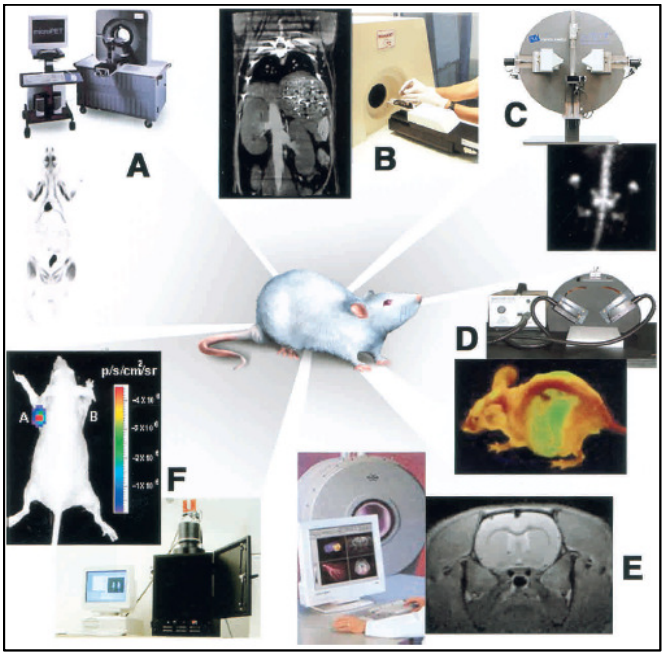

Figure 3: *Graphic representation of typical instruments available, and illustrative examples of the variety of images that can be obtained with in vivo imaging techniques: (A) microPET (B) microCT (C) microSPECT (D) fluorescence imaging (E) microMRI (F) bioluminescence imaging.*

Each technology is characterized by specific features: spatial and temporal resolution, penetration depth, energy used to generate the image, need/availability of contrast agents, threshold of detection. Furthermore, all these techniques differ for the type of information provided which could be, anatomical or functional. So, each methodology should be used with different efficiency, in relation to the application.

There are three general categories of molecular imaging approaches in living subjects: direct imaging, indirect imaging and surrogate imaging [68]:

- direct imaging: the image is the result of molecular probe localization at the target, directly and in a single stage. The extent of this localization (image intensity) relates directly to the interaction with the target, and each molecular probe is specific to one target.
- indirect imaging: is based on reporter gene expression imaging. The cells or animals are engineered to express a gene codifying for a reporter protein, whose expression is easily detectable and quantifiable through imaging procedures, immunohystochemistry and enzymatic assays. The expression of the reporter is induced after the occurrence of a specific molecular event. Following that, a molecular probe (a substrate or a ligand) specific for the reporter protein (an enzyme or receptor) is used to image its expression. Different reporter genes have been used ranging from intracellular enzymes to

transmembrane transporter and receptors. In the case of stem cell studies, reporter genes could be used to image *in vivo* long term stem cell viability. For this purpose, reporter genes driven by constitutive promoters (e.g., cytomegalovirus or CMV, β-actin, ubiquitin), are usually used. On the other hand reporter genes driven by a tissue specific promoter (e.g. the neuronal promoter MAP2 or the muscular promoter Myogenin) can be used for the study of stem cell or progenitors differentiation.

- Surrogate imaging: is also called 'physiological' or 'metabolic' imaging. These imaging strategies reflect downstream effects of the expression of one or more endogenous genes and/or molecular pathways involved in the metabolism, in order to describe the physiologic or pathologic conditions of tissues.

The majority of current clinical applications of molecular imaging use the principle of 'direct' imaging, mainly because of the longstanding and established practice of probe or target development and the extensive use in clinical nuclear medicine. As evidence, most cell therapy protocols, [69][70][71], opted for direct labelling strategy for MRI because of its high resolution. Moreover, many contrast agents, e.g. magnetic nanoparticles like Endorem® with an iron-oxide core, are already approved for clinical use and can easily be translated for human cell labelling.

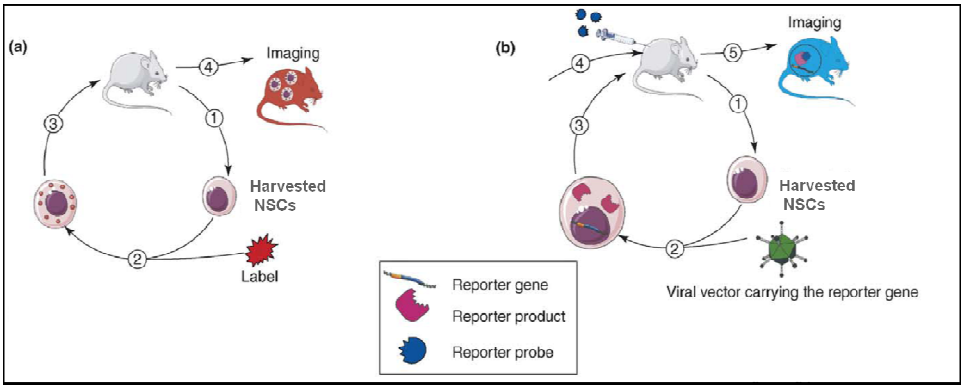

Figure 4: *Schematic representation of the direct and indirect imaging strategy. (a) Direct labelling procedures (b) Indirect imaging.*

Figure 4 displays the different phases of direct and indirect labelling: the advantages of direct imaging is the easy labelling protocols respect on the difficulty of engineering the cells [72]. In fact, the direct labelling consists of the aspecific internalization of a detectable agent (contrast agent or fluorescent probe) in a specific cell population or its specific binding to a molecular target in study. The great disadvantage of direct imaging, however, is that this approach does not enable long-term monitoring of cell viability and proliferation in the body because the label is lost or diluted owing to apoptosis or mitosis, respectively.
The indirect approach, based on cell engeenering, is essential for the imaging of proliferating cell populations during their migration, activation and division in fact

modifying stem cells (SCs) or immune cells with a reporter gene the entire cell progeny can trap the reporter probe, without loss of labelling [72] (figure 5).

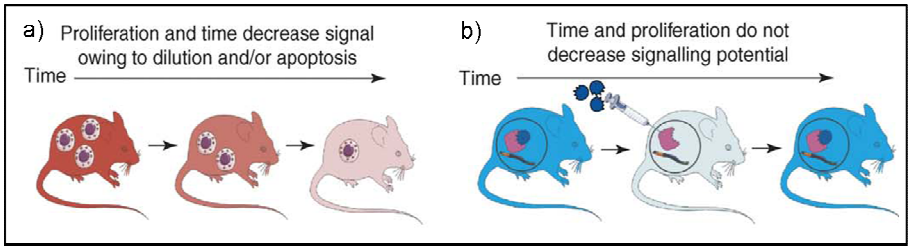

Figure 5: *Imaging of cell progeny over time.*

Molecular imaging in living subjects offers distinct advantages when compared with conventional *in vitro* and cell culture research techniques in biology. Although *in vitro* studies in basic biological research have been, and remain, a mainstay for defining biochemical and gene expression pathways, the *in vitro* approach has been less successful in deciphering physiological whole-body contributions of proteins, in which redundancies and differences in regulation can alter the outcome from that initially predicted [73]. In contrast to cell and tissue culture, *in vivo* animal models allow the assessment of phenomena such as tolerance, complementation, and redundancy in biological pathways [74]. Molecular imaging permits both the temporal and the spatial biodistribution of a molecular probe and related biological processes to be determined in a more meaningful manner throughout an intact living subject. Visualization of functions and interactions of a particular gene becomes easier in a more realistic manner that respects the dynamics of complex biological networks and of complete and holistic biological systems in the entire living subject [75].
Furthermore, they allow a repetitive, non-invasive, uniform and relatively automated study of the same living subject using identical or alternative biological imaging assays at different time points, thus harnessing the statistical power of longitudinal studies, and reducing the number of animals required (according to the 3R principle: Refine, Reduce, Replace) and cost. Moreover, each animal will be followed up as an individual being, thereby turning the cluster of animal models into an experimental group that can be compared directly with the treatment groups generally enrolled in clinical trials.

5.1. Optical Imaging

Optical imaging techniques reveal photons at different wavelengths (in visible and infrared ranges), resulting from bioluminescence (BLI) and fluorescence (FLI) events, by using highly sensitive charge-coupled device (CCD) cameras.
CCD cameras operate by converting light photons at wavelengths between 400 and 1000 nm that strike a CCD pixel with an energy of just 2–3 eV into electrons. A CCD contains semiconductors connected so that the output of one serves as the input of the next. In this way, an electrical charge pattern, corresponding to the

intensity of incoming photons, is read out of the CCD into an output register and amplified at the edge of the CCD for digitization.
The thermal energy in the CCD chip results in constant electrons release (termed "dark current"), determining formation of background noise. This is dramatically reduced by cooling CCD chip: dark current falls 10 fold every 20° C decrease in temperature (*e.g.* for BLI imaging, CCD cameras are usually cooling to –120° C to –150° C).
The derived image is a color image superimposed on a gray-scale photographic image of the small animal using overlay and image analysis software [76].

5.1.1. Bioluminescence imaging (BLI)

BLI imaging is based on the use of reporter genes encoding enzymes able to produce emission of photons in the presence of specific substrates, in the wavelength range of 485-613 nm.
The major limitation to the use of bioluminescent reporters is that the low energy photons emitted are absorbed and scattered in the tissue volume encountered on their path from the emission site to the detector system. It has been calculated that about 90% of the BLI signal is attenuated per centimeter of tissue depth. So, the amount of photons detected may not be proportional to the reporter expression or may be insufficient to visualize the enzymatic activity present in the most inner organs of the most common laboratory animals, including mice [77].
The most used reporter enzymes are Luciferases. After injection of a substrate, in presence of specific cofactors (*e.g.* Mg^{2+}, oxygen, ATP, etc.), the substrate is oxydated with production of photons. Many Luciferases with matching substrates are available.
The most useful Luciferase for molecular imaging is firefly (*Photinus pyralis*) Luciferase (and its substrate, D-luciferin). Firefly Luciferase catalyzes the transformation of its substrate D-luciferin into oxyluciferin in an oxygen and ATP-dependent process, leading to the emission of photons with a peak wavelength of 560 nm, and a wide emission that goes beyond 600 nm, characterized by a sufficient penetrance across small animal tissues. Furthermore, the non-immunogenic substrate luciferin, either i.v. or i.p. injected, diffuses within minutes throughout the entire animal body and is rapidly taken up by cells.
However, also Renilla Luciferase, green or red click beetle (*Pyrophorus plagiophthalamus*) Luciferases, and Gaussia Luciferase have been used. Both Renilla and Gaussia Luciferases emit blue light, which is highly attenuated in living tissue, and possess high bursting activity, therefore requiring care and precision in the readout timing. Moreover, their substrate, coelenterazine, has been shown to be transported by the multidrug resistance transporter Pgp as well as to interact efficiently with superoxide anion and peroxynitrate in light-producing reactions, thereby complicating applications of Renilla and Gaussia Luciferases *in vivo* [78].
Despite the ease of use, the low costs and the short acquisition time, this technique depends on pharmacokinetic of biodistribution of the substrate, does not provide fully quantitative data and in general offers mainly planar imaging datasets, therefore imposing some positional uncertainty of the attained signal.

5.1.2. Fluorescence imaging (FLI)

Fluorescent imaging is based on the detection of photons (wavelength range: 442-800 nm) produced by the return to the ground state of electrons excited by laser

photostimulation. These photons can be revealed by CCD-camera by using specific filters to select excitation and emission band and to reduce noise background. In this technique the influence of tissue scattering and absorption is doubled compared to bioluminescent probes, because light must cover two-folds the signal-detector distance (excitation and emission pathways).
Examples of fluorescent proteins are green fluorescent protein (GFP), red fluorescent protein (RFP). Despite largely used for *in vitro* study, not all these proteins are useful for *in vivo* studies, because of their photon wavelength emission, often under 600 nm. With the introduction of redshifted fluorescent proteins and injectable near-infrared fluorescent probes, the progression in highly sensitive photon detection device development and *in vivo* microscopy (confocal and multiphoton), and the advances in mathematical modeling of photon propagation in tissues it has been possible to develop innovative macro- and microscopic FLI imaging modalities such as FLI tomography, spectrally resolved whole body FLI imaging, and intravital multiphoton imaging [78].
In 2004 a report appeared describing new fluorescent reporters developed by mutagenesis process. These new genes were able to emit photons of several wavelength but with a more consistent set into the red spectrum. These proteins have emission maxima as long as 649 nm, but suffer from low quantum yields and then low brightness that limits their application *in vivo* [79].
In 2007 a brighter red-shifted fluorescent protein was described by Shcherbo *et al* [80]. This protein, named Katushka, is originated from the sea anemone *Entacmaea quadricolor*. Its excitation peak is at 588 mm and the emission peak is at 635 nm, both of which are relatively non-absorbed by tissues and hemoglobin. Katushka has many favorable properties in addition to its absorption and emission peaks, including a rapid maturation time of 20 min. Importantly, an extinction coefficient of 65 000 $M^{-1}cm^{-1}$ and quantum yield of 0.34 make Katushka the brightest fluorescent protein with an emission maximum beyond 620 nm. In cells, Katushka has no visible aggregates or other toxic effects.
For what concern FLI, cell labeling is also possible with direct strategies. There are commercially available protein that are trapped by cell membrane, such as PKH26, VivoTag, Alexafluor [81], or fluorescent nanoparticles, such as Quantum Dots [82] [83]. These molecules offer certain advantages: faster labelling procedures and lower costs.
Although exciting advances are emerging, FLI imaging still suffers from pitfalls such as, high autofluorescence in the blue-green window resulting in low signal-to-noise ratios, fluorophore photo-bleaching, and high levels of photon attenuation and scattering in living tissues. However, imaging of fluorescent proteins (preferably monomeric red-shifted reporters) has an important advantage over other imaging modalities with genetically encoded reporters, *i.e.*, no substrate is required, which uncouples read-out from substrate pharmacokinetic and thereby enables true real-time imaging. In addition, sub-cellular localization is possible by correlative microscopic analysis.

5.2. Nuclear Imaging (PET/SPET)

PET and SPET are both radionuclide imaging techniques, yet they differ substantially in the type of radionuclide employed to label the tracer and method of data acquisition [84].

Both the techniques record high-energy γ-rays emitted from within the subject during a physical decay event occurring in instable nuclides.
With regard to PET imaging, natural biological molecules can be labelled with a positron-emitting isotope. The most used isotopes are ^{15}O, ^{13}N, ^{11}C, and ^{18}F; other less commonly used positron emitters include ^{14}O, ^{64}Cu, ^{62}Cu, ^{124}I, ^{76}Br, ^{82}Rb, and ^{68}Ga. Natural decay of these radioisotopes produces emission of a proton from its nucleus, that annihilates with a nearby electron: this interaction is able to produce two 511 keV γ-rays that are emitted simultaneously about 180° apart.
For SPET, single photon emitting isotopes (*e.g.*, ^{99m}Tc, ^{111}In, ^{123}I, ^{131}I) can be used for imaging living subjects. These radioisotopes are characterized by emitting photons of different energy (*e.g.* ^{111}In decay with emission of two photons of 171 e 245 keV, ^{99m}Tc with one photon of 140keV) [84][85].

Several molecules have been labelled with these radionuclides, to be used for classical applications. Once injected into the organism in study, they distribute with the blood stream and accumulate in relation to a specific process: perfusion, metabolism, receptor expression.
Progresses have been made in developing more and more specific probes for every molecular target to be studied but a hard multidisciplinary work has to be done for each new tracer from the chemical synthesis, the labelling procedure, to the pharmacokinetic evaluation and the analysis of sensitivity and specificity as well as of its reliability. It takes many years before a new tracer can be used in every day life.

Both PET and SPET imaging are highly dynamic methods permitting the study of biodistribution, localization and elimination of the tracer during time in the whole organism.
Detection of γ-rays is achieved through an array of scintillation crystals able to convert γ-ray energy into visible light, suitable light sensors that convert light into electrons, read-out electronics, and image processing units.
The coincidence detection of both γ-rays in PET within nanoseconds of each other defines the line of response in space and thus the direction of flight.
The reconstruction software measures the coincidence events at all angular and linear positions to reconstruct an image that depicts the localization and concentration of the positron-emitting radioisotope within a plane of the scanned organ.
In the SPET acquisitions, otherwise, to locate the source of an admitted photon, its direction of incidence into the detection system needs to be accurately fixed and its interaction location determined in the position sensitive detector. Lead or tungsten collimators are perforated plates that define the angle of photon incidence and are, therefore, positioned in front of the detector during SPET acquisition. Collimator design is a compromise between spatial resolution and sensitivity (see appendix 5 for more details).
In contrast to SPET, attenuation (quantifiable reduction in events present at the face of the detector due to absorption or scatter through tissues) of the emitted radiation in PET can be corrected precisely because the total length through the body determines the attenuation factor along a coincidence line. By doing so, quantitative information about the tracer distribution can be obtained. If single

photon emitters are used, the direction of flight has to be determined by geometric collimation.
An important principle to note is that as all isotopes used result in two γ-rays of the same energy, if two molecular probes, each with a separate isotope, are injected simultaneously, it would not be possible for the PET detectors to distinguish them. Therefore, to investigate multiple molecular events, molecular probes are usually injected separately, allowing for the decay of one isotope prior to administration of the other. SPET, on the other hand, does allow simultaneous detection of multiple events owing to the use of multiple isotopes, each with different-energy γ-rays [65].
Several reporter gene systems have been developed for nuclear imaging studies. A well-studied strategy is the reporter gene *hsv1-tk* whose protein product (herpes simplex virus type 1 thymidine kinase [HSV1-TK] enzyme) can be imaged with the specific radiolabelled substrate (^{18}F-fluoropenciclovir, ^{18}F-FPCV) and imaged by PET imaging [86].
Even if Iodinated substrates have been developed for the use of this reporter system in SPET imaging (FIAU, uracil nucleoside derivatives labeled with radioactive iodine) [87].
These radiolabelled reporter probes are transported into cells, and are trapped as a result of phosphorylation by HSV1-TK. When used in non-pharmacological tracer doses, these substrates can serve only for imaging without the well-known toxic suicide effects. More recently, a mutant version of this gene, *HSV1-sr39tk*, was derived using site-directed mutagenesis to obtain an enzyme more effective at phosphorylating ganciclovir (and also less efficient at phosphorylating thymidine) with consequent gain in imaging signal [88].
The Dopaminergic type 2 receptor (D_2R) gene has also been validated for PET imaging as reporter gene. ^{18}F-fluoroethylspiperone (FESP), a radiolabeled inhibitor of such receptor characterized by high affinity, can be used as reporter probe ligand [89].
More recently, a mutant D_2R that uncouples signal transduction while maintaining affinity for FESP has also been reported [90].
In SPET imaging, Na^+/I- symporter has been largely used as reporter gene. In this case Iodide ($^{123}I^-$) is specifically transported into cells by the ATP-dependent symporter, and accumulated proportionally to the reporter expression level.
Once transported into cells, $^{123}I^-$ is not modified and then is free to get out again from the cell. This is a drawback of the use of this symporter. It has been estimated that 80% of the $^{123}I^-$ transported by the NIS goes out from the cell during the first hour from the tracer administration [91] [92].
Moreover, it is possible to label cells directly for nuclear imaging by other strategy, besides gene reporter. Labelled molecular probes or tracers can be introduced into the subject, and then PET or SPET imaging can follow the distribution and concentration of the injected molecules.
In this field, the most commonly used radiotracers are: 99mTc-HMPAO, 111Indio-Oxine and 18F-FDG. These radiotracers are used for the *ex vivo* a-specific labelling of the cells that, once reinfused, can be followed by PET/SPET *in vivo*.
One of the advantages of PET is that drugs or existing molecules known to interact with a specific target can be modified with a radiolabel while minimally perturbing the parent molecule. These probes serve quite a useful role in monitoring "downstream" changes in pathology, but do not generally serve to characterize changes early in a disease process. Currently, molecular imaging probes with

greater specificity and targeting potential can be made by using antibodies, ligands, or substrates that can specifically interact with targets in particular cells or sub-cellular compartments. One easy and useful molecule of this type is [^{18}F-FDG], 18F-2-fluoro-2-deoxyglucose. In the cells, this radioligand is phosphorylayed by hexokinase, providing information about cell metabolism. Despite the specificity of the molecular probes exemplified above, background noise can be substantial with this approach. This is because the scanner cannot distinguish the parent tracer from the bound or metabolized tracer, and as such, time is required to allow the parent tracer to clear. To circumvent this relative drawback, another category of specific imaging probes consists of activatable or "smart" probes (also referred to as sensors or beacons). These can only be detected once they have interacted with their target, and have been developed mainly for optical and magnetic resonance imaging applications [65].

5.3. Magnetic Resonance Imaging

MRI is widely used for imaging soft tissues. Nuclei (the most used is ^{1}H due to the water's abundance in the body) placed in a strong magnetic field align their spin to the magnetic field. Radiofrequency (RF) pulses induce some of the magnetically aligned nuclei to alter the alignment of their spins. When the RF pulse is turned off, the nuclei realign with the magnetic field, generating an electromagnetic flux that provides information about the environment of the resonating nuclei (for more details, see appendix 2 and 4).

In animal models, different reporter genes have been studied by MRI. Principal feature of this type of labeling approach is the ability of reporter to modify the relaxing process of expressing cells. The most used reporter genes are based on the enzyme-based strategy [93]:

1) enzyme-based cleavage of functional groups that block water (proton) exchange or protein binding of MR contrast agents, *i.e.* β-galactosidase. This enzyme is able to cleave off galactose to a gadolinium based substrate (EgadMe) and this results in inner sphere relaxation enhancement and increased contrast. A convenience of using β-galactosidase reporter system is the low background contrast, as there is no natural endogenous expression of the enzyme;

2) expression of surface receptors that enable binding of specific MR contrast agents, *i.e.* transferrin receptor. After systemic injection of transferring-monocrystalline iron oxide nanoparticles, this agents is retained to expressing receptor, generating a major contrast;

3) expression of para- and anti-ferromagnetic (metallo)proteins involved with iron metabolism, such as transferrin receptor, ferritin and tyrosinase. For example, the last enzyme is part of the melanin synthesis pathway: it catalyzes the oxidation of tyrosine-yielding dioxyphenylalanine that is converted in melanin at the end of the whole process, that has high affinity for iron, accumulating it and generating a resonance signal [94].

On the other hand, to generate contrast in MRI, several contrast agents have been developed, also approved for clinical use. Among these agents T2-weighted iron oxide nanoparticles represent the most sensitive agent used in both animal and human applications. In general, any particle larger than 50 nm is termed superparamagnetic iron oxide nanoparticles (SPIO, as Endorem®), while particles smaller than 50 nm are called ultra small superparamagnetic iron oxide (USPIO).

Currently, SPIO is the only T2 contrast agent approved by FDA for MRI, and there are several reasons for its popularity. First, the particles are usually non-toxic to cells, and the particle is biodegradable *in vivo*. Second, it is a negative contrast probe, so it provides clear contrast to the background of the soft tissue, that generally are bright. Third, the particles can remain inside terminally differentiated cells throughout their lifetime, thus allowing long-term studies. Fourth, due to its sensitive signal, SPIO-based imaging requires a much smaller concentration than gadolinium, which makes SPIO more suitable for labelling human cells than other contrast agents [95].
SPIO-based MR imaging can be used for tracking diffent type of cells, including stem cells and progenitor cells. For not phagocytic cells, such as neural stem cells, a transfecting reagent may be required to load the particles. One examples id the addition of protamine sulphate, which is conventionally used in the clinic as antidote to heparin anticoagulation but also as a transfection agent in molecular biology [96].

5.4. Application of Imaging in Cell Therapy

In general, nuclear imaging modalities, such as SPET and PET, are highly sensitive (detecting fmol levels of probe), quantitative, inherently tomographic methods and can be used in humans. However, nuclear imaging demands sophisticated instruments, committed personnel, readily available in-house production of radiopharmaceuticals, and stringent dependency on tracer biodistribution.
On the other hand, BLI imaging of Luciferase reporters provides a relatively simple, robust, cost-effective, and extremely sensitive means to image fundamental biological processes *in vivo* thanks to exceptionally high signal-to-noise levels, but, unfortunately, it is not translatable to human study.
MRI is characterized by high spatial resolution and provides anatomical images, but its low sensitivity requires longer image-acquisition time and a higher amount of contrast agents. Moreover, the complexity of this technique requires the supervision of a specialized technician for instrument use.
Furthermore, nuclear and optical techniques lack anatomical information, thus new scanners combined with computed tomography (CT) have been produced.

With regard to the stem cell tracking, the ideal imaging/agent should provide the following information:

- Real-time visualization of stem cell delivery
- Determination of location(s) of cells over time
- Quantification of numbers of viable transplanted stem cells
- Long-term quantification of transplanted stem cell survival
- Study of interaction between stem cells
- Study of interaction of stem cell with its microenvironment
- Study of differentiation capacity of stem cells

The chosen labelling modality should not interact with the normal functions of the stem cell. Otherwise, one would not be able to study accurately the biology of

these cells over time. In addition, issues such as biocompatibility, toxicity, and safety not only to the stem cell but most importantly to the individual should also be considered, and included in the decision of which modality to use.
All imaging modalities have a certain degree of background/non-specific signal (that may interfere with the signal under study). The preferred imaging modality should be one that provides a good contrast between background and the target signal under study, achieving a large signal-to-noise ratio. Furthermore, it should have good specificity (negative study in the absence of what is being studied, stem cells in this case). Only then it will be possible to use these modalities to study stem cell biology.
The main objective of regenerative medicine, and thus of stem cell imaging, is its clinical application. It is generally agreed upon that before its clinical use, therapeutic strategies should be tested in clinical models of disease. Thus, an ideal imaging modality should be flexible across different imaging modalities, both in terms of spatial resolution and system sensitivity (the lowest amount of activity or numbers of cells that can be detected by that specific modality)[97].
As regards to the pharmaceutical research, the ideal molecular imaging technique should be characterized by high temporo-spatial resolution, high sensitivity, and high specificity, and it should also be translatable into the clinical setting. The ideal technology fulfilling all these criteria does not exist and compromises are to be searched for. There is increasing interest in constructing models that can be *in vivo* by means of different imaging modalities (multimodal imaging) combining the positive features of the single imaging techniques and overcoming their limits [94].
Several studies were performed in cell therapy protocols and in immune therapeutic protocols.
The development of stem or progenitor cell transplantation protocols for tissue regeneration and repair benefit greatly from *in vivo* assays that can rapidly assess the extent of cell survival and localization of transplanted cells. In the past years, these measures relied on histological analyses and required serial sacrifices of animals. That way, real-time data pertaining to cell migration and survival over time could not be assessed. Among the various imaging modalities that have been developed, several offer opportunities in this type of investigation. Magnetic resonance imaging (MRI) and fluorescence imaging provide means of tracking transplanted cells *in vivo* [98] [99] [100] [101].
Recent studies have revealed the effectiveness of neural stem or progenitor cells (NSPCs) transplantation in the treatment of Parkinson's disease, multiple sclerosis, brain ischemia, and trauma of CNS, including spinal cord injury (SCI) [102] [103] [104] [105] [106] [107].
Thanks to MRI techniques, Guzman et al. have demonstrated that human central nervous system stem cells, previously directly labelled with superparamagnetic iron oxide (SPIO), transplanted either to the neonatal, the adult, or the injured rodend brain respond to the cues characteristic for the ambient microenvironment resulting in distinct migration patterns.
Politi et al., in a 2007 study, labelled with Resovist® the NPCs and monitored their accumulation following i.v. injection in mice with experimental autoimmune encephalomyelitis (EAE), the animal model of multiple sclerosis. With a human MR scanner, they were able to visualize transplanted cells as early as 24 hours posttransplantation in up to 80% of the brain demyelinating lesions. Neuropathological analysis confirmed the presence of transplanted NPCs

exclusively in inflammatory demyelinating lesions and not in normal-appearing brain areas providing evidence that clinical-grade human MR can be used for noninvasive monitoring and quantification of NPC accumulation in the central nervous system upon systemic cell injection [108].

Sykova *and* Jendelova studied the fate of implanted rat bone marrow stromal cells (MSCs) and mouse embryonic stem cells (ESCs) labelled with iron-oxide nanoparticles (Endorem®) and human CD34+ cells labelled with magnetic MicroBeads (Miltenyi) in rats with a cortical or spinal cord lesion.

Cells were grafted intracerebrally, contralaterally to a cortical photochemical lesion, or injected intravenously. MRI images permitted to visualize labelled MSCs, ESCs, and CD34+ cells in the lesion as a hypointensive signal, persisting for more than 50 days. These studies demonstrated that grafted adult as well as embryonic stem cells labelled with iron-oxide nanoparticles migrate into a lesion site in brain as well as in spinal cord.

Several studies, conducted by De Vries et al [109] has recently shown the utility of the non-invasive MRI technologies also for monitoring, in humans, immune-therapy based on DCs previously matured and loaded with tumour-derived antigenic peptide. Together with other clinical and preclinical studies [110][111][112], this work demonstrated that the imaging of DC migration through MRI gives the highest spatial resolution among non-invasive modalities, with exquisite dynamic information and anatomical contrast [113].

The studies on animal models, using nanoparticles of iron oxide [114][115] permitted to demonstrate the potential for non-toxic labelling of haematopoietic bone marrow-derived and mesenchimal stem cell populations without affecting their transdifferentiation capacity. Iron oxide labelling can also be used to track smaller numbers of cells in homing experiments enabling the *in vivo* identification of the mesenchimal stem cells which migrated to infarcted myocardium after intravenous administration.

Adult farm pigs were subjected to experimental MRI, and MSCs were injected intramyocardially under x-ray fluoroscopy. The labelled cells could be detected in the myocardium, with different shapes because of the different distribution in the damaged organ [114]. In the cardiovascular setting, besides, this cell labelling technology could be coupled with direct delivery methods through endomyocardial injections, demonstrating that transplanted cells could be imaged shortly after delivery with a high degree of spatial resolution using MRI [114].

With regard to the direct labelling for optical imaging, Hoshino et al [116] reported a successful labelling of bone marrow–derived mesenchimal stem cells with IR-786 (a NIR fluorophore) and their subsequent *in vivo* tracking for 90 minutes after intracoronary cell injection in a swine model of myocardial infarction.

The imaging in the NIR window (700-900 nm) has the advantage to be characterized by low absorption by intrinsic photoactive molecules, thus allowing light to penetrate several centimetres into the tissue giving the possibility to be used in big animals.

Gorio et al. [33] have labelled stem cells from dermis with PKH 26, a stable cell membrane fluorescent labelling, in order to localize them after their transplant into gracilis and cuneate fascicle at 3 mm caudally or rostrally to the spinal lesion site. The cell labelling permitted to demonstrate that when cells were transplanted into the spinal cord after traumatic injury, they were able to migrate into the lesion

cavity but their differentiation was dependent upon the time interval between lesioning and cell transplantation (submitted paper or Data not yet published).
In spite of MRI and fluorescent imaging are very useful in tracking transplanted cells *in vivo*, these techniques can be constrained by sensitivity and/or retention of the label [117][118][119].

The first imaging data on stem cell therapies by nuclear imaging and in particular by SPET and ^{111}In-oxine, were based on the intravenous injection of labelled MSCs [120][121]; the data allowed to conclude that the radiolabelling of MSCs is feasible, providing a good spatial resolution, but, as a consequence of the significant lung activity due to i.v. administration of MSCs –which obscures the assessment of myocardial cell trafficking- alternative routes of administration should be investigated for this application [120]. When ^{111}In^{111}–labelled endothelial progenitor cells were injected intraventricularly in the infarcted rat myocardium, labelled cells were found to accumulate in the hearth, but the overall radioactivity in the organ was only around 4.7% of the injected dose [122]. These data suggested that in loco injection is an efficient route of administration and that only a small number of cells ultimately home to injured myocardium, corroborating the high sensitivity of the nuclear imaging technique.
Several studies in the field of neuroscience reported the possibility to track also neural stem cells or progenitors by the use of nuclear imaging techniques.
Lappalainen et al. demonstrated, in 2008, using the SPET imaging, the accumulation of neural progenitor cells into internal organs after systemic administration in middle cerebral artery occlusion rats [123].
In this work they evaluated the feasibility of small animal SPET/CT in assessing the definite accumulation of ^{111}In-oxine-labeled human embryonic stem (ES) cell-derived neural progenitors and rat hippocampal progenitors after intravenous or intra-arterial administration (femoral vein vs. common carotid artery) in middle cerebral artery occlusion (MCAO) and sham-operated rats. Cell detection was carried out immediately and 24 h after the infusion using a SPET/CT device.
The results permitted to demonstrate that after intravenous injections both cell types accumulated primarily into internal organs, instead of brain. In contrast, after intra-arterial injection, a weak signal was detected in the ischemic hemisphere. These data showed that the small animal SPET is a powerful technique to study the whole body biodistribution of cell-based therapies and that intravenous administration is not an optimal route to deliver neural progenitor cell-containing transplants into the brain after MCAO in rats.

To circumvent the problem of signal loss due to dilution with cell division, typical of the direct labelling techniques, the research is focusing its attention on the reporter gene techniques. The aim is to integrate a reporter gene into the cells before transplantation. Such an approach that has been used for cell tracking and survival studies uses cells labelled with the luciferase gene and instruments for BLI [124], as described in the previous paragraph (5.1). BLI has been shown to be a useful tool for tumour, immune, and hematopoietic cell tracking studies. Usually, third-generation self-inactivating lentiviral vector system based on human immunodeficiency virus type 1 (HIV-1) is used. This viral vector offers safe, high titer transduction and efficient integration into cells irrespective of their state of division [125][100][126].

Okada et al., in order to monitor engrafted neural stem cells in the spinal cord injury, used a lentiviral vector to achieve efficient delivery and stable expression of both luciferase and green fluorescent protein (GFP) in primary cultured NSPCs. To determine the optimal timing of transplantation for SCI, they transplanted transfected NSPCs at different times relative to injury and observed differences in survival, migration, and differentiation of NSPCs.
In other studies based on bioluminescence imaging, embryonic rat H9c2 cardiomyoblasts expressing Firefly Luciferase as reporter gene were injected in the myocardium of rats [127]. Drastic reductions of signal intensity were noted within the first 1 to 4 days after transplantation, probably because of acute donor cell death following inflammation, ischemia, and apoptosis, as displayed on the histology, but the signal was detectable until 16 days.
Reporter constructs with luciferase are also useful for the study of cell differentiation as described by Hawang et al. They imaged neuronal differentiation *in vivo* of F11 cells using dual reporters (sodium iodide symporter [NIS] and luciferase) coupled to a neuron-specific enolase (NSE) promoter [128].

The direct cell labelling is simple and allows to visualize the location of the therapeutic cells nevertheless it is not sufficient to permit a long-term study of variables such as cell survival and differentiation, that, instead can be monitored *in vivo* by the use of reporter genes and adequate promoters.
The combination of the two techniques would allow long-term studies useful for the therapeutic protocol set up. Furthermore it would allow the identification of early and intermediate checkpoints giving information about the progress of the treatment by the use of diagnostic procedures that can be translated into clinical use.
Regarding the choice of imaging techniques, a combination of different techniques would overcome the limitations of individual methods by providing more informative results.
In particular, the BLI for animal models together with MRI transferable to the clinic, would be the best solution because it would combine the high sensitivity of BLI and its ease of use with high spatial resolution of MRI. The development of even more efficient contrast agents and the use of ever higher magnetic field intensity scanners would also permit to obtain an even better sensitivity with the advantage to be clinically transferable.

Aim

The use of stem cells in cell-mediated treatments is of considerable interest in research for the regeneration and reconstitution of tissues damaged by trauma and degenerative and inflammatory diseases. Continuous progresses have been made in the ability to isolate stem cells, culture them and track their differentiation *in vivo*. Moreover, numerous treatment protocols have been tested in various animal models in which stem cells are extracted from healthy animals and implanted in diseased ones.
At the moment, one of the limits of stem cell therapy consists of the fact that treatment efficacy evaluation is based only on functional recovery several months after the transplant also by the use of classical imaging techniques.
Furthermore, important variables such as the distribution of the injected cells, target organ localization, cell survival, proliferation and differentiation cannot be evaluated in vivo with conventional techniques. All other variables listed here are evaluated *ex vivo* on samples from biopsies and tissues from transplanted animals by means of immunohistochemistry.
For these reasons, the aim of this study was the introduction of early check-points permitting the *in vivo* evaluation of cell localization after transplant using cell imaging techniques. In particular, we proposed the development of protocols for the *in vivo* visualization of mNSCs in the evaluation of treatment approaches of traumatic spinal cord injury.
By using imaging techniques, such as nuclear imaging (PET/SPET), magnetic resonance imaging (MRI), and optical imaging (BLI and FLI), the fate of the injected cells can be dynamically and functionally evaluated *in vivo* in space and time, permitting to define specific parameters for assessing treatment efficacy in the early phases. The imaging protocols provide objectively evaluable parameters for describing the progress of a cell-mediated therapy, so to correlate the distribution, survival, effective differentiation of the injected cells with functional recovery *in vivo* over time by combining anatomic findings with functional results.
The use of different imaging modalities has the advantage to combine the positive attributes and to overcome the limits of the single imaging techniques themselves.
Furthermore with these protocols, the number of needed experimental animals would be lower, thus reducing interindividual variability, since each animal would become its own control. In addition, with fewer animals and better evaluation, the number of stem cells needed per experiment could be reduced, making them available for further studies.

More in particular, in the course of this project, neural stem cells were isolated from the subventricular zone of adult CD1 mice brain and implanted into spine-injured animals models. The cells were directly labelled with magnetic particles or ^{111}In-Oxine for Magnetic resonance imaging (MRI) and nuclear imaging respectively. Early phases distributions were followed by scintigraphy while MRI. The cells were also indirectly labelled. NSCs were infected with a lentiviral vector containing Luciferase controlled by the PGK constitutive promoter. Bioluminescent imaging (BLI) provided information about cell distribution, and luciferase activity permitted in vivo evaluation of cell viability after transplant. All the information provided by the different *in viv*o imaging analyses will permit the direct evaluation of treatment efficacy in each single animal permitting to foresee eventual adjustments of the protocol for each single treated subject.

Materials and Methods

1. MURINE NEURAL STEM CELLS (mNSCs) COLTURE

Adult CD-1 albino mice weighing 25-30 g (Charles River) were anesthetized by intraperitoneal injection of 4% chloral hydrate (0.1 ml/10 gm body weight), then sacrified by cervical dislocation and neural stem cells were isolated as described by Gritti et al. [61]. Tissues were enzymatically digested at 37°C for one hour in 5% CO_2 in a solution containing cistein (Sigma) 0.2 mg/ml, EDTA (Sigma) 0.2 mg/ml papain (Worthington DBA) 1 mg/ml in EBSS (Enhanced Balanced Salt Solution) (Gibco). At the end of the digestion the tissue was spun at 123 g for 10 minutes, the supernatant removed and substituted with 1 ml of EBSS medium. The pellet was desegregated using a 1000 µl Gilson pipette, washed in EBSS and centrifuged with the same parameters of the previous one. The supernatant was removed leaving 200 µl and the pellet further desegregated by pipetting up and down with a 200 µl Gilson pipette and wash with EBSS and further centrifuged at 123 g for 10 minutes. The supernatant was finally discarded and the pellet re-suspended in 200 µl of medium containing EGF (20ng/ml)(Epidermal Growth Factor), bFGF (10ng/ml) (basic Fibroblast Growth Factor), DMEM/F12 medium 2 mM L-glutammine, 0.6% glucose, 9.6 gm/ml putrescine, 6.3 ng/ml progesterone, 5.2 ng/ml sodium selenite, 0.025 mg/ml insulin, 0.1 mg/ml transferrin, and 2 mg/ml heparin called growth medium. The cells were plated as 3500 cells/cm^2 in the appropriate volume of the aforementioned medium in a 25 cm^2 flask at 37°C in a humidified 5% CO_2 atmosphere. EDTA (Sigma-Aldrich), and incubated for 45 min at 37°C on a rocking platform. Tissues then were centrifuged at 123*g* and the supernatant was discarded. The pellet was re-suspended in 1 mL of EBSS and mechanically dissociated using an aerosol resistant tip (1000 µm Gilson Pipette). Cells were re-suspended in 10 mL EBSS and centrifuged at 123*g* for 10 min. The supernatant was discarded and the pellet re-suspended in 200 µL of EBSS. The pellet again was dissociated mechanically using an aerosol resistant tip (200 µm Gilson Pipette). Cells were re-suspended in 10 mL of EBSS and centrifuged at 123*g* for 10 min. The supernatant was discarded and the pellet resuspended in 1 mL of chemically defined DMEM-F-12 containing FGF2 (human recombinant, 10 ng/mL; Peprotech, Rocky Hill, NJ, USA, or Upstate Biotechnology, Lake Placid, NY, USA) and EGF (human recombinant, 20 ng/mL; Peprotech). The cells were counted and plated at 3500 cells/cm^2, the spheres formed after 5–7 d were harvested, collected by centrifugation (10 min at 123*g*), mechanically dissociated to a single-cell suspension, and re-plated in medium containing the appropriate GF(s) (19). This procedure was repeated every 3–5 d (passage) *in vitro* for up to 12 months. The total number of viable cells was assessed at each passage by Trypan blue exclusion. Stem cells used in these experiments were between the fifth to the fifteenth passage in culture.

2. NSCs LABELLING

2.1. Direct labelling

2.1.1. NSC labelling with SPIOs

Murine neural stem cells (mNSC) were freshly plated early in the morning. Six hours after, cells were labelled with different amounts of SPIOs (0 - 100 - 200 - 400 µg Fe/ml Endorem, Guerbet®; stock solution 11,2 mg Fe/ml) in the colture medium and incubated for 24,48 or 72 hours in presence of transfection agents such as PLL hydrobromide (Sigma-Aldrich; a stock solution at 2,4 mg/ml), polybrene (PB, Sigma-Aldrich; stock solution 10 mg/ml, used at 10 µg/ml) and protamine sulphate (PS, Sigma-Aldrich; stock solution 10 mg/ml). PLL and PS were tested at different ratio (Fe/PLL 1:0,03, 1:0,06 and 1:0,09 and Fe/PS 1:0,025 and 1:0,05). Cells were washed three times with PBS and Heparin (1U/ml).
After 24, 48 and 72 hours of incubation*,* cells were counted to analyse the viability by standard Trypan Blue exclusion test and then washed. Morphology (Perl's staining), iron content, and relaxation time reduction were analysed to evaluate the labelling efficiency and the capability of the cells to be detected *in vivo* by MRI. Part of the labelled cells were also plated and cultured for further 5 or 7 days for multipotency and differentiation capability analyses, respectively.

2.1.1.1. Perl's Prussian Blue Staining

After incubation with paramagnetic nanoparticles, the Prussian blue (PrB) staining (Perls' acid ferrocyanide) was used for the detection of iron within the cell cultures. This induces a reduction of ferric iron to the ferrous state with formation of a blue precipitate.
150.000 single-cell-dissociated SPIO-labelled NSCs harvested on glasses for microscopy using cytospin, were fixed with an alcoholic solution (Cervix fixative, J.T Baker). Prussian blue (PrB) staining was performed by incubation in a 1:1 mixture of 2% HCl (BDH Laboratory Supplies) and 2% potassium ferrocyanide (Merck) for 45 minutes at room temperature (24°C). A minimum of *n*° 7 nonoverlapping fields was counted for each sample. Cell membranes were counterstained by gram's Safranine solution (Merck). Data were expressed as mean percentage of PrB-positive cells (over total of counted cells).

2.1.1.2. Iron content evaluation

The iron content per cell was evaluated with the spectrophotometer analysis [129]
The absorbance (optical density) was measured using a Hewlett Packard 8452A diode array spectrophotometer (Hewlett Packard, Palo Alto, CA, USA).

2.1.1.3. Relaxation time measurements

Cells were washed as described above and then every sample was resuspended in 500 µL of 1%PFA at the same concentration. 2.5 ml of PBS were added and the samples were analysed at 40°C using a 0.47-T Bruker Minispec mq20 relaxometer (see 1.3.3 paragraph and appendix 2 and 3 for details) with the following parameters: 12.000 pt reading single scan, delay of 2 sec, gain of 64, dummy shot of 0.

2.1.2. NSC labelling with ^{111}In-oxine

$1x10^6$ cells were incubated for 30 minutes with 60 µCi of ^{111}In-oxine and Tris-HCl 5M (pH7) buffer. The cells were washed in PBS and injected into the tail vein of a spinal cord injured mice.

2.2. Indirect labelling

2.2.1. Lentiviral production

Helper Lentiviral vectors of third generation (pMD2g-VSV-G, pMDLg-RRE and pRSV-Rev) useful for the viral production for stem cells infection were offered by Dr. Rivella's Laboratory (Cornell University, New York) and were amplified in DH-5alpha bacteria (NEB), purified with an endotoxin free DNA extraction kit (Invitrogen) and diluted in TE buffer.
The pCLL.PGK.Luc.WPRE (PLW) plasmid, containing the Luciferase gene controlled by the constitutive promoter PGK, was previously cloned in our laboratory.
The lentiviral vectors were producted as described by Tom Dull et al. [130].
The vector copy number (VCN) viral titer ($7,62x10^5$ TU/ml) was calculated on HeLa cell lines through the amplification of the lentiviral specific WPRE region from genomic DNA of Hela infected cells by the use of the Real-Time PCR technique [131] and its comparison to a curve of DNA standards with known VCN.

2.2.2. NSCs Infection

NSCs were infected with 5 MOI of PLW lentiviral vectors and polybrene (8 µg/ml).

The luciferase expression was evaluated after the cell lysis, by CCD camera using a luciferase activity assay (Promega) and the data obtained were normalized on the total protein concentration.

3. EVALUATION OF LABELLED NSC FEATURES

3.1. Stem cells features maintenance

The maintenance of the capability of labelled NSCs to form new neurospheres was visualized by optical microscopy while the maintenance of specific neural stem cells marker expression was evaluated in immune-Fluorescence.
180.000 labelled NSCs were dissociated to a single-cell suspension, were harvested on glasses for microscopy using cytospin, and were fixed with an alcoholic solution (Cervix fixative, J.T Baker).
NSCs were permeabilyzed by a solution TRITON 0,1 % and PBS 0,01M (200 µl/well) and incubated with the primary antibodies anti-nestin (monocl.1:100; Pharmingen, San Jose, CA, USA)). Nuclei were stained with DAPI. The detection of immunocomplexes was performed using the appropriate secondary antibodies conjugated with either Texas Red or fluorescein isothiocyanate (Jackson Immunoresearch Laboratories).

3.2. Cell differentiation

The neural differentiation was evaluated by Immune-fluorescence for GFAP (marker of astrocytes), Gal-C (marker of oligodendrocytes) and β-tubulin III (neuronal marker) expression.
NSCs, after the dissociation were plated, at the density of 40,000 cells/cm^2, on coverslips pre-coated with adhesion molecules (Matrigel™) placed into the wells of a 48 multiwell plate. The NSC differentiation was achieved colturing stem cells in presence of serum and removing the growth factors (EGF and FGF). Differentiation and expression of various epitopes were achieved within 7 days. Differentiated NSCs were fixed with 4% paraformaldehyde in PBS for 5 minutes at room temperature, and, then, washed with PBS. Cells were used for immunocytochemical staining.
The immunostaining was performed as follows: the coverslips were incubated for 90 min at 37°C (or overnight at 4 °C) in PBS containing 10% normal goat serum (NGS), 0.3% Triton X-100, and the appropriate primary antibodies or antisera. After thorough washing with PBS and 10% NGS, cells were incubated for 45 minutes (room temperature) with secondary antibody (anti mouse or rabbit) conjugated with the Alexa Fluor dyes 488 or 543nm (Invitrogen, Carlsbad, California). The cells were then counterstained with the DNA-binding dye 4'-6'-diamidino-2-phenylindole (DAPI) (2 µg/ml in PBS) for 10 minutes at room temperature, twice washed in PBS followed. Coverslips containing the stained differentiated cells were mounted onto glass slides and examined under a fluorescence microscope (Leica, Wetzlar, Germany). Acquisition of the stained cells was performed using the image-analysis software (Leica, Wetzlar, Germany) or by confocal microscope Leica SP2 microscope with He/Kr and Ar lasers (Leica, Wetzlar, Germany). In control experiments, primary antibodies were either omitted or replaced with equivalent concentrations of unrelated IgG of the same subclass. Moreover, in double labelling experiments, sections incubated with one primary antibody and two secondary antisera revealed no appreciable cross-reactions.
Neural differentiation was assessed by immunocytochemistry with antibodies against: β-tubulin III (monocl. 1:100; Sigma), microtubule-associated protein 2

(MAP-2; monocl. 1:200; Sigma), glial fibrillary acidic protein conjugated with cy3 fluorocrome (GFAP-cy3; monocl. 1:50; Roche, Basel, CH).

4. SPINAL CORD INJURY

4.1. Animals

Adult CD1 mice weighing 28 to 30 g were used. A standard dry diet and water were available ad libitum. All experimental protocols were approved by the Review Committee of the University of Milan and met the Italian guidelines for laboratory animals, which conform to the European Communities Directive of November 1986 (86/609/EEC)
The animals were kept for at least 3 d before the experiments in standard conditions (22 ± 2° C, 65% humidity, and artificial light between 08:00 a.m. to 08:00 p.m.).

4.2. Spinal Cord Injury with UTS Impactor

The traumatic SCI was performed by means of the UTS impactor as described by Gorio et al [5].
Animals were previously anesthetized by i.p. injection (10 ml/kg) of 4% chloral hydrate (Sigma-Aldrich, St. Louis, MO) and laid over a mat kept at the temperature of 38°C.A laminectomy of the T8 and T9 vertebral level was performed on anesthetized mice. The lateral processes of T8 and T10 vertebras were cleared of the muscle to allow the stabilization of the vertebral column using forceps attached to the impactor-clamping platform, and a contusion injury was induced on the exposed cord using the impactor device. The impounding piston was positioned 1 mm above the exposed cord at T8 and T9 and set for an excursion of 3 mm. A force of 50 Kd for 2 seconds was applied, which was followed by an automatic return of the impactor rod. The muscle and skin were sutured, after the injury, with a reabsorbing string (Etichon).
Before awakening, they were treated with buprenorphine (0.03 mg/kg) (Sigma-Aldrich) for pain and penicillin G (10,000 U/kg; Sigma-Aldrich) as antimicrobial agent.
To prevent the sepsi post-operation, in the next days all mice were treated with 100 ml of subcutaneously injected ampicillin (100 mg/Kg, Farmitalia) and 1 ml of physiologic solution.
Each experimental group was constituted by at least 15 animals.

4.3. Experimental Groups for Transplantation

The animals were divided into four experimental groups: 1) spinal cord injured CD1 mice injected with $1{,}5x10^5$ of labelled NSCs directly into the spinal cord used as positive control; 2) spinal cord injured CD1 mice injected with $1x10^6$ of labelled NSCs into the tail vein; 3) Naïve control mice not laminectomized and not injured; 4) spinal cord injured mice transplanted with phosphate buffer (PBS) by i.v.(Mock mice).

5. *IN VIVO* IMAGING

5.1. Nuclear Imaging

Nuclear imaging of the early phases distribution was performed, on the four experimental groups, for 3 days soon after the injection of ^{111}In-I-oxine labelled cells using a new very compact gamma camera prototype (Hi-Cam), developed in collaboration with the Politecnico of Milan, constituted by Silicon Drift Detectors (SDD) and characterized by a high spatial resolution (< 1mm), a FOV of 5x5 cm^2 and a Sensitivity of 272 cpm/microCi using a parallel hole collimator and of 282 cpm/microCi using a Pin hole collimator.Being Hi-Cam a prototype, no standard acquisition sequences were available: for each image, timing of acquisition was depending on the radioactivity of the injected cells.

5.2. MRI

After the incubation with the SPIO-containing medium, cells were washed twice in phosphate-buffered saline (PBS), and once in PBS added with heparin (1U/ml) and viable cells were counted by trypan blue exclusion.
All mice were previously anesthetized with an intraperitoneal injection of 4% Chloralium solution. Then cells or PBS were injected into the spinal cord or into the tail vein of the injured mice. The injection was performed the same day of the injury in every experiment.
MRI imaging was performed, on the four experimental groups, from 1 week after the transplant up to 2 months using 7T MR scanner (Bruker).
Anesthetized animals (isofluoran gas anaesthesia) were positioned prone on the animal bed and inserted in the radiofrequency coil (diameter of 38 mm) inside the magnet. Scout transverse images were acquired for correct positioning of interest region. Different MR sequences were tested in order to optimize spinal cord visualization and signal contrast:

- Spin Echo (MSME) sequence, (matrix 256x128; TR/TE: 1200/12 ms; 2 averages; acquisition time: 5' 7"; fat suppression used) permitted to obtain images for morphological analysis of tissues and organs,
- Gradient Echo (FLASH) sequence (matrix 256x128; TR/TE: 1200/10 ms; 2 averages; acquisition time: 5' 7") permitted to enhance the iron signal, with a decreasing on morphology definition.
- Fast spin echo (RARE) sequence (matrix 256x128; TR/TE: 2000/56 ms; e average; acquisition time: 4'16'') permitted to enhance the iron signal maintaining a good morphological resolution.

All animals were acquired in sagittal, coronal (5 slices of 0.7 mm of thickness; FOV 4x4 and spatial resolution of 156 µm x 312 µm) and axial plans (12 slices of 0.7 mm of thickness; FOV 3x3 and spatial resolution of 117 µm x 234 µm).
Once a week a small group of animals were sacrificed and the spinal cords were collected, embedded in formalin and sectioned, in order to perform Perl's staining, as described above.
Sections of the spinal cords were analysed by optical microscopy at 5X, 20X and 40X original magnification to confirm the homing of labelled NSCs.

5.3. In vivo Bioluminescence imaging (BLI)

The NSCs were infected with the PLW lentiviral vector and analyzed for cell viability and for the maintenance of phenotypical and functional features as previously described.
Xenogen-IVIS Lumina cooled CCD optical macroscopic imaging system was used for BLI after an i.p. injection of D-luciferin (80 mg/kg body weight). Mice injected with lentivirally infected mNSCs were acquired every day, for the first week after the transplant and then once a week for a month. Serial images were initially acquired from 5–35 min after D-luciferin administration in order to find the time window providing the maximum signal intensity. Since the signal intensity peaked at 15 min after D-luciferin administration, followed by a plateau of 25 min, this time window was chosen for the next acquisitions. Naïve control mice not laminectomized and not injured and mock mice were acquired as negative controls. All images were analyzed with Living Image software (Xenogen).

6. STATISTICAL ANALYSIS

Statistical analysis was performed with a Student's *t* test. For the open field score, repeated. measure ANOVA and Bonferroni/Dunn test were used. Significance was accepted at $P < 0.05$.

Results and Discussion

1. NSCs DIRECT LABELLING FOR MRI

1.1. NSC labelling with SPIOs

In CNS disorders characterized by neuronal or glial loss (e.g. Parkinson's disease, Multiple sclerosis, stroke and spinal cord injury), the NSC-based replacement therapies represent a promising alternative therapeutic approach. However there are some relevant issues that needed to be solved before translating such therapies to human application: 1) the route of cell administration and cell homing; 2) persistence and the differentiation of transplanted cells into the targeted tissue. Furthermore, the integration of transplanted cells into the host tissue and the maintenance of cell viability and functionality are important goals to be achieved. To better understand these events for a future translation in humans of such promising therapies the research would benefit from a reliable non invasive imaging system able to follow *in vivo* the fate of transplanted cells.

Among the different imaging techniques, MR imaging presents numerous advantages, since it offers both near-cellular (i.e., 25-50 μm) resolution and whole body imaging along with excellent soft tissue contrast. MRI is characterized by a high spatial resolution and a direct anatomical correlation, which permits relatively precise localization of transplanted labelled cells. Furthermore this technique is still commonly used in clinical practice and in particular for the study of human CNS and represents a good tool for diagnosis, patient examination and monitoring.

In order to develop a methodology for the *in vivo* monitoring of murine adult NSC trafficking, we set up a specific labelling protocol with paramagnetic nanoparticles (MNPs) and analyzed the maintenance of their phenotypical and functional features once incubated with paramagnetic nanoparticles such as new neurosphere formation and the maintenance of differentiation capability.

Commercial MNPs, called Endorem® (FDA approved), are formed by a core of iron coated with dextran (called ferumoxide) with an hydrodynamic ray of about 100 μm. These MNPs can be resuspended in cell colture medium and internalized by NSCs.

Cell labelling was carried out by either direct exposure of the cells to the SPIOs (Endorem, Guerbet ®) or by complexing the SPIOs to different carriers such as poly-L-lysine (PLL), polybrene (PB) and protamine sulphate (PS). To further optimize the loading protocol also different times of incubation of the cell with the iron containing colture medium were used.

Labelling efficiency was calculated by analyzing the percentage of cells positive to the specific iron staining Perl's while cell viability after labelling was evaluated by the Standard Trypan Blue Exclusion Test.

In preliminary studies, murine NSCs, were incubated for 24h with different amount of SPIOs (25–50–100-200-400 μg Fe/ml, Endorem ®). After the Perl's staining, it was possible to observe an increase in iron content per cell in relation to the iron concentration in the medium and to the different carriers (figure 1 and graph 1).

The incubation with SPIOs in presence of polybrene or PLL also tested at different ratios with respect to the nanoparticles (Fe/PLL 1:0.03; 1:0,06; 1:0,09) didn't increase the labelling efficiency (data not shown), on the contrary the use of PS (ratio Fe/PS 1:0.025) as carriers, permitted to obtain the higher labelling degrees (94,5% of labelling efficiency).

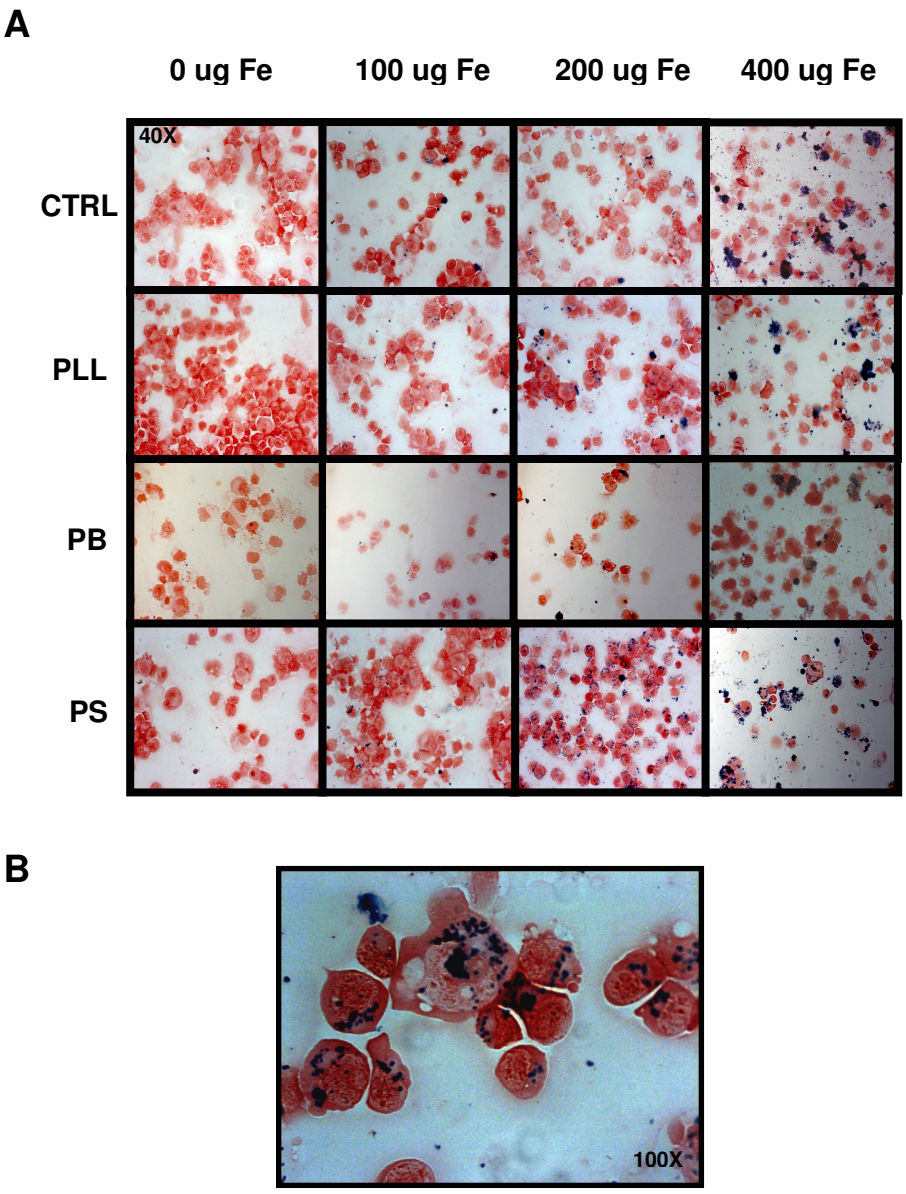

Figure 1: *Adult neural stem cells isolated from the SVZ of CD1 mice labelled with different amounts of SPIOs (0, 100, 200, 400 µg/m Fel) in the presence or absence of different transfection agents such as poly-L-Lysine (PLL), polybrene (PB), protamine Sulphate (PS) for 24h (A). Prussian blue staining of labelled cells permitted to reveal an increase in cell iron content in relation to the amount of SPIOs in the cell culture medium and to the presence of transfectants. 400 µg Fe/ml with or without tranfectants resulted in cell suffering and aberrant morphology. 200 µg Fe/ml in presence of PS for 24 hours, seemed to be the best labelling condition (B).*

Lower iron concentrations (25-50 µg Fe/ml) were early discarded because of their low labelling efficiency. On the contrary, higher iron concentrations (400 µg Fe/ml) resulted in evident toxicity and lower cell viability as demonstrated by the figure 1 and the graph.
200 µg Fe/ml (Endorem®) in presence of PS has initially been chosen as the best labelling condition in term of iron content/cell (110pg Fe/cell), labelled cell rate and cell viability.

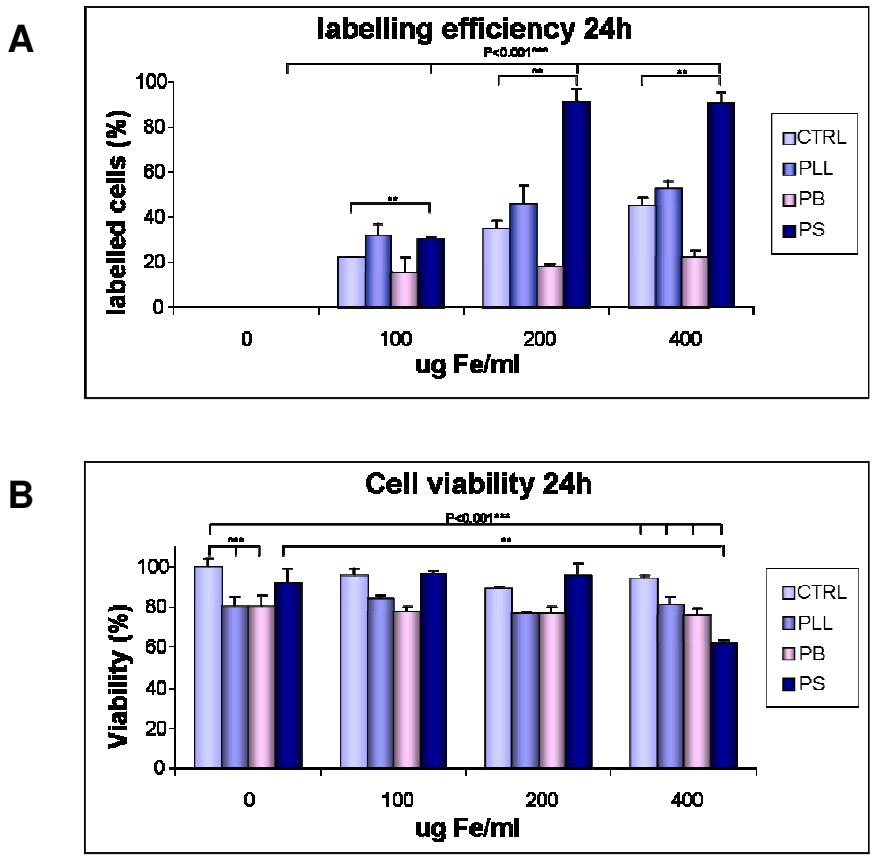

Graph 1. *The percentage of Iron-positive cells increased in proportion to the iron content in the medium and in the presence of PS (A). In particular we obtained 94,5%±1 iron-positive cells in the samples incubated with 200 µg Fe/ml for 24h in the presence of PS (p<0.001 compared to control). Higher amount of Iron (400 µg Fe/ml) enhanced the percentage of labelled cells (A) but strongly decreased the viability (P<0.001) (B). Labelling with 100 and 200 µg Fe/ml in the presence of different transfection agents (PLL, PB, PS) did not reduce cell viability compared to the respective control. The presence of trasfection agents PLL and PB in the medium, decreased the percentage of viable cells (P<0.001) whereas the presence of PS did not influence cellular viability (B).*

A higher PS concentration (ratio Fe/PS 1:0.05) was tested in order to further increase iron internalization.
There were no significant differences, in terms of viability and proliferation, between mNSCs, incubated for 24h with 200 µg Fe/ml in presence or absence of different amount of PS, and non labelled cells (graph 2).
The percentage of viable cell was 85% for Fe/PS 1:0.025 ratio and 77% for Fe/PS 1:0.05 ratio compared to the 95% of the control (with no PS). On the contrary, the percentage of iron positive cells increased in proportion to the PS content in the medium. In particular 94,5% of labelling efficiency was obtained in the samples incubated with Fe/PS 1:0.025 ratio and 99% in the samples incubated with Fe/PS 1:0.05 ratio (graph 2).
The spectrophotometer analysis revealed an increase of the iron content from 110 pg Fe/cell to 210 pg Fe/cell increasing PS concentration even if by using the higher Fe/PS ratio cell morphology resulted in higher vacuolization (figure 2). In order to perform an efficient labelling protocol able to track the cells without perturbing their features and functionality, the lower PS concentration has been chosen.

A

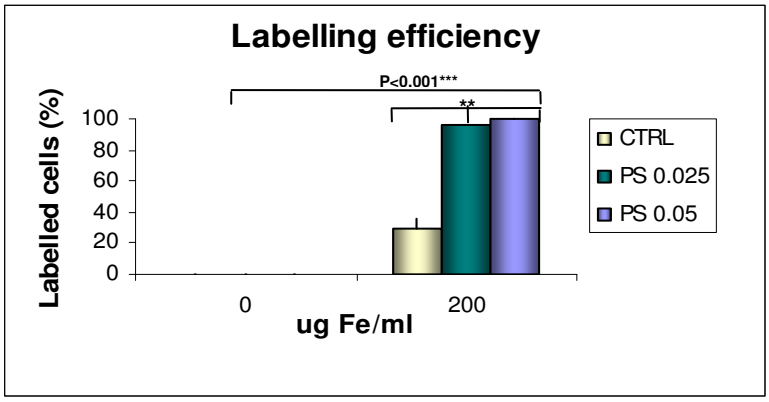

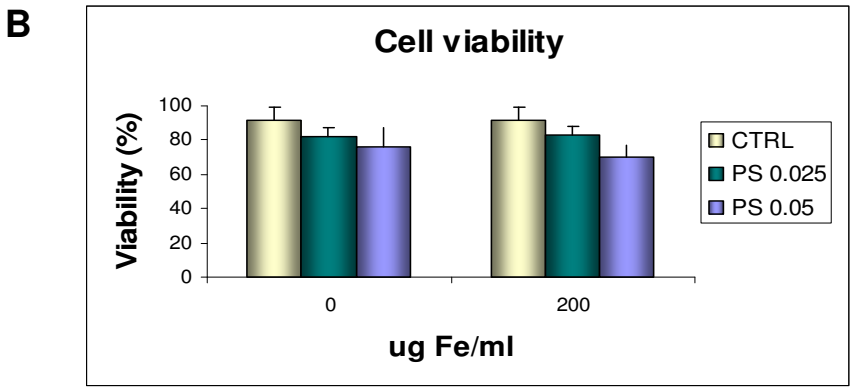

Graph 2. *Set up of PS concentration. The percentage of Iron-positive cells increased in proportion to the PS content in the medium (A). Higher amount of PS (Fe/PS 1:0.05 ratio) enhanced the percentage of labelled cells (99%) compared to Fe/PS 1:0.025 ratio (94,5%) (P<0.001) (A) and did not significantly influence cell viability (B) compared with the respective controls.*

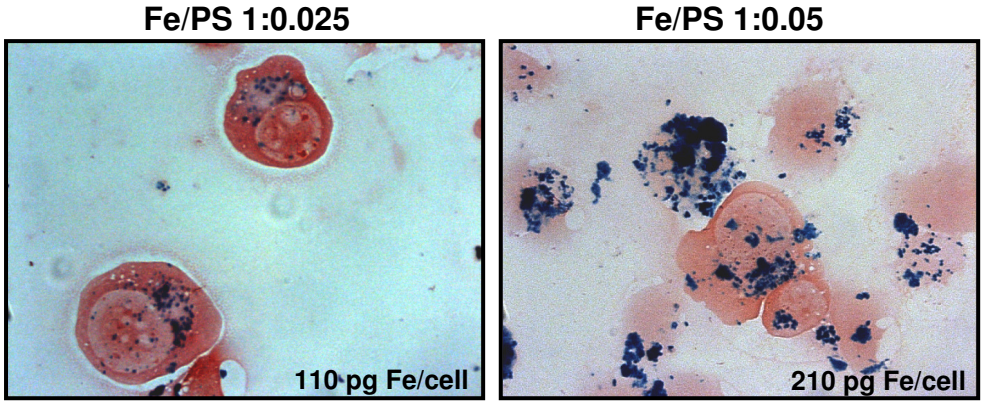

Figure 2. *Set up of PS concentration. Cells incubated with the Fe/PS 1:0.05 ratio show a higher iron content per cell compared with Fe/PS 1:0.025 ratio, as demonstrated by the blue inclusions visible in optic microscopy after PERL's staining, but the cells appear more vacuolized and with an aberrant morphology.*

Therefore, kinetic studies were performed by incubating mNSCs with the MNPs for different incubation time (24-48-72h) to identify the optimal incubation time needed for cell loading. Prussian Blue Staining (Perl's) demonstrated that the iron content/cell increased in proportion to the time of incubation (figure 3, images are only representative of the cell iron load, are not objective index of viability, labelling

efficiency and iron content) and the relassometric results confirmed these data (graph 3).

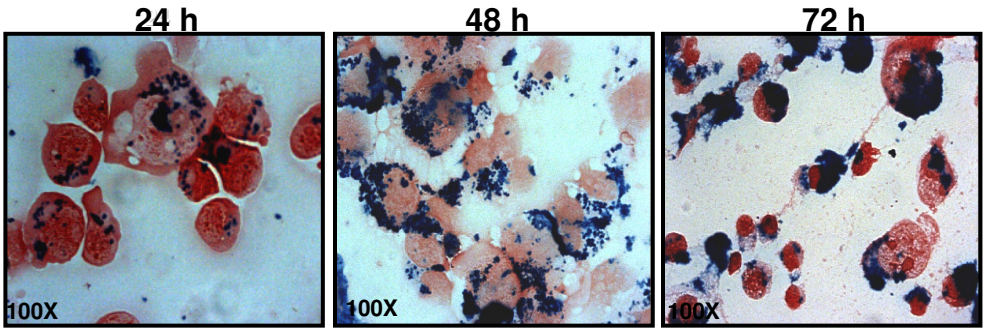

Figure 3. *PERL's Staining of incubation studies (100X o.m.). The images displayed NSCs incubated with 200 µg Fe/ml and PS for different times (24-28 and 72h). An increased iron content per cell was visible in proportion to the incubation time. At 48 and 72h of incubation, NSCs were characterized by cell vacuolization and an aberrant morphology.*

Longer incubation times (48h and 72h), even if increased the iron internalization and the iron content per cell, resulted in marked toxicity and aberrant morphology as demonstrated by the Perl's staining (figure 3). Furthermore the labelling efficiency did not increase in a statistically significant way.

A

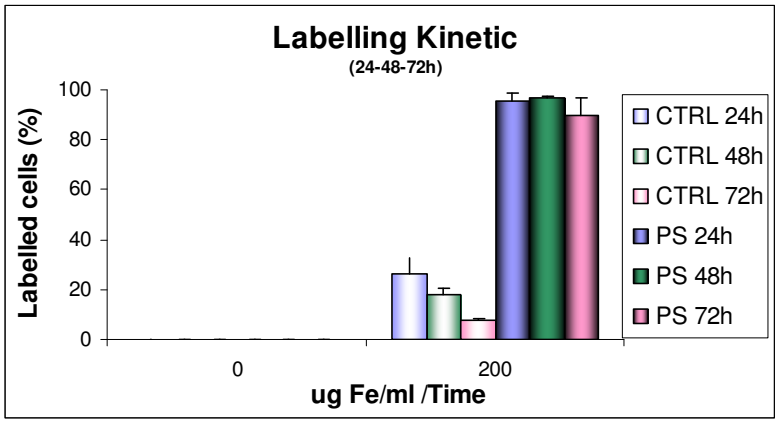

B

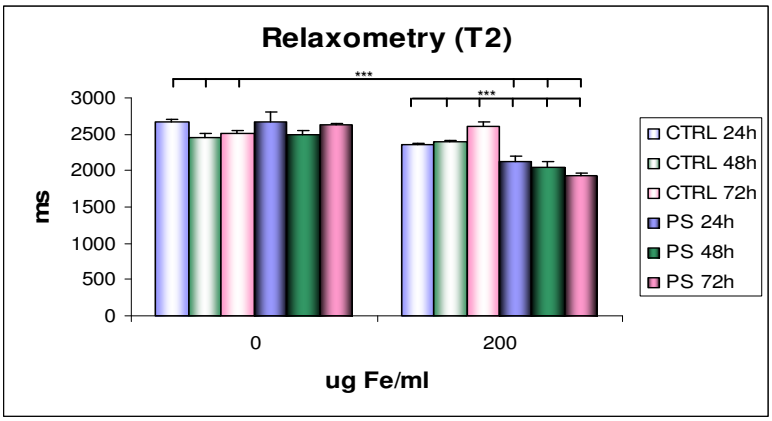

Graph 3. *Labelling kinetic studies. The percentage of Iron-positive cells did not increase in proportion to the incubation time of NSCs with the labelled medium (A). As resulted by the relaxometric assay, T2 decreased in proportion to the incubation time (P<0.001) probably due to the increase of iron content per cell(B).*

The 24 hours of incubation appeared to produce an optimal labelling, also in relation to viability: as a matter of fact, a time of incubation longer than 24 hours resulted in a significant decrease in viability (Data not shown).

1.2. Evaluation of labelled NSC features

After the labelling protocol set up and before proceeding with the *in vivo* experiments, it was demonstrated that labelling NSCs is feasible and does not impair cell viability and biological characteristic *in vitro*. In particular was evaluated the maintenance of the phenotypic and functional features such as the maintenance of the expression of typical neural stem cell marker, of the self-renewal capability and the maintenance of the differentiation ability demonstrating the inertness of SPIOs and lentiviral infection on neural stem cells.

1.2.1. Stem cells features maintenance

Initially, it was analyzed the effect of NSC labelling with SPIOs, regarding cell proliferation capability, by demonstrating the maintenance of the ability to form new neurospheres.
In particular, NSCs washed and replated after the labelling with Endorem® (200 µg Fe/ml with PS ratio 1:0.025 for 24h of incubation) maintained the capability to form new floating neurospheres, as can be seen in the optical microscopy images (figure 4), demonstrating the maintenance of self-renewal capability. In fact, neurospheres were visible since 5 days after SPIO-labelled cell replating compared to the control non labelled cells.

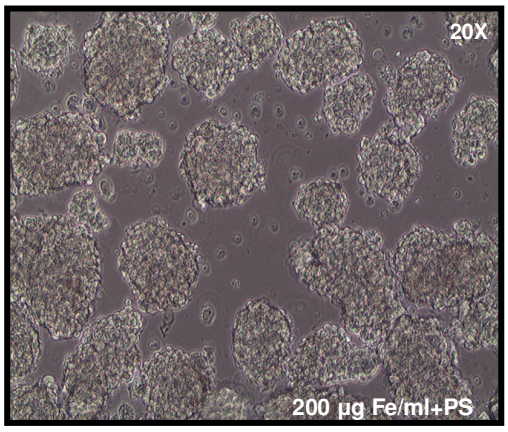

Figure 4. *Optical Mycroscopy of NSCs. NSCs labelled directly with Endorem® maintained the capability to form new neurospheres, as displayed in the figure A (after 5 day of culture) if replated soon after labelling, demonstrating their maintenance of the self-renewal capability.*

Furthermore, labelling of NSCs with Endorem® did not affect expression of major antigens of immature neural stem cells (such as nestin).
In fact, as displayed by immune-fluorescence (figure 5), labelled NSCs maintained their ability to express nestin (green).

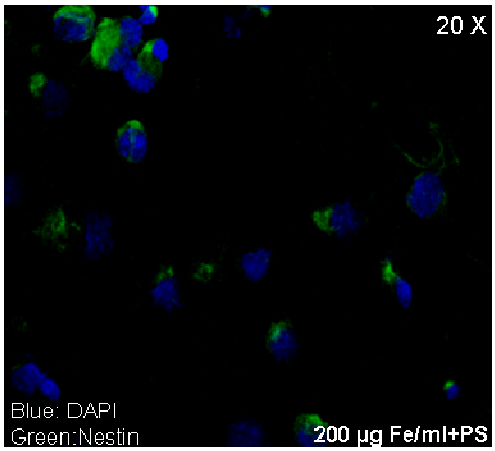

Figure 5. *NSCs labelled directly with SPIOs maintained the expression of nestin (green), typical neural stem cell marker, as displayed in the figure confirming the maintenance of staminality. Nuclei were stained as internal control (DAPI, blue) (20X magnification).*

1.2.2. Cell differentiation

In order to establish if labelling procedures could influence proliferation ability of NSCs, the cells were induced to differentiate and successively were analyzed by immune-fluorescence for GFAP (marker of astrocytes), Gal-C (marker of oligoderocytes) and β-tubulin III (neuronal marker) expression.
Figure 12 demonstrates that NSCs, replated on matrigel immediately after their labelling with SPIOs (200 µg Fe/ml and PS for 24h) and deprived of mitogenic factors, maintained their ability to differentiate in neurons (figure 12A), astrocytes (figure 12B) and oligodendrocytes (figure 12C).
Since the labelling efficiency was of 94,5%, the majority of differentiated cells contained the iron nanoparticles, as demonstrated by Perl's staining (figure 12D) of the same cells before the differentiation induction, and this confirmed that the labelling procedure did not inhibit cell differentiation.

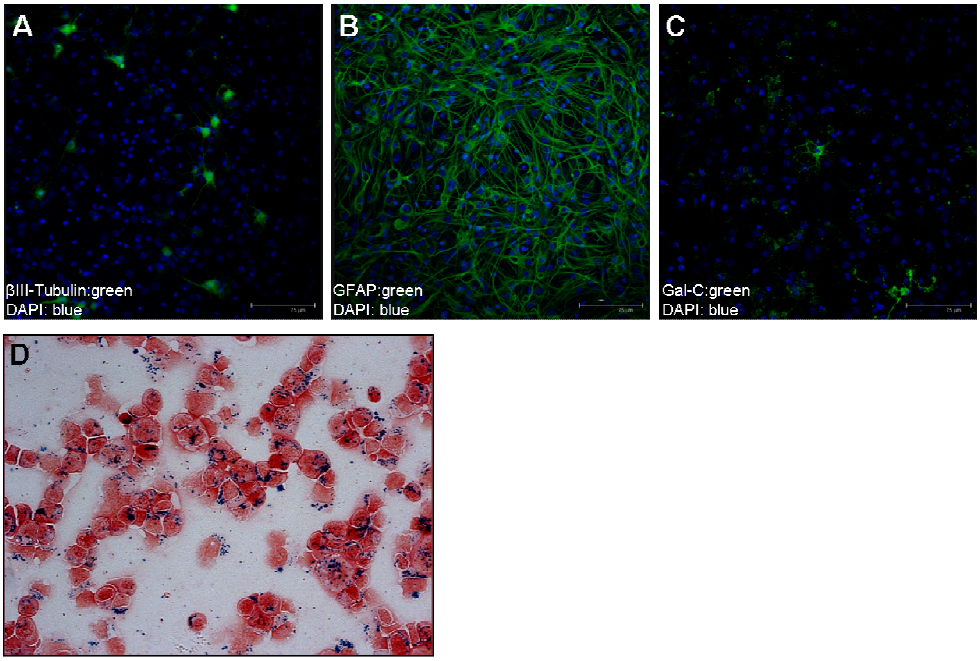

Figure 6. *Immune-fluorescence assay on differentiated SPIO-labelled NSCs. NSCs replated on matrigel immediatly after their labelling with SPIOs (200 µg Fe/ml and PS ratio Fe/PS 1:0,025) for 24h, maintained the ability to differentiate in neurons (A) (Anti- β-tubulin III Antibody, green), in astrocytes (B) (anti-GFAP Antibody, green) and in oligodendrocytes (C) (Anti-Gal-C Antibody, green). Nuclei were counterstained with DAPI (blue).*
The optical image (D), displayed the Perl's staining of the same labelled NSCs before the induction to differentiate (40X o.m.).

1.3. In vivo MRI

Having established a protocol allowing efficient labelling of mNSCs (in terms of number of labelled cells and intensity of labelling) using SPIOs without an overall short-term or delayed toxicity and functional cell impairment, It was assessed whether SPIO-labelled cells could be visualized by MRI after their transplantation into animal models of traumatic spinal cord injury.
For this intent $1,5x10^5$ labelled NSCs were intramedullary injected and followed by MRI. Initially two conventional MRI sequences were tested: the spin-echo sequences and the gradient-echo sequences. While the spin-echo sequences permitted to obtain images for morphological analysis of the site of injury, the gradient-echo permitted to enhance the iron signal, with a decreasing on morphology definition so, to obtain complete information, all these sequences were required.
Preliminary results, demonstrated the possibility to detect SPIO-labelled NSCs by MRI techniques as shown in figure 7. In fact a hypointense signal due to iron presence within the injected cells was detectable in the site of injury after their intra-medullary injection and the signal was persistent also two months after the transplant.

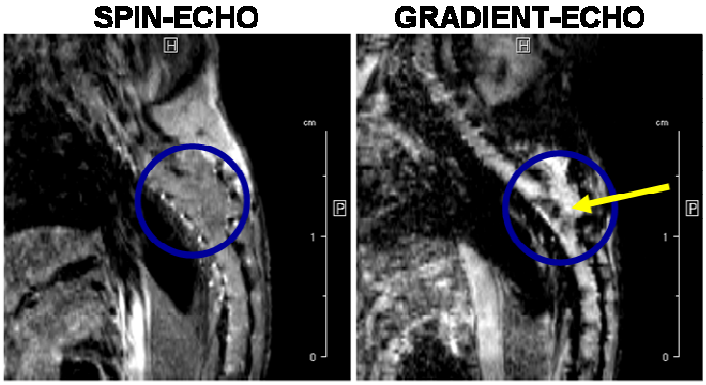

Figure 7. *In vivo MR imaging (Spin-Echo, MSME and Gradient-Echo, FLASH, sequences) sensibility tests on injured spinal cord mice. The spin-echo sequences furnished only morphological informations but were not able to detect the labelled cells. SPIO-labelled cells were detectable by the use of gradient-echo sequences, 7 days after the cell injection into the spinal cord. The yellow arrows identified the presence of SPIO-labelled cells.*

After two months mice were sacrificed and the spinal cords were collected and sliced for the histological analysis. Perl's staining on corresponding serial sagittal sections cut from the same spinal cord after the MRI procedure confirmed the presence of iron-labelled cells into the site of injury (figure 8).

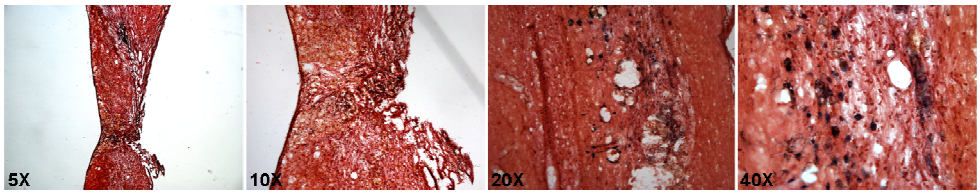

Figure 8. *Histological analysis of collected injured spinal cord of positive control mice i.s. injected with SPIO labelled cells, after the MRI (Gradient-echo sequences). The Prussian blue staining confirmed the presence of SPIO-labelled cells into the lesion site.*

Gradient-echo sequences, therefore was initially used to visualize the fate of NSCs after their therapeutic administration ($1x10^6$ labelled cells injected) into the tail vein for the treatment of traumatic spinal cord injury.
The figure 9 shows the presence of an hypointense signal into the site of injury since day 21 after their injection and the signal was persistent also two month after the transplant (not shown).

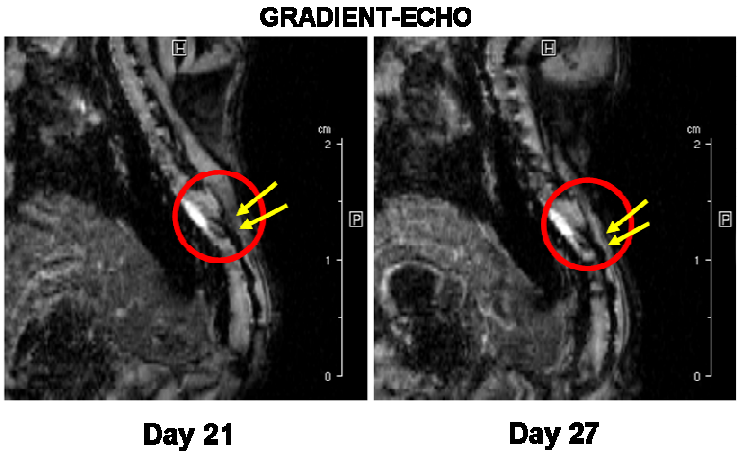

Figure 9. *In vivo MR imaging (Gradient-Echo, FLASH, sequences) of SPIO-labelled NSCs injected intravenously in an experimental model of traumatic spinal cord injury. Sagittal MRI images of the spinal cord at 21 and 27 days post cell injection showed the presence of T2 hyporintense signal in the dorsal portion of the spinal cord (yellow arrows).*

After two month mice were sacrificed and the spinal cord was extracted and analyzed by *ex vivo* MRI to confirm that the signal was not due to any artefacts.
MRI on isolated spinal cord, acquired both in axial and sagittal plan, confirmed the presence of typical regions of hypointense signal attributable to SPIO-labelled cells

(figure 10), as further demonstrated by Perl's staining on corresponding serial sagittal sections cut from the same spinal cord after the MRI procedure (figure 11).

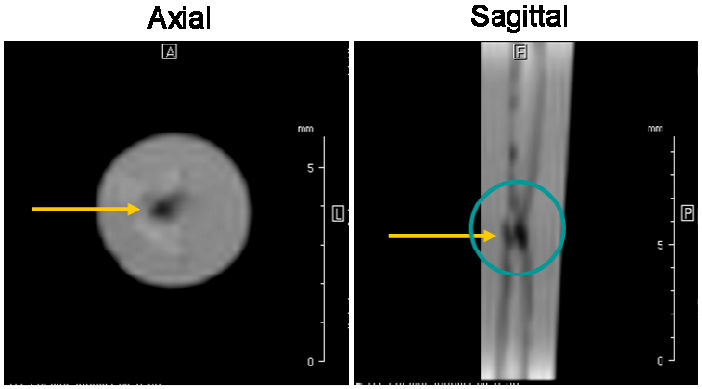

***Figure 10**. Ex vivo MR imaging of the injured spinal cord, axial (sx) and sagittal (dx) sections.*

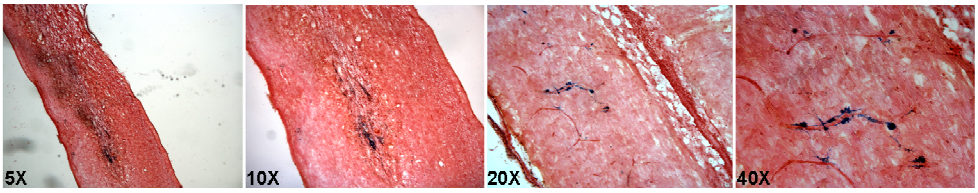

***Figure 11**. Histological analysis of collected injured spinal cord after the MRI (Gradient-echo sequences). The Prussian blue staining confirmed the presence of SPIO-labelled cells into the lesion site.*

For the following *in vivo* NSC tracking experiments, RARE sequences, strongly weighted in T2, were tested in order to obtain an image with a clearly visible iron signal in combination with a good morphological resolution.
The RARE images were demonstrated to be more sensitive in revealing the presence of the SPIO-labelled cells. In fact, an hypointense signal was detectable since 7 day after the cell administration into the tail vein both in sagittal plan (figure 12) and coronal plan (figure 13).

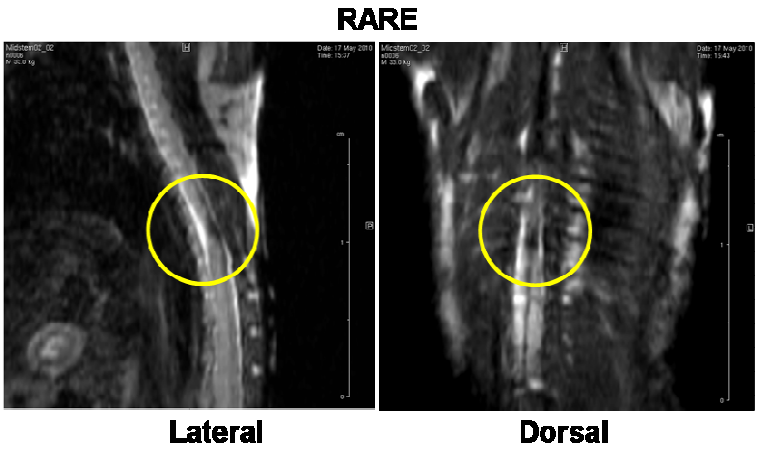

***Figure 12**. In vivo MR imaging (RARE sequences) of SPIO-labelled NSCs injected intravenously in experimental model of traumatic spinal cord injury. Sagittal and dorsal MRI images of the spinal cord just at 7 days post cell injection showed the presence of T2 hyporintense signal in the dorsal portion of the spinal cord (yellow circles).*

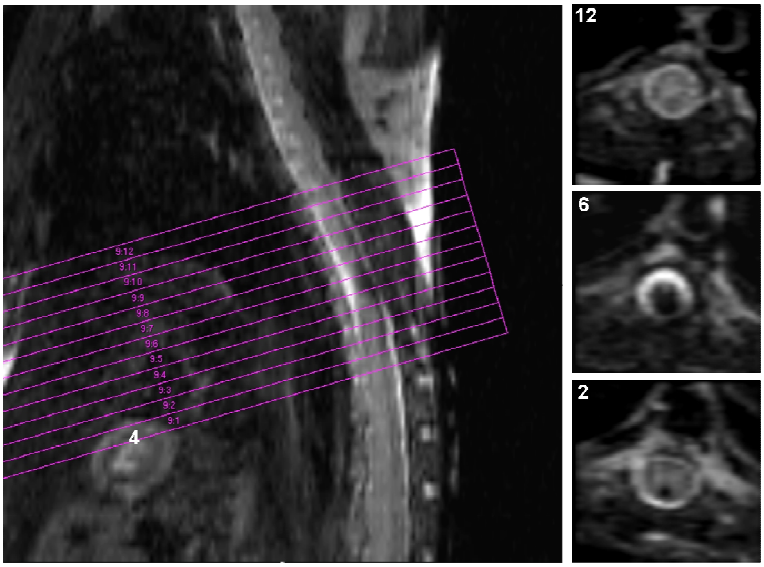

***Figure 13**. Magnification of an in vivo MR image (RARE sequences) of the injured spinal cord 7 day after labelled cell injection. The sagittal figure on the left showed a red grid dividing into 12 axial slices the region containing the hypointense signal. The figures on the right showed the most representative axial MR image acquired at the level of the slice 12, 6 and 2 respectively. Also coronal images confirmed the presence of T2 hypointense signal in the dorsal portion of the spinal cord.*

After one week mice were sacrificed and the spinal cord was extracted and analyzed by *ex vivo* MRI.
The presence of typical regions of hypointense signal was revealed also by *ex vivo* MRI on isolated spinal cord, acquired both in axial and sagittal plan, demonstrating that the signal was not due to any artefacts (figure 14).

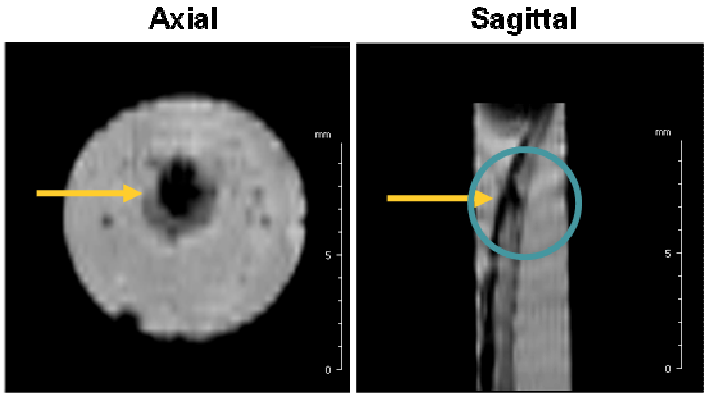

***Figure 14**. Ex vivo MR imaging of the injured spinal cord at one week after the SPIO-labelled cells injection, axial (sx) and sagittal (dx) sections.*

The histological analysis on corresponding serial sagittal sections cut from the same spinal cord after the *ex vivo* MRI procedure, confirmed the presence of SPIO-labelled cells in the dorsal portion of the spinal cord (on the left), in proximity of the lesion site.

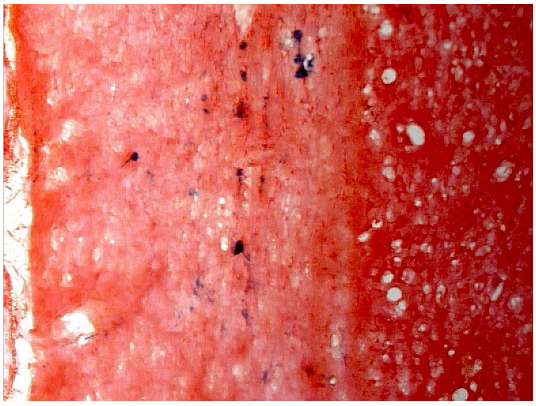

***Figure 15.** Histological analysis of collected injured spinal cord after the MRI (RARE sequences). The Prussian blue staining confirmed the presence of SPIO-labelled cells in the dorsal portion of the spinal cord (on the left), into the lesion site (20X o.m.).*

The 40X o.m. permitted to highlight that the labelled cells have emitted some protrusions, probably due to their effective differentiation once established to the lesion site (figure 16 A). Furthermore a lot of cells are detectable in proximity of blood vessels demonstrating their distribution trough the blood flow (figure 16 B).

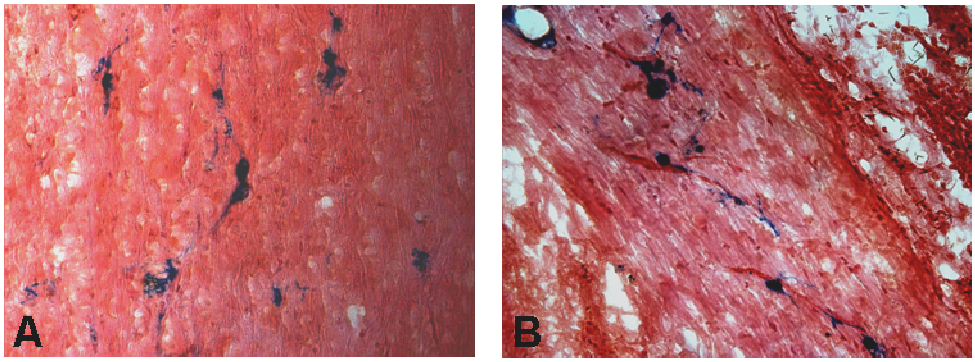

Figure 16. *Histological analysis of collected injured spinal cord after the MRI (RARE sequences). The 40X o.m. of the Prussian blue stained sections permitted to highlight the protrusions emitted by the SPIO-labelled cells localized into the site of injury.*

2. DIRECT LABELLING FOR NUCLEAR IMAGING

2.1. NSC direct labelling with ^{111}In-oxine

Since it was difficult to study the early phases of the NSC distribution by MRI, mNSC were labelled with ^{111}In-oxine .^{111}Indium is indeed characterized by a γ-decay that emits two photons, having a 173 and 240 keV energy respectively and a half life of 69 hours. Imaging can be performed also 24 and 48 hours after injection, with good resolution. The radioisotope is linked with 8-hydrossichinoline (oxine), a chelating agent by which it forms a lipophilic complex that is able to penetrate the cell membrane. When the complex reaches the cytoplasm, it dissociates, leaving ^{111}Indium firmly linked to nuclear and cytoplasmic proteins with a stable interaction that lasts for more than 24 hours.
In particular, several incubation time were tested in order to increase the labelling efficiency. The cells were initially incubated with ^{111}In-oxine for 15 minutes as described by De Vries et al. [70] with 60% of efficiency. A higher incubation time was tested in order to further increase the labelling efficiency. Labelling efficiency of mNSCs incubated for 30 minutes with ^{111}In-oxine was of 99,4% .
NSC viability was not affected by the labelling procedures (data not shown).
Therefore, the final results demonstrated that cell labelling with ^{111}In-oxine can be used for *in vivo* imaging of NSC migration by means of nuclear techniques and by exploiting the higher sensitivity of SPET with respect to MRI.

2.2. In vivo planar SPET imaging

One million of NSCs were labelled with 60 μCi of ^{111}In-oxine and injected in the tail vein of CD1 spinal cord inured mice (for further details about animal models, see Materials and Methods, paragraph 1.5.1).
The pictures were taken with a digital camera separated from the γ-camera and were overlaid with the photon emission map. This shrewdness permitted to overcome the intrinsic limit of the nuclear based imaging techniques: the lack of anatomical information. SPET images fail to localize exactly the source of the emitted photon, and indeed the emission map results to be only a bi-dimensional projection of a three-dimensional mouse model.
The image, shown in figure 20, was taken 30 min after injection demonstrates that, in the early phases post-injection, stem cells can be detected within the filter organs of the animals (lung, liver and kidneys). As a confirmation, acquiring the image 1 h later, no more detectable signal was visible in the same area (data not shown).

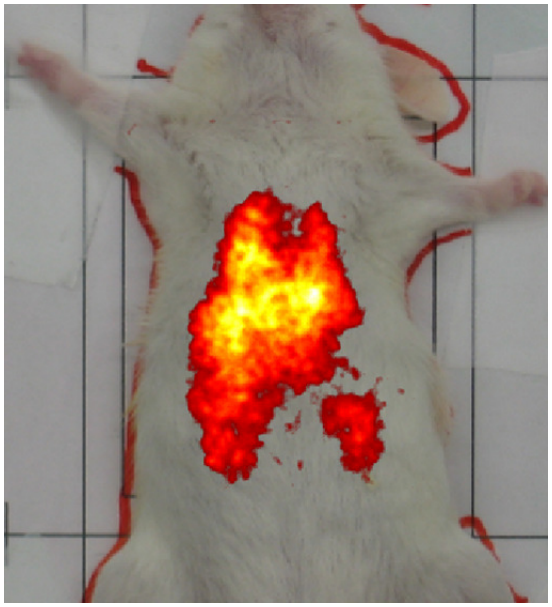

Figure 17. *Nuclear imaging of NSCs labelled with ^{111}Indium-oxine. Labelled cells were visible in the filter organs (lungs, liver and kidneys) 30 minutes after their injection into the tail vein.*

The data obtained demonstrated the efficient cell distribution through the blood flow (figure 17). Furthermore this technique revealed the great sensitivity of the prototypical sensor we used that was provided by the Politecnico of Milan (Professor Carlo Fiorini).

3. INDIRECT LABELLING FOR BLI

3.1. Lentiviral production and NSCs infection

Helper Lentiviral vectors of third generation (pMD2g-VSV-G, pMDLg-RRE and pRSV-Rev) useful for the viral production for stem cells infection were offered by Dr. Rivella's Laboratory (Cornell University, New York) and were amplified in DH-5alpha E.Coli (NEB), purified by an endotoxin free DNA extraction kit (Invitrogen) and diluted in TE buffer.
The pCLL.PGK.Luc.WPRE (PLW) plasmid, containing the Luciferase gene controlled by the constitutive promoter PGK, was previously cloned in our laboratory (figure 18).

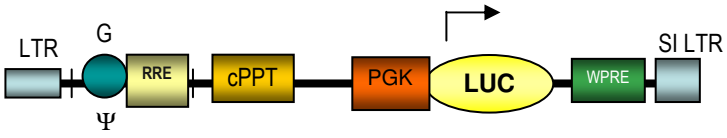

Figure 18 . *Schematic reproduction of the lentiviral vector PLW.*

The lentiviral vectors were produced as described by Tom Dull et al. [132]
The vector copy number (VCN) viral titer ($7{,}62 \times 10^5$ TU/ml) was calculated on HeLa cell lines through the amplification of the lentiviral specific WPRE region from genomic DNA of Hela infected cells by the use of the Real-Time PCR technique [133] and its comparison to a curve of DNA standards with known VCN.
NSCs were infected with 5 MOI of PLW lentiviral vectors and polybrene (8 µg/ml) and the luciferase expression was evaluated after the cell lysis, by CCD camera using a luciferase assay (Promega) and the data obtained, as counts (i.e. photon emitted), were normalized on the total protein concentration. Luciferase expression obtained was around $4{,}24 \times 10^8$ counts/mg of protein and the luminescence was clearly visible by CCD camera (figure 19).

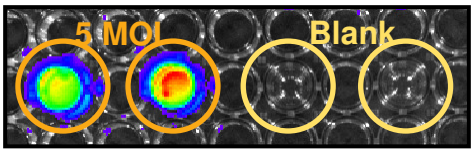

Figure 19. *In vitro bioluminescence assay on NSCs infected with 5 MOI of the lentiviral vector PLW.*

3.2. Evaluation of labelled NSC features

To confirm that lentiviral transduction had not altered the properties of NSCs, immune-fluorescence and optical microscopy were performed as previously described.
In particular, NSCs washed and replated after the infection with PLW vector (5 MOI), maintained the capability to form new floating neurospheres, as shown by optical microscopy images (figure 20), demonstrating the maintenance of self-renewal capability, even if the lentiviral infection with PLW seemed to slow the proliferation rate since the neurospheres were visible only 7 days after cell plating compared to the 5 days of non infected control cells. This is probably due to the integration of PLW DNA in the genome of the NSCs that interfere with the DNA replication.

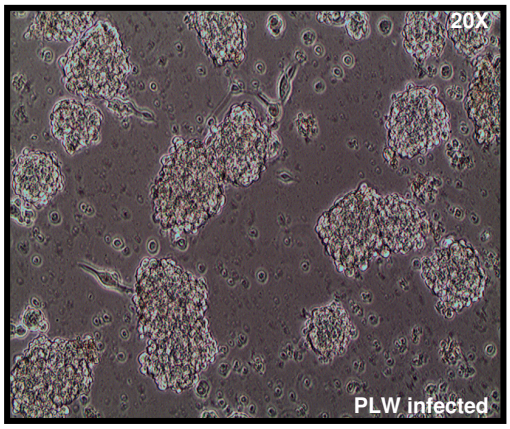

Figure 20. *Optical Mycroscopy of NSCs. NSCs labelled indirectly with PLW maintain the capability to form new neurospheres, as shown in the figure (after 7 day of colture) if replated soon after labelling, demonstrating their maintenance of the self-renewal capability.*

Furthermore, labelling of NSCs with PLW did not affect nestin expression (antigens of immature neural stem cells).
In fact, as shown by immune-fluorescence (figure 21), infected NSCs maintained their ability to express nestin (green).

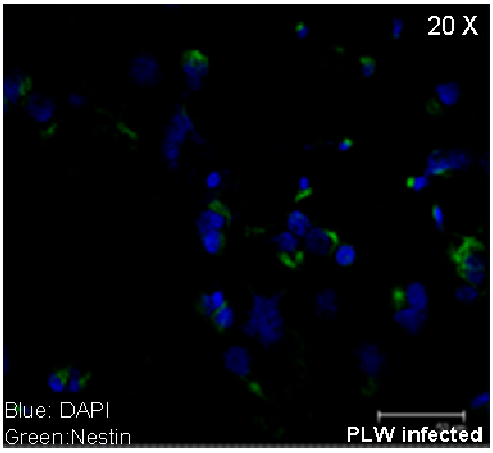

Figure 21. *NSCs infected with PLW vector maintain the expression of nestin (green), typical neural stem cell marker, as shown in the figure confirming the maintenance of staminality. Nuclei were stained as internal control (DAPI, blue). (20X magnification).*

3.3. In vivo Bioluminescence imaging (BLI)

In the research of cell-therapy, the accuracy of transplantation is a fundamental premise. In this study the BLI was used as a tool helping the evaluation of the transplant success.

One of the advantages of the BLI is the capability to detect only viable grafted cells since the Luciferase reaction is dependent upon oxygen and ATP, furthermore the BLI permits to obtain data easily and faster compared to other imaging techniques such as MRI. One of the limits of BLI is its lower anatomical resolution.

To examine the engrafted cells viability once arrived in the lesion site, 1×10^6 of infected NSCs were injected into the tail vein of CD1 spinal cord injured mice.

The accuracy of transplantation was confirmed immediately after transplantation using BLI. The day after the cell transplantation, D-luciferine was intraperitoneally administrated (80 mg/kg body weight). Five minutes after D-luciferin injection, images acquisition started (Xenogen-IVIS Lumina). In the set up experiments, serial images were acquired from 5 to 35 min after D-luciferin administration in order to study the kinetic of distribution and metabolism of the luciferine. The luminescence peak was found between 15 and 25 minutes after D-luciferin injection (data not shown). So this time was chosen as for animal acquisition.

Mice injected with lentivirally infected mNSCs were acquired every day, for the first week after the transplant and then once a week for a month.

NSCs, infected with the viral vector PLW, and intramedullary injected, produced a very high signal localized in the site of injection. On the other hand, intravenously injected cells were detectable since one week after the transplant within the lesion

of injured mice (figure 22) demonstrating the presence of viable cells and confirming MRI data, furthermore the signal was detectable also 6 weeks after the transplant demonstrating cell survival into the lesion site.

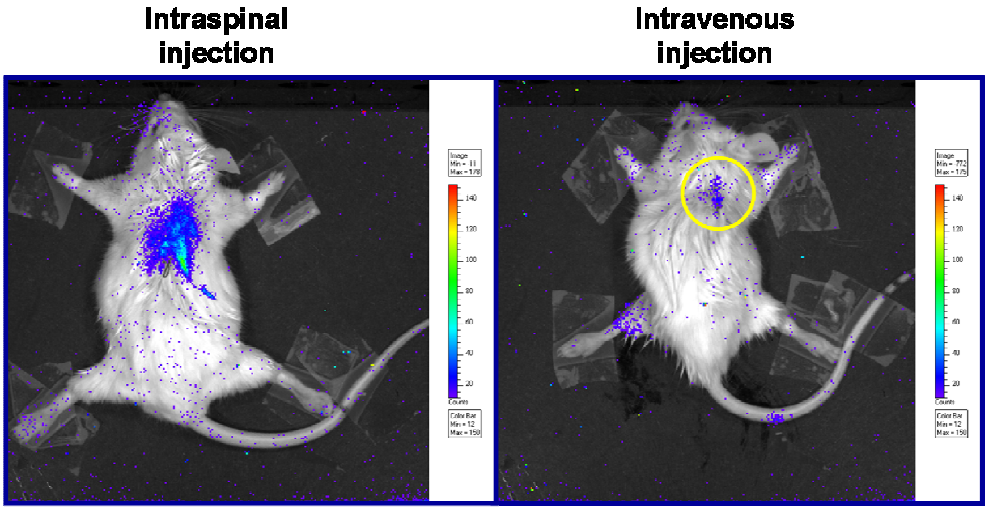

Figure 22. *In vivo bioluminescence image of NSCs infected with pCLL.PGK.Luc.WPRE (PLW) vector. 1x10^6 infected cells were injected into the tail vein of injured mice (figure on the right). All the mice, used as internal positive controls, were stereotactically injected, with 1,5x10^5 infected cells, directly into the injured spinal cord (figure on the left). Luciferase activity was detectable in the lesion site, 1 week after their injection into the tail vein.*

Conclusions

Cell-based therapy has been announced as being a promising, novel therapeutic strategy for recovery from various diseases. In particular, two big branches can be identified: the stem cell-mediated therapy and the immunotherapy.
The use of stem cells in cell-mediated therapy is of considerable interest for studying the regeneration and reconstitution of tissues in damages caused by trauma as well as in inflammatory and degenerative diseases.
More in particular, NSC-based therapeutic approaches have recently become the subject of study due to their huge potential for application in both cell-based and gene therapy of CNS disorders.
These cells, originated from the SVZ of CD1 mice, are able to differentiate into many neuronal cell types *in vitro,* such as neurons, astrocytes an oligodendrocytes and to restore structure and function of the nervous system in diseased animal models.
Preliminary data obtained with this type of treatment have demonstrated its efficacy as proved by motor recovery assessed by motor behavioural test.
Once the efficacy and safety of these novel therapeutic approaches will be fully demonstrated in preclinical models of CNS disorders, they will rapidly move towards clinical testing. Furthermore, controversial, issues remain unresolved with respect to the molecular mechanisms underlying cell mediated treatments. To this purpose, molecular and cellular imaging retains a fundamental role not only in preclinical studies, but also in clinical practice, since the possibility to accurately evaluate at the early stage of the treatment the precise delivery and/or homing of cells to target tissues is crucial for the clinical success of such applications.
Indeed, non-invasive, imaging-based methods have been recently developed to *in vivo* follow transplanted cells that had been previously labelled with different protocols. These imaging techniques allow to track the localization, distribution and migration of administered cells once introduced into the living model. The ability to track the location of cells will allow several questions to be answered: 1) if injected through the vein, where do these cells go? 2) if implanted, do cells remain in the site of implantation or do they migrate to the target tissue? 3) once arrived to the target organ or tissue, how do they interact with their microenvironment or with the resident cells? 4) how long can injected cells survive? 5) can transplanted cells differentiate into the desired tissues?
Furthermore, the use of imaging techniques permits to introduce early and intermediate check points of cell-mediated treatment efficacy being previously evaluated only by the final functional recovery and provides direct and clear parameters able to depict cell behavior after injection.
In general, successful *in vivo* imaging requires a cell to be labelled, so as to provide sufficient contrast for detection by imaging instruments. Cell labelling can be performed by following two different strategies: direct and indirect protocols. The direct labelling methodology is based on the use of contrast agents, such as paramagnetic nanoparticles and fluorescent or radioactive molecules that a-specifically enter the cell membrane and label cells, while the indirect strategy exploits the genetic engineering of cells through introducing reporter genes coding for reporter proteins within the host genome. The use of contrast agents permits to label the cells easily, and so to perform different types of imaging. The imaging modalities available are indeed very different from each other in terms of spatial resolution, sensitivity, type of information provided (anatomical or functional information), depth of tissue penetration and the type and amount of required

probe. For these reasons, very often a multimodal approach is needed to overcome the intrinsic limitations of each single imaging technique and provide more informative data.
Our studies demonstrated that direct labelling procedures with paramagnetic nanoparticles of NSCs is efficient and safe. In particular, we used SPIOs (Endorem®) as a contrast agents and protamine sulphate (PS), being both FDA approved for clinical use. Dose-response and incubation time studies were performed so that the specific optimal dose and time of incubation should be identified. In particular, for NSCs, the best labelling condition is the incubation with 200 µg of iron/ml of culture medium for 24 hours in presence of PS (ratio Fe/PS 1:0,025) .
Once the best labelling protocols were identified, we demonstrated that after the labelling, there was no alteration of the NSC phenotype or its behaviour in different conditions and that an intracellular iron level of 110 pg/cell resulted to be able to produce a good signal in MRI.
Another problem in the setting up of a cell imaging protocol is the need to visualize even small amounts of cells in the target organ. Our data demonstrated that MRI was able to show NSC accumulation within the target tissue with a good sensitivity even if MRI technique for its complexity and the long time of acquisition do not permit to follow early phases distribution. Furthermore MRI needed an expert technician for images acquiring and reading.
A partial solution to this problem can be found by using a-specific long term labels such as radionuclides, whose half life were consistent with the cell cycle duration and with the kinetic of the process to be studied in order to have enough time to reveal the desired check point. This is the case of the NSCs labelled with ^{111}In-Oxine that, having a half time of 69 hours, permits to follow early phase distribution from the site of injection.
Nuclear imaging demonstrated that the prototypical sensor (provided by the Politecnico of Milan, Professor Carlo Fiorini) has a good sensitivity: it is able to image circulating NSCs, even though only in a bi-dimensional perspective, and to integrate the information deriving from MRI studies, so that the combination of MRI and scintigraphy permits to merge the special high resolution of MRI with the high sensitivity and the whole body images of scintigraphy thus allowing to partially overcome the disadvantages of each single technique.
As far as it is concerned, NSC imaging by MRI provided good anatomical information that permitted to localize accurately the presence of iron, due to injected NSC within the spinal cord.
The setting up of an imaging protocol to visualize proliferating cells has to take into account the dilution of the label through cell generations occurring in direct labelling strategies and the fast decay of radioactive signal that limits the possibility to track cells to short periods of time. The unique global solution to this problem is the use of reporter genes for the engineering of the cells that have to be studied *in vivo* in order to pass the biomarker, reporter protein, from a cell unaltered over time to the cell litters.
In our study, NSCs were engineered to express the reporter gene luciferase under the control of a constitutive promoter (PGK). The great advantages of the BLI is that permits to acquire only viable cells because the reaction needs of oxygens and ATP, provides informations for long times only requiring the addiction of the substrate of the enzyme (luciferine) and lacks background noise.

Furthermore our data demonstrated the feasibility and sensitivity of BLI in revealing luminescent cell accumulation even if this technique lacks of anatomical resolution and the labelling process is quite elaborated.
Furthermore cell engineering is not always possible because of the danger in producing cell genetic modifications or because of the possibility to evoke an immune response against the reporter protein when this is reintroduced into the living model.
In this context, indirect cell labelling provide the means for the long term study of parameters describing the efficacy of a cell-mediated treatment permitting the identification of important early intermediate points fundamental for the estimation of treatment efficacy that can be studied easier with direct labelling strategies. The identification and the exploiting of these intermediate points could change also the clinical approach in the evaluation of treatment efficacy not basing only on the final long term recovery of function or tumour shrinkage but to the *in vivo* study of their molecular and cellular bases. In this scenario, the treatment scheduling could potentially be improved, making it possible to keep each phase of the treatment under observation.

The data reported in this thesis permit us to validate our labelling protocols as efficient strategies to follow *in vivo* the cells that are systemically administered to mouse models. They thus demonstrate the value of our models for the *in vivo* study of important variables for the evaluation of the efficacy of a cell-mediated therapy: first of all the cell ability to *in vivo* migrate and localize into the target, that is the first step of an efficient therapeutic protocol.
However, to evaluate the cell-mediated treatment efficacy it is necessary to perform further experiments in order to correlate the *in vivo* evaluated cell localization and differentiation with the restoration of spinal cord injury.
Furthermore all data obtained by imaging methods will be compared and correlated with data on motor recovery by different behavioural tests (BMS scale).
The route of administration, the scheduling of treatment and the potential use of adjuvant pharmacological treatments will be evaluated. Genetic engineering of NSCs will be carried out to make them able to express a reporter gene (Luciferase or Katushka) under control of a neuron specific promoter- to *in vivo* visualize their neuronal differentiation.
The anatomical information provided by MRI will permit to have a global view of the system and will thus allow the evaluation of specific parameters linked to the cell-mediated treatment as the spinal cord morphology, and will at the same time highlight the cell population in study and its effect on the organism.

Appendix

1. PRINCIPLES OF NMR

Nuclear Magnetic Resonance (NMR) deals with the interaction between an oscillating magnetic field and the net magnetization of a sample, which originates from its constituent nuclei in the presence of a static magnetic field .
The nuclei at the centre of atoms are electrically charged for the presence of protons. In addition to this property many, but not all, atomic nuclei (isotopes or nuclides) possess an angular momentum or spin I (figure 1), which is caused by the rotation of nucleus about its axis.

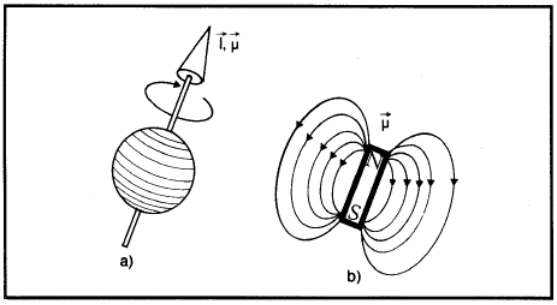

Figure 1: *representation of an atomic nucleus having a nuclear spin*

Principally, the nuclear spin follows the rules of quantum mechanics. A rotating charge (circular current) induces a magnetic dipole (μ) (Figure 1); thus, all atomic nuclei with spin I behave as tiny compass needles. As long as no external magnetic fields exist these "compass needles" are statistically oriented in all possible spatial directions (figure 2a).

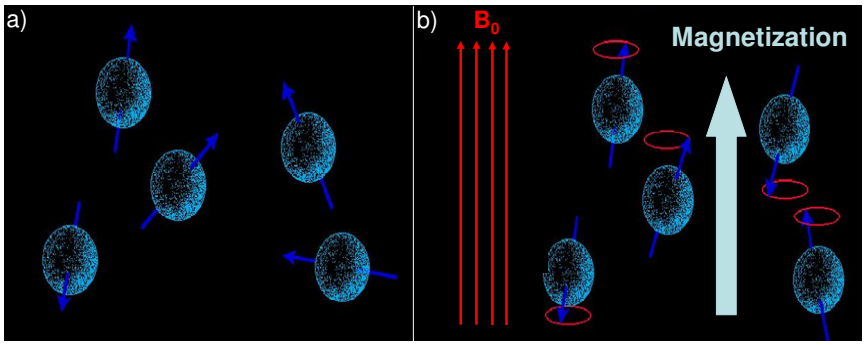

Figure 2: *orientation of the nuclear magnetic dipole moment.*

However, if we subject a substance to a magnetic field (B_0), the magnetic dipoles strive to align themselves along the direction of the magnetic field, and the magnetization precesses along a conical path around the B_0 field direction (figure 2b). According to quantum mechanics, an angular momentum can have only a restricted number of alignments with respect to the magnetic field. Hence, the

angular momentum of, for example, the hydrogen nucleus (proton, ^1H), which has spin I = 1/2, can have only two (2I + 1) possible stable orientations relative to the magnetic field B_0: one parallel to the magnetic field, the other anti-parallel to it (figure 3).

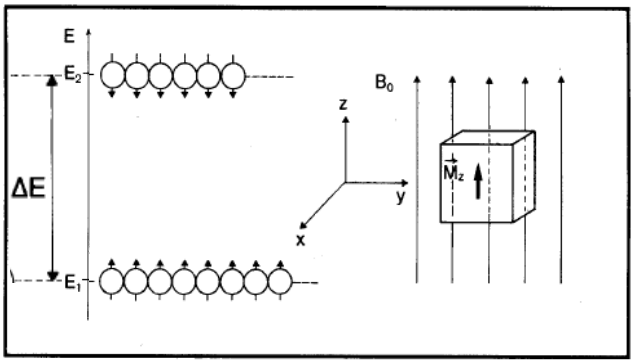

Figure 3: *Representation of energy level differences during spin alignment and representation of the build-up of macroscopic magnetization M_z of a sample*

The two spin states differ in their energy (figure 3) so that the probability of finding a spin in a certain state is not uniform. A parallel orientation obviously means less energy than an antiparallel direction. The difference in energy ΔE (Figure 3) is proportional to the field strength B_0: this means that doubling the field strength entails a doubling of energy difference . There is in addition a temperature effect: at absolute zero all the nuclear spins are aligned along the field direction, whereas at room temperature the thermal energy works against alignment, i.e. temperature interferes with an ordered arrangement. As a result, the two energy levels are not equally populated and there is a slight predominance of vectors in the parallel configuration, according to the Boltzmann's law distribution. At a typical magnetic field strength at room temperature and in thermal equilibrium, for every one million nuclei at the higher energy level one million and six nuclei would exist at the lower energy level. Consequently, a macroscopic magnetization M_z in the magnetic field results as the sum of all microscopic nuclear magnetic dipole moments (Figure 3) and this magnetization can be detected. The net magnetization lies along the axis of the main magnetic field (in general defined as the z-axis) and is named "Longitudinal Magnetization".

The nuclei of atoms placed in a magnetic field are not exactly aligned along the direction of the lines of force of the field: the magnetic axis of each nucleus tends to be disposed in an oscillating way along the vector of field itself, as with the needle of the compass. This oscillation combines with the motion of spin, giving rise to a complex movement of rotation on a conical surface (Figure 4) having its axis along the direction of stable magnetic field. This movement is called precession of the nuclei, and is similar to the motion of a gyroscope that oscillates on its axis of rotation due to the gravity field of the earth. The speed of precession is proportional to the magnetic field strength and is different for each atom. The precession rate is called Larmor frequency, and, for hydrogen nucleus, is in the range of radiofrequencies (figure 4).

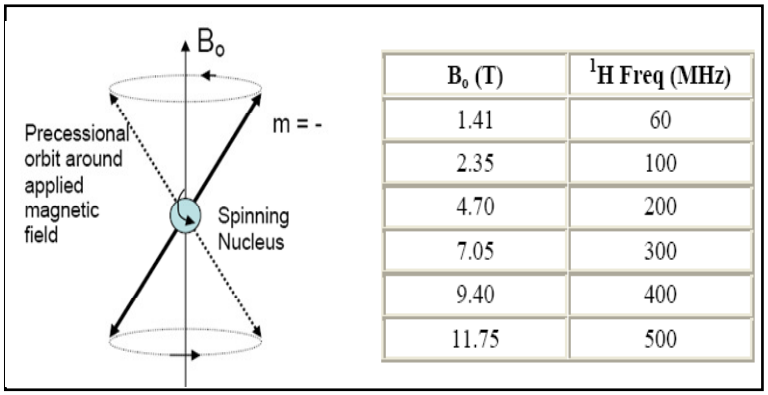

B_0 (T)	^{1}H Freq (MHz)
1.41	60
2.35	100
4.70	200
7.05	300
9.40	400
11.75	500

Figure 4: *schematic representation of precession movement and value of Larmor frequency for different intensity of B_0*

If we irradiate the sample with radio waves (in the MHz frequency range) the proton will absorb the energy and be promoted to the less favourable higher energy state and the precession rate of all nucleus is in the same position of conic surface. This energy absorption is called resonance because the frequency of the applied radiation and the precession coincide or resonate.
The resulting effect of the nucleus in phase concordance is the formation of a new magnetization vector along the xy plane (perpendicular to B_0 vector), named Transverse Magnetization (figure 5a).

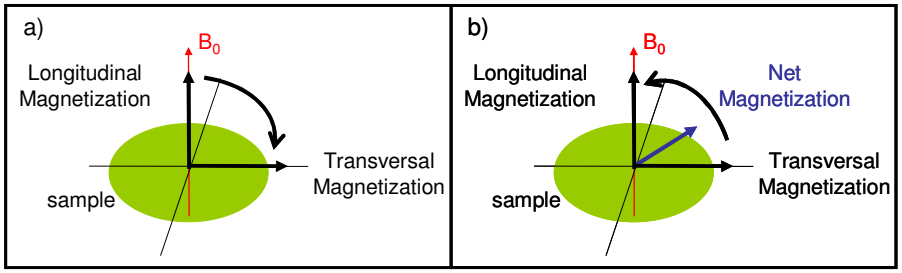

Figure 5: *relative position of longitudinal and transverse magnetization in presence a) or absence b) of a radiofrequency.*

When radiofrequency pulse is removed, nuclei start losing their stored energy, generating radiofrequency waves that can be detected. During this phenomenon, the net magnetization from the xy plane will rotate back until it is aligned again with B_0 (full recovery of longitudinal magnetization)(Figure 5b). At the same time all spins will spread out and loose coherence with each other and the x-y component of the magnetization will gradually disappear.
The recovery of longitudinal magnetization occurs with a time constant T1, referred to as T1 o spin lattice relaxation time: the energy is just handed over to their surroundings, the so-called lattice. The gradual loss of transversal magnetization

occurs with a time constant T2, referred to as T2 or spin-spin relaxation time Each nucleus in fact is influenced by the small magnetic fields from neighbouring nuclei, which are somehow characteristics for a tissue. Since the nuclear spin relaxation processes depend on the existence of molecular motions to generate a randomly varying magnetic field, we can get valuable information about these motions, and therefore about the type of tissue, from the relaxation rates.

1.1. Contrast agents

Magnetic relaxation can be enhanced using contrast agents. In fact spin-lattice relaxation T1 and spin-spin relaxation T2 may be shortened considerably in presence of paramagnetic species. The resulting effect is a change in the MR signal.

Magnetism is a fundamental property of matter. Substances are divided in three classes, according to their magnetic properties: diamagnetic, paramagnetic, and ferromagnetic. Diamagnetic substances do not exhibit magnetic properties Paramagnetic species instead, do not exhibit magnetic properties outside a magnetic field, but when placed in a magnetic field exhibit a slight positive interaction with it. . Paramagnetic species do not retain any magnetization in the absence of an externally applied magnetic field and this is the difference with the ferromagnetic substances

Paramagnetic species are used to generate contrast in NMR and MRI. They have unpaired electrons with associated magnetic fields which are approximately one thousand times stronger than those corresponding to water protons. Such substances therefore interact with water protons exactly as surrounding protons but with much stronger magnetic fields, causing a stronger impact on their relaxation rates.

Some examples are molecular oxygen, stable radicals (i.e. nitroxide radical) or metal ion (i.e. many transition metal ions).

Radicals generally cause damage to the living tissues. Therefore, they are not suitable candidates for medical MRI purposes. The paramagnetic effect of oxygen, although demonstrable, seems too weak for practical applications. Paramagnetic metal ions do show suitable effect which depends on their number of unpaired electrons.

There are many transition and lanthanide metals with unpaired electrons , but for the metal to be effective as a relaxation agent, their electron spin-relaxation time must match the Larmor frequency of the protons. This condition is best met for the Fe^{3+}, Mn^{2+} and Gd^{3+} ions.

The main problem with this paramagnetic heavy metal ions is that in their native form they are toxic. Research is focused on the development of stable paramagnetic ion complexes. Both the metal ion and the ligand usually exhibit substantial toxicity in the unbound state: together, however, they may create a thermodynamically and kinetically stable compound which is well tolerated.

Gadolinium (Gd) is the paramagnetic substance most commonly used as MR contrast agent. It is chelated to DTPA (Gd-DTPA) to solve toxicity problems.

A relatively new type of paramagnetic contrast agents are the so-called superparamagnetic iron oxide (SPIO) based colloids. They consist of non-stoichiometric microcrystalline magnetite cores which are coated with dextranes (in ferumoxide) or siloxanes (in ferumoxils). Commercially available iron oxide contrast

agents include Endorem®, Feridex IV® and Sinerem®. The compositions and physicochemical properties of non-stoichiometric magnetite are continuously variated between those of Fe_3O_4 and Fe_2O_3. Conceptually, these cation-deficient, inverse-spinel phases are formed by partial oxidation of Fe(II) in stoichiometric magnetite.

2. PRINCIPLES OF RELASSOMETRY

Relaxometry is an instrument able to acquire the NMR (nuclear magnetic resonance) signal produced by nuclei of test samples. It is formed by a circular coil capable of generating a uniform magnetic field, a generator, a receveir of, respectively, radiofrequency (RF) pulse and output, and a computer for processing signals received (figure 1).

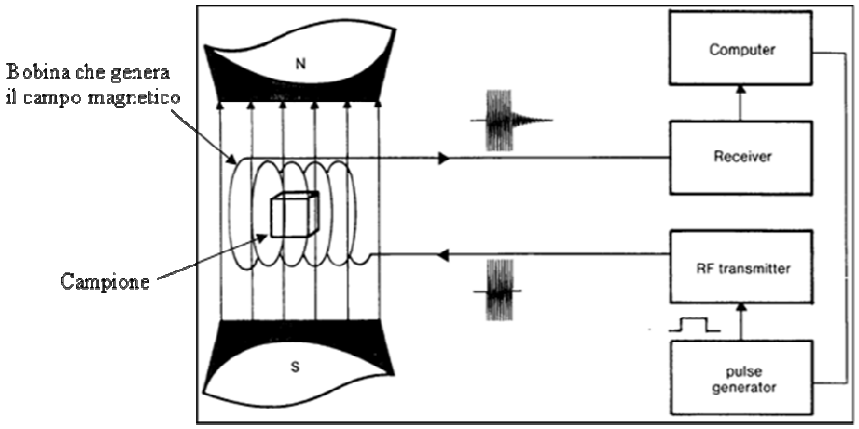

Figure 1: *Block diagram of an NMR system*

To obtain measures "weighed" in a selective manner according to the time T1 (recovery of longitudinal magnetisation) or T2 (loss of transversal magnetization), it is essential to use specific sequences of nuclear excitation and collection of signals: by varying the types of acquisition and/or regulatory factors of the sequences will be possible to have images with desired weighing.
The most common sequence is the sequence Spin-Echo (SE), which allows to get values weighed in T2 without the interference of the inhomogeneities of the magnetic field. This sequence is also highly flexible and, by varying some parameters of its acquisition, it is possible to obtain also measures in T1 weighted and proton density.
The sequence Spin-Echo was now here described in detail.
The transverse magnetization is sensitive to the intrinsic inhomogeneities which are inevitably present in any magnetic field: they would lead to a false interpretation of results, because they determine an apparent more rapid decay of T2, due to the spontaneous dephasing of nuclei of atoms excited. To eliminate this problem, the rephasing signal of nuclear spin after an RT pulse at 180° (respect to magnetic field) was recording with Spin Echo sequence.
In practice, each SE sequence is composed of an initial pulse at 90° which aim is to bring the magnetization on the transverse plane. At this point, the spin direction of the protons begins to de-phase of on the basis either of their T2 and nor of the inhomogeneities of the magnetic field: if the signal was measured at this time, you collect a FID signal (Free Induction Decay, namely the spontaneous fall of the magnetization in the absence of other pulses) (figure 2).

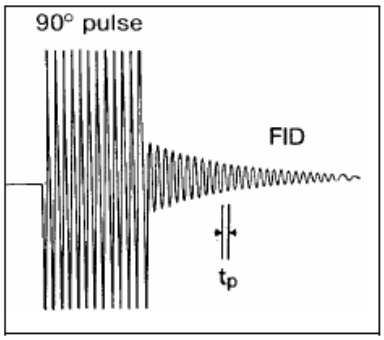

Figure 2: *RT pulse with decaying NMR signal*

Then a pulse at 180° was applied: note that, since the magnetization vector is currently on the transverse plane, this impulse at 180° has the effect to " flip" the orientation of the spin direction. In this way, after a time equal to twice the time elapsed between the pulse at 90° and 180°, the precession of the nuclei back into phase and the transverse magnetization takes a maximum value that is measured by the instrument (in fact with the application of a 180° pulse, this fanning-out is at least partially inverted so that phase coherence is again established for a short time and a "spin-echo" signal can be obtained).
If a whole series of 180° pulses are applied, it results in a continuous rephasing of the nuclei in the opposite direction, with production of a succession of spin-echoes, and because no energy is added at the system, each registration of signal T2 is worth less and less, and this way permitted the record of the fall of the transverse magnetization (the phase relationship at time $2t_1$ gradually disappears again producing a signal which looks like a FID) (figure 3). This sequence, comprising one 90° pulse followed by a series of 180° pulses, is termed a "Carr-Purcell sequence".

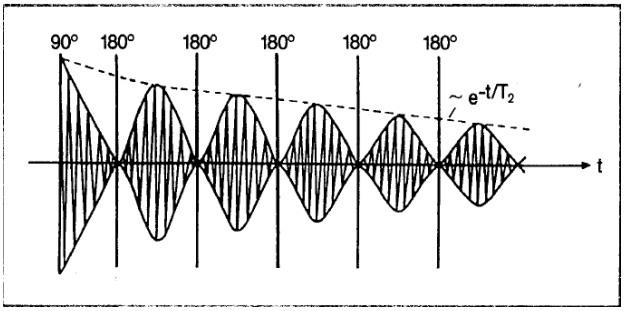

Figure 3: *Carr Purcell Sequence for the determination of the transverse relaxation time T2*

The SE sequence is characterized by three fundamental parameters that must be programmed by the operator, and whose values determine the characteristics of the final images. First, the repetition time of pulse at 180° (namely number of points, represents a discretisation of the total time of measurement), that is the

parameter which decides the length of the sequence and the start of a subsequent phase of acquisition. Secondly, the interval between pulse at 90° to 180° determines the time to echo (π), which is equal to twice this value, since half the time is spent to allow the de-phasing of the precession of protons (interval between pulse at 90° and 180°) and the other half, just the same, spends between 180° pulse and collection of eco of spin resulting by rephasing. Finally, the presence of a possible repetition pulse at 180° within a given sequence is determined by the echo number. This repetition allows the collection of late echoes, useful for evaluating the signal deriving from sample test characterized by long T2.

3. PRINCIPLES OF MRI

When NMR is used for imaging, we refer to Magnetic Resonance Imaging (MRI). Hydrogen is by far the most commonly observed nucleus in MRI, because of its favourable magnetic properties and its abundance. ^{1}H-MR images reflect the density of hydrogen, main component in tissues as water or fat. To be more precise , MR signal intensity reflects the number of MR-visible protons in a unit volume of tissue; in other words it reflects the density of mobile hydrogen nuclei influenced by their chemical environment, which causes magnetic relaxation times, T1 and T2, to occur (see appendix 2 for details about the physical basis of MR signal).
Principal components of an MR imaging system are : the main magnet, that generate the magnetic field and polarizes the sample, the magnetic field gradients, for spatial reconstruction and localization of signal, and the radiofrequency coils to transmit and/or receive the MR imaging signal (figure 1). The whole system is controlled by one or more computer and associated signal processing equipment.

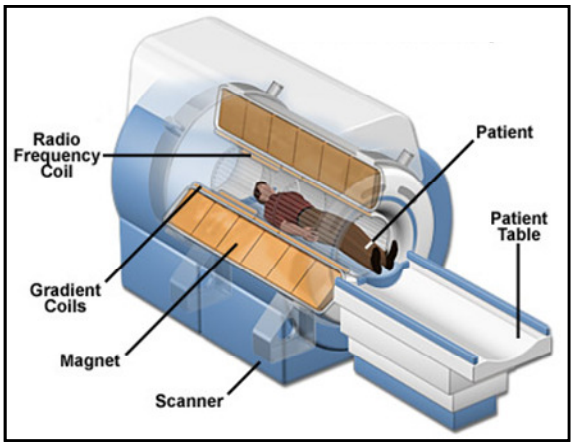

Figure 1: *Schematic representation of MRI components.*

The magnet
The magnet is the largest and most expensive component of the scanner, and its strength is measured in Tesla (T). Clinical magnets generally have a field strength in the range 0.1—3.0 T, with research systems available up to 9.4 T for human use and 21 T for animal systems. The homogeneity of the basic magnetic field over the examination volume should be as high as possible to ensure low image distortion and high signal homogeneity (high potential signal to noise ratio for good image quality). Besides, the homogenous examination volume should be as large as possible. A cylindrical main magnet with the homogeneous volume centred on the central axis fulfils all these requirements and, therefore, represents the most frequent magnet design today, and in general it is based on the use of superconducting electromagnet.
When a niobium-titanium or niobium-tin alloy is cooled by liquid helium to –269°C it becomes a superconductor, losing resistance to the flow of electrical current and

can have extremely high field strengths, with very high stability. The construction of such magnets is extremely costly, and the cryogenic helium is expensive and difficult to handle. However, despite their cost, helium cooled superconducting magnets are the most common type found in MRI scanners today.
Most superconducting magnets have their coils of superconductive wire immersed in liquid helium, inside a vessel called a cryostat. Despite thermal insulation, ambient heat causes the helium to slowly boil off. Such magnets, therefore, require regular topping-up with liquid helium. Generally a cryocooler, also known as a coldhead, is used to condense some helium vapour back into the liquid helium bath. Several manufacturers now offer 'cryogenless' scanners, where instead of being immersed in liquid helium the magnet wire is cooled directly by a cryocooler.
When a sample is placed into the scanner, it creates the inhomogeneities in the field, causing region showing no signal and spatial distortion in the acquired images. To restore the field homogeneity, a set of shim coils are included in the scanner. These are resistive coils, usually at room temperature, capable to produce secondary magnetic fields which correct inhomogeneities and errors in the magnetic field strength. This process of “shimming” is usually automated.

The gradient system

The magnetic field gradients give rise to linear variations of magnetic field strength. In fact, gradient coils are used to spatially encode the positions of protons by varying the magnetic field linearly across the imaging volume.
In order to produce an image, 3 gradients in 3 orthogonal orientations are used: one gradient is used to “locate” the level of each plane and is known as “slice gradient”; the other two gradients are used to locate points within each plane. They are called “frequency” and “phase encoding” gradients.
Gradient coils are usually resistive electromagnets powered by sophisticated amplifiers which permit rapid and precise adjustments of field strength and direction.
Scan speed depends on the gradient system performance, and the optimal system must be able to cover large examination volume in the shortest possible time. In general, the gradient system requirements can be best met with a cylindrical design that fits magnet geometry.

The Radiofrequency system

The radiofrequency (RF) system consists of a RF transmit coil, positioned inside the magnet, for selective RF excitation of the spins and a RF receiver coil system for picking up the weak RF signal resulting from excited nuclei (figure 2).

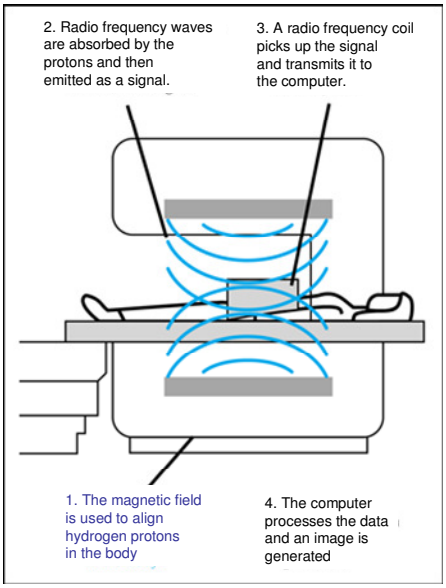

Figure 2: *representation of Radiofrequency system.*

Often both transmit and receive functions are performed by the same coil; nevertheless in some systems, it is advantageous to employ separate transmit and receiver coils. In general, the radio frequency (RF) transmission system consists of an RF synthesizer, a power amplifier and a transmitting coil, whereas the receiver consists of the coil, a pre-amplifier and a signal processing system.
Radiofrequency coils can be constructed with a variety of geometries and they are increasingly built for specific applications; however, large cylindrical volume transmit RF coils with a conductor geometry similar to a birdcage are typically used.

Image formation

The radiofrequency signal picked up by the receiver at the end of an acquisition doesn't have an intrinsic spatial information: it is not able to discriminate signal deriving from different points of the sample, and cannot be used to reconstruct an image. The passage between raw signal and image formation is based on a process of spatial codification, with attribution of a specific frequency and resonance phase for each point of the space: this is possible thanks to the application of the gradients (see paragraph above).
This way, at each different point of the examined space, identified through a frequency and phase codification, is assigned a numeric value of intensity that is translated in a different intensity of grey scale on the image.
One of the big advantages of MRI over other imaging techniques is its ability to image non-invasively slices of an object at any arbitrary position, thickness and orientation. This is obtained by applying an RF pulse with a range of frequencies together with a slice magnetic field in the proper orientation. This range of frequencies associated with the RF pulse is referred to as the "bandwidth" and directly determines the slice thickness. Slice thickness can also be altered by

changing the slope of the gradient (a very strong gradient allows the reading of thinner slices, and vice versa).

An MR image is essentially a two-dimensional representation of the intensity of the magnetic properties of the observed nucleus as a function of its distribution in space.

Many factors affect signal intensity and contrast of an MR image. They include intrinsic factors like proton density, T1 and T2 relaxation times and diffusion, as well as extrinsic or experimental factors, such as parameters of acquisition.

One of the biggest advantages of MRI is that image contrast can be optimized for specific purposes and the choice of pulse sequences determines the weighting and the quality of the images. A multitude of sequences are available in MRI through conventional (Spin Echo and Gradient Echo sequences), fast imaging and ultra fast imaging.

4. PRINCIPLES OF SPECT

SPECT (Single Photon Emission Computed Tomography) tomograph is a device able to detect high energy photons emitted from the subject under examination, following the administration, generally by intravenous injection, of radioactively labelled tracers. After reaching the target organ, the tracers are retained there as a result of transport, binding to receptors and antigens, reaction with enzymes, biochemical and mechanical trapping, phagocytosis, or a combination of the above.

The labelled tracers contain an excited nucleus -as a radionuclide- which is unstable and can spontaneously stabilize to a less-excited system. The resulting transformation alters the structure of the nucleus and causes the emission of either a photon or a high-velocity particle with a mass (such as an electron, alpha particle, or other type). The radioactive decay is a random process on the atomic level, in that it is impossible to predict when a given atom will decay, but given a large number of similar atoms the decay rate, on average, is predictable, and can be used to image a specific process or cells. One of the main advantages of the nuclear imaging techniques is their very high sensitivity, when compared with other in-vivo imaging techniques.

SPECT is based on the use of radiotracers labelled with a radionuclide, such as ^{99m}Tc, ^{123}I, ^{125}I, ^{111}In and ^{201}Tl, that decays with emission of single photons with different energy (e.g., ^{111}In has two emission lines at 171 and 245 keV, ^{99m}Tc has a single line at 140 keV). To locate the source of an emitted photon, its direction of incidence into the detection system needs to be accurately selected and its position of interaction determined in the position sensitive detector.

Principal components that comprise a SPECT imaging system include: the collimator, a scintillation crystal, the position sensitive photo-detector, which is traditionally based on photomultiplier tubes, and the readout electronic, which is dependent on the type of photo-detector used and gives information about the position of interaction and the energy of each detected gamma photon (figure 1).

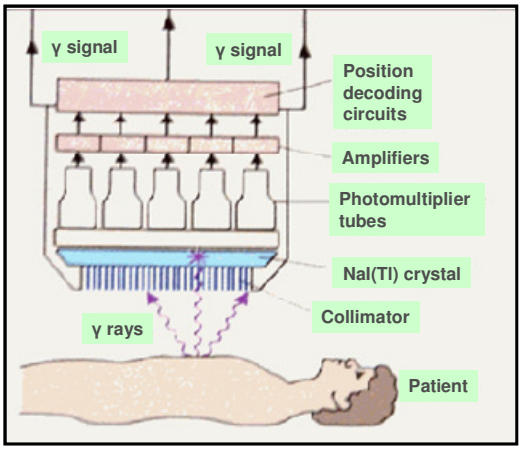

Figure 1: *schematic representation of a gamma camera.*

The collimator is a device made of a high-Z material such as lead, which selects gamma rays along particular directions in order to form an image on the sensitive area of the gamma-camera. There are different options for the collimator geometry, among which one of the most commonly used is the parallel holes. In this case, the holes of the collimator are parallel and permit the passage only of the photons perpendicular to the surface of the photodetector. The image obtained is thus the projection of the distribution of the radio tracer inside the patient on a plane parallel to the scintillator crystal or the photo-detector. This kind of collimator is also the one which has been used during the measurements with the Hi-Cam Gamma Camera prototype (see next paragraph).
The scintillation crystal is the fundamental constituent of a gamma camera: its function is to convert the high energy gamma photons into many lower energy photons, usually in the visible range, which can easily be detected by the photo-detector. On the contrary, without a scintillator, the photo-detector would be almost transparent to the gamma radiation and wouldn't provide any useful signals.
The gamma photon, leaving the patient and impinging on the scintillator, is called the primary photon. When it interacts with the scintillator, it leaves part or all of his energy inside the crystal and, with part of the lost energy, a certain number of lower energy photons, called secondary photons, are generated. The energy spectrum of the secondary photons generated is usually composed of one or two close lines, which depend on the scintillator used. This means that, at a first degree of approximation we can consider that all the secondary photons have the same energy. Due to the conservation of energy and the fact that the secondary photons have the same energy, the number of secondary photons is proportional to the amount of energy lost inside the scintillator by the primary photon. For example, if we consider only the events in which the primary photon has released all of his energy inside the crystal, i.e. the photopeak in the energy spectrum, the number of secondary photons is proportional to the energy of the photon emitted by the radio-tracer.
The way the primary photon looses energy inside the crystal can be described in short as follows: when the gamma photon leaves the patient, it knocks the crystal and loses energy, determining the production of a high energy ionizing electron (figure 2).

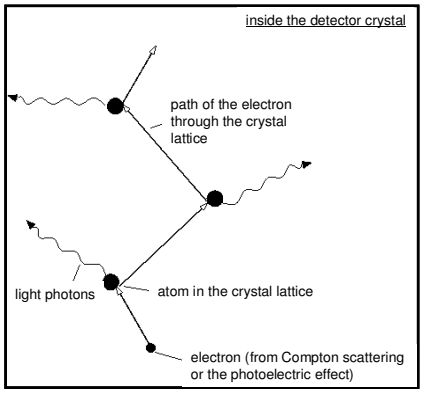

Figure 2: *events that happened inside the crystal.*

The generated electron loses its kinetic energy in the form of thermal energy, light photons or by ionizing other electrons, which again will loose their energy inside the crystal through the same mechanisms, until all the electrons find a minimal energy state. At the end of the process part of the energy of the primary photon is converted into many secondary photons, while the rest of the energy is "lost" in non-radiative transitions, which convert it in thermal energy inside the crystal.
At the energies relevant for the SPECT there are two ways the primary photon can make the first interaction with the scintillator: the photoelectric effect and the Compton effect (see figure 3). In the first case, all the energy of the gamma photon is lost inside the crystal, generating the photopeak in the energy spectrum, while in the second case only part of the energy remains inside the crystal, because the rest is taken away by the deviated gamma photon.

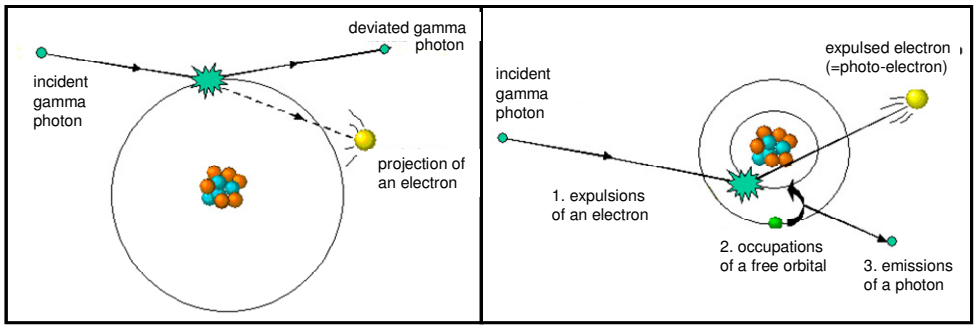

Figure 3: *graphic representation of Compton effect (left panel) and photoelectric effect (right panel).*

There are many different kinds of scintillators, but the most common in the gamma cameras are the inorganic scintillators. They are high-Z crystals, so that they have a high stopping power for the primary photons, and are transparent to the visible light, in order to let the secondary photons reach the photo-detector. The most important figures of Merit of the scintillator are usually considered the light yield, i.e. the total number of secondary photons generated per unit energy deposited inside the crystal, the stopping power for high energy photons and the decay time constant, i.e. the time in which the secondary photons are generated, after the detection of the primary photon. Being one of the most important parts of the gamma cameras, a big amount of research has been done in order to optimize the parameters of the scintillator, so that nowadays many kinds of inorganic scintillators are available. The most common are NaI(Tl), CsI(Tl), used for Hi-Cam prototype (see next paragraph), or, more recently, $LaBr_3$(Ce).
The secondary photons are detected by the photo-detector, which is placed at the opposite side of the scintillator, with respect to the collimator. Its function is to convert the secondary photons into a proportional electronic signal. One very common photo-detector, for these application, is the photomultiplier tube, or PMT. Inside the photomultiplier, there is a photocathode, which absorbs the visible

photons generating free electrons, that are subsequently accelerated in a vacuum tube by a sequence of dynodes, having a positive potential increasing proportionally to the distance from photocathode. Along their path inside the tube, the interaction of the electrons with dynodes determines the formation of new electrons, obtaining a signal amplification. At the and of the tube there is the anode, which collects all the electrons and generates an electric signal whose amplitude is proportional to the number of secondary photons interacting at the photocatode and thus also to the total energy released in the scintillator by the gamma photon.
With respect to the simplifies structure described above, some modification have been implemented, in order to add position sensitivity to certain types of PMTs and actually record the image generated by the collimator.

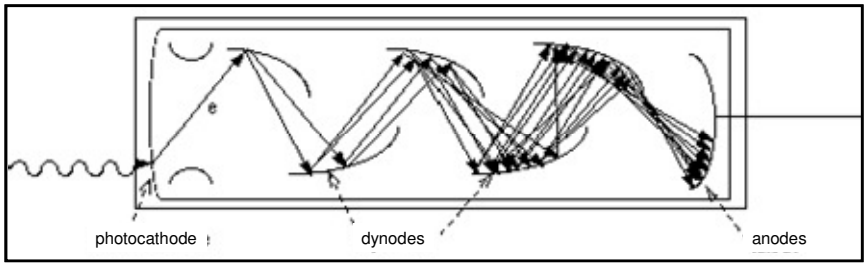

Figure 4: *schematic representation of a photomultiplier.*

More recently, different photo-detectors, based on solid-state silicon devices, have been proposed in order to improve performances of the gamma cameras. In particular, the aim of the use of silicon devices is to get better energy performance, spatial resolution, more compactness, lower cost and less sensitivity to magnetic fields, with respect to PMTs, which could allow their use in integration with MRI. All these solution, however, are under research and the widespread photo-detector for gamma cameras remains the PMT. For example, the Hi-Cam gamma camera is a research project for evaluating the use of a very peculiar type of silicon detector, the Silicon Drift Detector (SDD), as the photo-detector in a high resolution gamma camera.
In origin the SPECT was used only for human studies, but recently it has been rescaled for studies in small animals, and an examples is the prototype of microSPET used in this project, that will be briefly explained follow.

4.1. Hi-Cam: a new prototype of microSPET

Hi-Cam prototype is a high resolution, small Field Of View (FOV), compact gamma ray imager, based on the Anger camera principle. Thanks to its characteristics, the potential applications of the imager in human medicine are in the field of intra operative probes and of cancer diagnosis, staging and therapy control. Moreover, the probe could be useful in pre-clinical validation of new drugs carried out with in vivo studies on small animals. The most relevant and innovative characteristic of

the Hi-Cam imager is the use of a non-standard silicon photo-detector for scintillation light readout. This detector is the Silicon Drift Detector, or SDD, which is characterized by a very low electronic noise, reached without any internal charge multiplication mechanism. Moreover, custom anti reflective coatings have been implemented on the entrance window of the detector, in order increase the Quantum Efficiency (QE). Thanks to these characteristics, the statistical and noise contributions to the energy resolution in gamma ray spectroscopy are reduced, eventually yielding to an improved image quality.

The Hi-Cam imaging instrument is composed, starting from top, by a collimator, a single scintillator crystal, which covers all the units of the array of photo-detectors and converts the high energy γ-photons into many visible ones, and the photo-detector array, which converts the light into electric signals.

The position of interaction of the gamma photons inside the crystal is obtained by the scintillation light distribution among the elements of the array. The signals of the photo detectors are amplified and filtered by a multi-channel analog readout electronics and then sent to an acquisition board, where they are converted to digital values and sent to a PC. Finally, on the PC, a digital algorithm reconstructs the position of interaction of the photons in the crystal.

The scintillator is made of CsI:Tl, which has a high light output, but a long decay time constant. The results confirm good performances, such as an energy resolution of 5.38 % on the ^{57}Co peak, indicating that the SDD is an almost noiseless detector in the measured energy range, between 50 KeV and 700 KeV.

The readout electronics is designed specifically for the Hi-Cam project and is composed of ten, 8-channel ASICs (Application Specific Integrated Circuits). Every single channel features a low noise preamplifier, a 6th order semi-gaussian shaping amplifier with selectable gain and peaking times in the μs range, a peak stretcher and a baseline holder. The 8-channel chip also features an analog multiplexer, registers for threshold programming, and some logic necessary for the multiplexer to work and for interfacing with the rest of the system. The acquisition system converts the peak values of the semi-gaussian shaping amplifiers, shifted out from the multiplexer, with a precision of 13 bits. The converted data are then stored in a FIFO memory for buffering and sent to the host PC, through a high-speed USB interface. Both the control of the acquisition board and the digital processing of the data, for calculating the position of interaction of the gamma photon inside the crystal basing on the Anger logic, is done on the PC.

Bibliography

[I] Gorio A, Madaschi L, Di Stefano B, Carelli S, Di Giulio AM, De Biasi S, Coleman T, Cerami A, and Brines M; "Methylprednisolone neutralizes the beneficial effects of erythropoietin in experimental spinal cord injury", *Proc Natl Acad Sci U. S. A.*, Vol. 102, 2005, pp.16379–16384.

[2] Kwon BK, Borisoff JF and Tetzlaff W, "Molecular targets for therapeutic intervention after spinal cord injury", *Mol Intervent,* Vol. 2, 2002, pp. 244–258.

[3] Bethea JR, "Spinal cord injury-induced inflammation: a dual-edged sword", *Prog Brain Res* , 2000, Vol. 128, pp. 33–42.

[4] Gris D, Marsh DR, Oatway MA, Chen Y, Hamilton EF, Dekaban GA, Weaver LC, "Transient blockade of the CD11d/CD18 integrin reduces secondary damage after spinal cord injury, improving sensory, autonomic, and motor function", *J Neurosci*, Vol. 24, 2004, pp. 4043–4051.

[5] Gorio A, Madaschi L, Zadra G, Marfia G, Cavalieri B, Bertini R and Di Giulio AM, "Reparixin, an Inhibitor of CXCR2 Function, Attenuates Inflammatory Responses and Promotes Recovery of Function after Traumatic Lesion to the Spinal Cord", *J Pharmacol Exp Ther*, Vol. 322, no. 3, 2007, pp. 973-981.

[6] Anderson DK, Howland DR, Reier PJ "Foetal neural grafts and repair of the injured spinal cord", *Brain Pathol*, Vol. 5, 1995, pp. 451–457.

[7] Bernstein JJ, Goldberg WJ, "Foetal spinal cord homograft ameliorate the severity of lesion-induced hind limb behavioural deficits"*, Exp Neurol* , Vol. 98, 1987, pp. 633–644.

[8] Reier PJ, Bregman BS, Wujek JR, "Intraspinal transplantation of embryonic spinal cord tissue in neonatal and adult rats", *J Comp Neurol*, Vol. 247, 1986, pp. 275–296.

[9] Tessler A, Himes BT, Houle J, "Regeneration of adult dorsal root axons into transplants of embryonic spinal cord", *J Comp Neurol* , Vol. 270, 1988, pp. 537–548.

[10] Bregman BS, Kunkel-Bagden E, Reier PJ, "Recovery of function after spinal cord injury: mechanisms underlying transplant-mediated recovery of function differ after spinal cord injury in newborn and adults rats", *Exp Neurol*, Vol. 123, 1993, pp. 3–16.

[11] Ribotta M, Orsal D, Feraboli-Lohnherr D, "Kinematics analysis of recovered locomotor movements of the hindlimbs in paraplegic rats transplanted with monoaminergic embryonic neurons", *Ann NY Acad Sci,* Vol. 860, 1998, pp. 521–523.

[12] Stokes BT, Reier PJ, "Foetal grafts alter chronic behavioural outcome after contusion damage to the adult rat spinal cord", *Exp Neurol*, Vol. 116, 1992, pp. 1–12.

[13] Anderson DK, Reier PJ, Wirth ED, "III Delayed grafting of foetal CNS tissue into chronic compression lesions of the adult cat spinal cord", *Restor Neurol Neurosci*, Vol. 2, 1991, pp. 309–325.

[14] Application of Current Statutory Authorities to Human Somatic Cell Therapy Products and Gene Therapy Products, Notice, Oct 14, 1993 (Federal Register). (Notice from the Center for Biologics Evaluation and Research, Center for Drug Evaluation and Research, Center for Devices and Radiological Health, U.S. Food and Drug Administration).

[15] Redmond, DE Jr, Bjugstad KB, Teng YD, Ourednik V, Ourednik J, Wakeman DR, Parsons XH, Gonzalez R, Blanchard BC, Kim SU, Gu Z, Lipton SA, Markakis EA, Roth RH, Elsworth JD, Sladek JR Jr, Sidman RL, Snyder EY, "Behavioral improvement in a primate Parkinson's model is associated with multiple homeostatic effects of human neural stem cells", *Proc Natl Acad Sci U S A*, Vol. 104, no. 29, 2007, pp. 12175-80.

[16] Ryu, JK, Cho T, Wang YT, McLarnon JG, "Neural progenitor cells attenuate inflammatory reactivity and neuronal loss in an animal model of inflamed AD brain", *J Neuroinflammation*, Vol. 6, 2009, pp. 39.

[17] Blurton-Jones, M, Kitazawa M, Martinez-Coria H, Castello NA, Müller FJ, Loring JF, Yamasaki TR, Poon WW, Green KN, LaFerla FM, "Neural stem cells improve cognition via BDNF in a transgenic model of Alzheimer disease", *Proc Natl Acad Sci U S A*, Vol. 106, no. 32, 2009, pp. 13594-13599.

[18] Bacigaluppi, M, Pluchino S, Peruzzotti Jametti L, Kilic E, Kilic U, Salani G, Brambilla E, West MJ, Comi G, Martino G, Hermann DM, "Delayed post-ischaemic neuroprotection following systemic neural stem cell transplantation involves multiple mechanisms", *Brain*, Vol. 132 (Pt 8), 2009, pp. 2239-2251.

[19] Snyder EY, Taylor RM, Wolfe JH, "Neural progenitor cell engraftment corrects lysosomal storage throughout the MPS VII mouse brain", *Nature*, 1995, Vol. 374, pp. 367–370.

[20] Meng XL, Shen JS, Ohashi T, Maeda H, Kim SU, Eto Y, "Brain transplantation of genetically engineered human neural stem cells globally corrects brain lesions in the mucopolysaccharidosis type VII mouse", *J Neurosci Res*, 2003, Vol. 74, pp. 266–277.

[21] Eto Y, Shen JS, Meng XL, Ohashi T, "Treatment of lysosomal storage disorders: cell therapy and gene therapy", *J Inherit Metab Dis*, Vol. 27, 2004, pp. 411–415.

[22] Arvidsson A, Collin T, Kirik D, Kokaia Z, Lindvall O, “Neuronal replacement from endogenous precursors in the adult brain after stroke”, *Nat Med*, Vol. 8, 2002, pp. 963–970.

[23] Brundin L, Brismar H, Danilov AI, Olsson T, Johansson CB, “Neural stem cells: a potential source for remyelination in neuroinflammatory disease”, *Brain Pathol*, Vol. 13, 2003, pp. 322–328.

[24] Pluchino S, Zanotti L, Rossi B, Brambilla E, Ottoboni L, Salani G, Martinello M, Cattalini A, Bergami A, Furlan R, Comi G, Constantin G, Martino G, “Neurosphere-derived multipotent precursors promote neuroprotection by an immunomodulatory mechanism” *Nature*, Vol. 436, 2005, pp. 266–271.

[25] Singh SK, Hawkins C, Clarke ID, Squire JA, Bayani J, Hide T, Henkelman RM, Cusimano MD, Dirks PB, “Identification of human brain tumour initiating cells”, *Nature*, Vol. 432, 2004, pp. 396–401.

[26] Mezey E, Key S, Vogelsang G, Szalayova I, Lange GD, Crain B, ”Transplanted bone marrow generates new neurons in human brains”, *Proc Natl Acad Sci USA*, Vol. 100, 2003, pp. 1364–1369.

[27] Bjo¨rnson CRR, Rietze RL, Reynolds BA, Magli C, Vescovi AL, ”Turning brain into blood: a hematopoietic fate adopted by adult neural stem cells *in vivo”*, *Science*, Vol. 283, 1999, pp. 534–537.

[28] Wurmser AE, Gage FH, “Stem cells: cell fusion causes confusion”, *Nature*, Vol. 416, 2002, pp. 485–487.

[29] Terada N, Hamazaki T, Oka M, Hoki M, Mastalerz DM, Nakano Y, Meyer EM, Morel L, Petersen BE, Scott EW, “Bone marrow cells adopt the phenotype of other cells by spontaneous cell fusion”, *Nature*, Vol. 416, 2002, pp. 542–545.

[30] Ying QL, Nichols J, Evans EP, Smith AG, “Changing potency by spontaneous fusion”, *Nature*, Vol. 416, 2002, pp. 545–548.

[31] McDonald JW, Liu XZ, Qu Y, Liu S, Michey SK, Turetsky D, Gottlieb DI, Choi DW, “Transplanted embryonic stem cells survve, differentiate and promote recovery of injured rat spinal cord”, *Nat Med* , Vol. 5, 1999, pp. 1410-1412.

[32] Ogawa Y, Sawamoto K, Miyata T, Miyao S, Watanabe M, Nakamura M, Bregman B, Koike M, Uchiyama Y, Toyama Y, Okano H, “Transplantation of in vitro-expanded foetal neural progenitor cells results in neurogenesis and functional recovery after spinal cord contusion injury in aduts rats”, *J Neurosci Res,* Vol. 69, 2002, pp. 925-933.

[33] Gorio A, Torrente Y, Madaschi L, Di Stefano A B, Pisati F, Marchesi C, Belicchi M, Di Giulio AM And Bresolin N, "Fate of autologous dermal stem cells transplanted Into the spinal cord after traumatic injury (TSCI)", *Neuroscience,* Vol. 125, 2004, pp. 179–189.

[34] Bjornson CR, Rietze RL, Reynolds BA, Magli MC, Vescovi AL, "Turning brain into blood: a hematopoietic fate adopted by adult neural stem cells *in vivo", Science,* Vol. 283, 1999, pp. 534–537.

[35] Schultz SS, Lucas PA, "Human stem cells isolated from adult skeletal muscle differentiate into neural phenotypes", *J Neurosci Methods,* Vol. 152, 2006, pp. 144–155.

[36] Riess P, Zhang C, Saatman KE, Laurer HL, Longhi LG, Raghupathi R, Lenzlinger PM, Lifshitz J, Boockvar J, Neugebauer E, Snyder EY, McIntosh TK, "Transplanted neural stem cells survive, differentiate, and improve neurological motor function after experimental traumatic brain injury", *Neurosurgery,* Vol. 51, 2002, pp. 1043–52, discussion 1052–44.

[37] Liker MA, Petzinger GM, Nixon K, McNeill T, Jakowec MW, "Human neural stem cell transplantation in the MPTP-lesioned mouse", *Brain Res*, Vol. 971, 2003, pp. 168–177.

[38] Akerud P, Holm PC, Castelo-Branco G, Sousa K, Rodriguez FJ, Arenas E, "Persephin- overexpressing neural stem cells regulate the function of nigral dopaminergic neurons and prevent their degeneration in a model of Parkinson's disease", *Mol Cell Neurosci,* Vol. 21, 2002, pp. 205–222.

[39] Hofstetter CP, Schwarz EJ, Hess D, Widenfalk J, El Manira A, Prockop DJ, Olson L, "Marrow stromal cells form guiding strands in the injured spinal cord and promote recovery", *Proc. Natl. Acad. Sci. U. S. A.*, 2002, Vol. 99, pp. 2199–2204.

[40] Bottai D, Madaschi L, Di Giulio AM and Gorio A, "Viability-Dependent Promoting Action of Adult Neural Precursors in Spinal Cord Injury", *Mol. Med 1*, Vol. 4, no. 9-10, 2008, pp. 634- 644.

[41] Gorio A, Gokmen N, Erbayraktar S, Yilmaz O, Madaschi L, Cichetti C, Di Giulio AM, Vardar E, Cerami A, and Brines M, "Recombinant human erythropoietin counteracts secondary injury and markedly enhances neurological recovery from experimental spinal cord trauma" *Proc. Natl. Acad. Sci. U. S. A.* ,Vol. 99, 2002, pp. 9450–9455.

[42] Sanchez-Ramos JSS, Samberg PR, "Adult bone marrow stromal cells differentiate into neural cells in vitro", *Exp Neurol* , Vol. 164, 2000, pp. 247–249.

[43] Brazelton TR, Rossi FM, Keshet GI, Blau HM, "From bone marrow to brain: expression of neuronal phenotypes to adult mice",*Science* , Vol. 290, 2000, pp. 1775–1779.

[44] Mezey E, Chandross KJ, Harta G, Maki RA, McKercher SR, "Turning blood into brain: cells bearing neuronal antigens generated *in vivo* from bone marrow", *Science*, Vol. 290, 2002, pp. 1779–1781.

[45] Toma JG, Akhavan M, Fernandes KJ, Barnabe-Heider F, Sadikot A, Kaplan DR, Miller FD, "Isolation of multipotent adult stem cells from the dermis of mammalian skin", *Nat Cell Biol*, Vol. 3, 2001, pp. 778–784.

[46] Mathai KI, Sasivadanan MS, Sudumbraker S M, Sahoo PK, "Stem ell therapy for spinal cord injury. A plea for rationality", *Indian journal of neurotrauma*, Vol. 5, no. 1, 2008, pp. 7-10.

[47] Conover JC, Ip NY, Poueymirou WT, Bates B, Goldfarb MP, DeChiara TM, Yancopoulos GD, "Ciliary neurotrophic factor maintains the pluripotentially of embyronic stem cells", *Development,* Vol. 119, 1993, pp. 559-565.

[48] Shimazaki T, Shingo T, Weiss S, "The ciliary neurotrophic factor/ leukemia inhibitory factor/gp130 receptor complex operates in the maintenance of mammalian forebrain neural stem cells", *J Neurosci,* Vol. 21, no. 19, 2001, pp. 7642-7653.

[49] Chojnacki AT, Shimazaki C, Gregg G, Weinmaster G, Weiss S, "Glycoprotein 130 signaling regulates Notch1 expresssions and activation in the self-renewal of mammalian forebrain neural stem cells", *Journal of Neuroscience,* Vol. 23, no. 5, 2003, pp. 1730-1741.

[50] Morrison SJ, Perez SE, Qiao Z, Verdi JM, Hicks C, Weinmaster G, Anderson DJ, "Transient Notch activation initiates an irreversible switch from neurogenesis to gliogenesis by neural crest stem cells", *Cell,* Vol. 101, no. 5, 2000, pp. 499-510.

[51] Doetsch R, Caille I, Lim DA, Garcia-Verdugo JM, Alvarez-Buylla A, "Subventricular zone astrocytes are neural stem cells in the adult mammalian brain", *Cell,* Vol. 97, 1999, pp. 703-716.

[52] Gaiano N, Nye JS, Fishell G, "Radial glial identity is promoted by Notch1 signaling in the murine forebrain", *Neuron,* Vol. 26, no. 2, 2000, pp. 395-404.

[53] Lim DA, Tramontin AD, Trevejo JM, Herrera DG, Garcia-Verdugo JM, Alvarez-Buylla A, "Noggin antagonizes BMP signaling to create a niche for adult neurogenesis", *Neuron,* Vol. 28, no. 3, 2000, pp. 713-726.

[54] Gross RE, Mehler MF, Mabie PC, Zang Z, Santschi L, Kessler JA, "Bone morphogenetic proteins promote astroglial lineage commitment by mammalian

subventricular zone progenitor cells", *Neuron,* Vol. 17, no. 4, 1996, pp. 595-606.

[55] Shou J, Rim PC, Calof AL, "BMPs inhibit neurogenesis by a mechanism involving degradation of a transcription factor", *Nat Neurosci,* Vol. 2, no. 4, 1999, pp. 339-345.

[56] Merkle FT, Mirzadeh Z, Alvarez-Buylla A, "Mosaic organization of Neural Stem Cells in the Adult Brain", *Science*, Vol. 317, 2007, pp. 381

[57] Morshead CM, van der Kooy D, "Postmitotic death is the fate of constitutively proliferating cells in the subependymal layer of the adult mouse brain", *J Neurosci,* V*ol.* 12, no.1, 1992, pp. 249-256.

[58] Morshead CM, Reynolds BA, Craig CG, McBurney MW, Staines WA, Morassutti D, Weiss S, van der Kooy D, "Neural stem cells in the adult mammalian forebrain: a relatively quiescent subpopulation of subependymal cells", *Neuron,* Vol. 13, no. 5, 1994, pp. 1071-1082.

[59] Reynolds BA, Weiss S, "Generation of neurons and astrocytes from isolated cells of the adult mammalian central nervous system", *Science,* Vol. 255, no. 5052, 1992, pp. 1707-1710.

[60] Kuhn HG, Winkler J, Dempermann G, Thal LJ, Gage FH, "Epidermal growth factor and fibroblast growth factor-2 have different effects on neural progenitors in the adult rat brain", *J Neurosci*, Vol. 17, no. 15, 1997, pp. 5820-5829.

[61] Gritti A, Frolichsthal-Schoeller P, Galli R, Parati EA, Cova L, Pagano SF, Bjornson CR, Vescovi AL, "Epidermal and fibroblast growth factors behave as mitogenic regulators for a single multipotent stem cell-like population from the subventricular region of the adult mouse forebrain" *J Neurosci,* Vol. 19, no. 9, 1999, pp. 3287-3297.

[62] Doetsch F, Petreanu L, Caille I, Garcia-Verdugo JM, Alvarez-Buylla A, "EGF converts transit-amplifying neurogenic precursors in the adult brain into multipotent stem cells", *Neuron,* Vol. 36, no.6, 2002, pp. 1021-1034.

[63] Sanai N, Tramontin AD, Hinojosa AQ, Barbaro NM, Gupta N, Kunwar S, Lawton MT, McDermott MW, Parsa AT, Verdugo JMG, Berger MS, Buylla AA, "Unique astrocyte ribbon in adult human brain contains neural stem cells but lacks chain migration" *Nature*, Vol. 427, 2004, pp. 740-744.

[64] Quiñones-Hinojosa A, Sanai N, Soriano-Navarro M, Gonzalez-Perez O, Mirzadeh Z, Gil-Perotin S, Romero-Rodriguez R, Berger MS, Garcia-Verdugo JM, Alvarez-Buylla A, "Cellular composition and cytoarchitecture of the adult human subventricular zone: a niche of neural stem cells ", *J Comp Neurol*. Vol. 494, no. 3, 2006, pp. 415-434.

[65] Massoud TK, Gambhir SS, "Molecular imaging in living subjects: seeing fundamental biological processes in a new light", *Genes and Development*, Vol. 17, 2003, pp. 545–580.

[66] Bulte JW, Kraitchman DL, "Iron oxide MR contrast agents for molecular and cellular imaging", *NMR in Biomedicine*, Vol. 17, 2004, pp. 484–499.

[67] Lewis JS, Achilefu S, Garbow JR, Laforest R, Welch MJ, "Small animal imaging. Current technology and perspectives for oncological imaging", *European Journal of Cancer*, Vol. 16, 2002, pp. 2173–2188.

[68] Massoud TF, Gambhir SS, "Integrating noninvasive molecular imaging into molecular medicine: an evolving paradigm", *TRENDS in Molecular Medicine*, Vol. 13, no. 5, 2007, pp. 183-191.

[69] Baumjohann D, Hess A, Budinsky L, Brune K, Schuler G, Lutz MB. "*In vivo* magnetic resonance imaging of DC migration into the draining lymph nodes of mice", *European Journal of Immunology*, Vol. 36, 2006, pp. 2544-2555.

[70] de Vries IJ, Lesterhuis WJ, Barentsz JO, Verdijk P, van Krieken JH, Boerman OC, Oyen WJ, Bonenkamp JJ, Boezeman JB, Adema GJ, Bulte JW, Scheenen TW, Punt CJ, Heerschap A, Figdor CG, "Magnetic resonance tracking of DC in melanoma patients for monitoring of cellular therapy", *Nature Biotechnology*, Vol. 23, no. 11, 2005, pp. 1407-1413.

[71] Lutz MB, Kukutsch N, Ogilvie ALJ, Rößner S, Koch F, Romani N, Schuler G, "An advanced culture method for generating large quantities of highly pure dendritic cells from mouse bone marrow", *Journal of Immunological Methods*, Vol. 223, 1999, pp. 77-92.

[72] Lucignani G, Ottobrini L, Martelli C, Rescigno M, Clerici M, "Molecular imaging of cell-mediated cancer immunotherapy", *Trends in Biotechnology, Vol.* 24, no. 9, 2003, pp.410-418.

[73] Livingston JN, "Genetically engineered mice in drug development", *Journal of International Medicine*, Vol. 245, 1999, pp. 627–635.

[74] Gassmann M, Hennet T, "From genetically altered mice to integrative physiology", *News in physiological sciences : an international journal of physiology produced jointly by the International Union of Physiological Sciences and the American Physiological Society*, Vol. 13, 1998, pp. 53–57.

[75] Massoud TK, Gambhir SS, "Molecular imaging in living subjects: seeing fundamental biological processes in a new light", *Genes and Development*, 2003, Vol. 17, pp. 545–580.

[76] Spibey CA, Jackson P, Herick K, "A unique charge-coupled device/xenon arc lamp based imaging system for the accurate detection and quantitation of multicolour fluorescence", *Electrophoresis*, Vol. 22, 2001, pp. 829-836.

[77] Ottobrini L, Ciana P, Biserni A, Lucignani G, Maggi A, "Molecular imaging: A new way to study molecular processes *in vivo*", *Molecular and Cellular Endocrinology*, Vol. 246, 2006, pp. 69-75.

[78] Gross S, Piwnica-Worms D, "Spying on cancer: molecular imaging *in vivo* with genetically encoded reporters", *Cancer Cell*, Vol.7, 2005, pp. 5-15.

[79] Shaner NC, Campbell RE, Steinbach PA, Giepmans BNG, Palmer AE, Tsien RY, "Improved monomeric red orange and yellow fluorescent proteins derived from *Discosoma sp*. red fluorescent protein", *Nature. Biotechnology*, Vol. 22, 2004, pp. 1567-72

[80] Shcherbo D, Merzlyak EM, Chepurnykh TV, Fradkov AF, Ermakova GV, Solovieva EA, Lukyanov KA, Bogdanova EA, Zaraisky AG, Lukyanov S, Chudakov DM, "Bright far-red fluorescent protein for whole-body imaging", *Nature Methods*, Vol. 4, 2007, pp. 741-6.

[81] Swirski FK, Berger CR, Figueiredo JL, Mempel TR, von Andrian UH, Pittet MJ, Weissleder R, "A Near-Infrared Cell Tracker Reagent for Multiscopic *In vivo* Imaging and Quantification of Leukocyte Immune Responses", *PLoS ONE*, Vol. 10, 2007, pp. 1-7.

[82] Noh YW, Lim YT, Chung BH, "Noninvasive imaging of dendritic cell migration into lymph nodes using nearinfrared fluorescent semiconductor nanocrystals", *The FASEB Journal*, Vol. 22, no. 11, 2008, pp. 3908-18.

[83] Sen D, Deerinck TJ, Ellisman MH, Parker I, Cahalan MD, "Quantum Dots for Tracking Dendritic Cells and Priming an Immune Response In vitro and *In vivo*", *PLoS ONE*, Vol. 3, no. 9, 2008, pp. 1-13.

[84] Lecchi M, Ottobrini L, Martelli C, Del Sole A, Lucignani G, "Instrumentation and probes for molecular and cellular imaging", *Quarterly Journal of Nuclear Medicine and Molecular Imaging*, Vol. 51, 2007, pp. 111-26.

[85] Rosenthal MS, Cullom J, Hawkins W, Moore SC, Tsui BM, Yester M, "Quantitative SPECT imaging: A review and recommendations by the Focus Committee of the Society of Nuclear Medicine Computer and Instrumentation Council", *Journal of Nuclear Medicine*, Vol. 36, 1995 pp. 1489-513.

[86] Iyer M, Barrio JR, Namavari M, Bauer E, Satyamurthy N, Nguyen K, Toyokuni T, Phelps ME, Herschman HR, Gambhir SS, "8-[F-18]fluoropenciclovir: An improved reporter probe for imaging HSV1-tk reporter gene expression *in vivo* using PET", *Journal of Nuclear Medicine*, Vol. 42, 2001, pp. 96-105.

[87] Tjuvajev JG, Finn R, Watanabe K, Joshi R, Oku T, Kennedy J, Beattie B, Koutcher J, Larson S, Blasberg RG, "Noninvasive imaging of herpes virus thymidine kinase gene transfer and expression: A potential method for monitoring clinical gene therapy", *Cancer Research*, Vol. 56, 1996, pp. 4087-95.

[88] Gambhir SS, Bauer E, Black ME, Liang Q, Kokoris MS, Barrio JR, Iyer M, Namavari M, Phelps ME, Herschman HR, "A mutant herpes simplex virus type 1 thymidine kinase reporter gene shows improved sensitivity for imaging reporter gene expression with positron emission tomography", *Proceedings of the National Academy of Sciences PNAS*, Vol. 97, 2000, pp. 2785-90.

[89] MacLaren DC, Gambhir SS, Satyamurthy N, Barrio JR, Sharfstein S, Toyokuni T, Wu L, Berk AJ, Cherry SR, Phelps ME, Herschman HR, "Repetitive, non-invasive imaging of the dopamine D2 receptor as a reporter gene in living animals", *Gene Therapy*, Vol. 6, 1999, pp. 785-91.

[90] Liang Q, Satyamurthy N, Barrio JR, Toyokuni T, Phelps MP, Gambhir SS, Herschman HR, "Non-invasive, quantitative imaging in living animals of a mutant dopamine D2 receptor reporter gene in which ligand binding is uncoupled from signal transduction", *Gene Therapy*, Vol. 8, 2001, pp. 1490-8.

[91] Haberkorn U, Henze M, Altmann A, Jiang S, Morr I, Mahmut M, Peschke P, Kübler W, Debus J, Eisenhut M, "Transfer of the human Na/I symporter gene enhances iodide uptake in hepatoma cells", *Journal of Nuclear Medicine*, Vol. 42, 2001, pp. 317-25.

[92] Cho JY, Xing S, Liu X, Buckwalter TL, Hwa L, Sferra TJ, Chiu IM, Jhiang SM, "Expression and activity of human Na^+/I^- symporter in human glioma cells by adenovirus-mediated gene delivery", *Gene Therapy*, vol. 7, 2000, pp. 740-9.

[93] Gilad AA, Winnard PT Jr, van Zijl PCM, Bulte JWM, "Developing MR reporter genes: promises and pitfalls", *NMR in Biomedicine*, Vol. 20, 2007, pp. 275-90.

[94] Martelli C, Libani IV, Lui R, Ottobrini L, "Imaging in drug development with reporter mice", *Minerva Biotecnologica*, Vol. 21, 2009, pp. 53-66.

[95] Pham W, Kobukai S, Hotta C, Gore JC. "Dendritic cells; therapy and imaging", *Expert Opinion in Biology and Therapy*, Vol. 9, no. 5, 2009, pp. 539-564.

[96] Arbab AS, Yocum GT, Kalish H, Jordan EK, Anderson SA, Khakoo AY, Read EJ, Frank JA, "Efficient magnetic cell labeling with protamine sulphate complexed to ferumoxides for cellular MRI", *Blood*, Vol. 104, 2004, pp. 1217–1223.

[97] Rodriguez-Porcel M, Wu JC, Gambhir SS, "Molecular imaging of stem cells", *StemBook* [Internet]. Cambridge (MA): Harvard Stem Cell Institute; 2008-. 2009.

[98] Lewin M, Carlesso N, Tung CH, Tang XW, Cory D, Scadden DT and Weissleder R, "Tat peptide-derivatized magnetic nanoparticles allow *in vivo* tracking and recovery of progenitor cells", *Nat Biotechnol*, Vol. 18, 2000, pp. 410–414.

[99] Bulte J W, Duncan ID and Frank JA, "*In vivo* magnetic resonance tracking of magnetically labeled cells after transplantation", *J Cereb Blood Flow Metab*, Vol. 22, 2002, pp. 899–907.

[100] Okada S, Ishii K, Yamane J, Iwanami A, Ikegami T, Katoh H, Iwamoto Y, Nakamura M, Miyoshi H, OkanoHJ, Contag CH, Toyama Y and Okano H, "*In vivo* imaging of engrafted neural stem cells: its application in evaluating the optimal timing of transplantation for spinal cord injury", *The FASEB Journa.,* Vol. 10, 2005, pp.1096.

[101] Graves EE, Weissleder R and Ntziachristos V, "Fluorescence molecular imaging of small animal tumour models", *Curr Mol Med*, Vol. 4, 2004 , pp. 419–430.

[102] Lindvall O, Kokaia Z, and Martinez-Serrano A,"Stem cell therapy for human neurodegenerative disorders-how to make it work", *Nat Med,* Vol. 10, 2004, pp. Suppl, S42–S50.

[103] Bjorklund A, Dunnett SB, Brundin P, Stoessl AJ, Freed CR, Breeze RE, Levivier M, Peschanski M, Studer L, and Barker R, "Neural transplantation for the treatment of Parkinson's disease", *Lancet Neurol*, Vol. 2, 2003, pp. 437–445.

[104] Hallbergson AF, Gnatenco C, and Peterson DA, " Neurogenesis and brain injury: managing a renewable resource for repair", *J Clin Invest*, Vol. 112, 2003, pp. 1128–1133.

[105] Jeong SW, Chu K Jung KH, Kim SU, Kim M, and Roh JK, "Human neural stem cell transplantation promotes functional recovery in rats with experimental intracerebral hemorrhage", *Stroke,* Vol. 34, 2003, pp. 2258–2263.

[106] Hofstetter CP, Holmstrom NA, Lilja JA, Schweinhardt P, Hao J, Spenger C, Wiesenfeld-Hallin Z, Kurpad SN, Frisen J, and Olson L, "Allodynia limits the usefulness of intraspinal neural stem cell grafts; directed differentiation improves outcome", *Nat Neurosci,* Vol. 8, 2005, pp. 346–353.

[107] Iwanami A, Kaneko S, Nakamura M, Kanemura Y, Mori H, Kobayashi S, Yamasaki M, Momoshima S, Ishii H, Ando K, et al., "Transplantation of human neural stemcells for spinal cord injury in primates" *J. Neurosci Res*, Vol. 80, 2005, pp.182–190.

[108] Politi LS, Bacigaluppi M, Brambilla E, Cadioli M, Falini A, Comi G, Scotti G, Martino G and Pluchino S, "Magnetic Resonance-Based Tracking and Quantification of Intravenously Injected Neural Stem Cell Accumulation in the Brains of Mice with Experimental Multiple Sclerosis", *Stem Cells,* Vol. 25, 2007, pp. 2583–2592.

[109] De Vries IJ, Lesterhuis WJ, Barentsz JO, Verdijk P, van Krieken JH, Boerman OC, Oyen WJ, Bonenkamp JJ, Boezeman JB, Adema GJ, Bulte JW, Scheenen TW, Punt CJ, Heerschap A, Figdor CG, "Magnetic resonance tracking of DC in melanoma patients for monitoring of cellular therapy", *Nature Biotechnology*, Vol. 23, no. 11, 2005, pp. 1407-1413.

[110] Ridolfi R, Riccobon A, Galassi R, Giorgetti G, Petrini M, Fiamminghi L, Stefanelli M, Ridolfi L, Moretti A, Migliori G, Fiorentini G, "Evaluation of *in vivo* labelled dendritic cell migration in cancer patients", *Journal of Translational Medicine*, Vol. 2, no. 27, 2004, pp. 27-37.

[111] Quillien V, Moisan A, Carsin A, Lesimple T, Lefeuvre C, Adamski H, Bertho N, Devillers A, Leberre C, Toujas L, "Biodistribution of radiolabelled human dendritic cells injected by various routes", *European Journal of Nuclear Medicine and Molecular Imaging*, Vol. 32, no. 7, 2005, pp. 731-41.

[112] Baumjohann D, Hess A, Budinsky L, Brune K, Schuler G, Lutz MB. "*In vivo* magnetic resonance imaging of DC migration into the draining lymph nodes of mice", *European Journal of Immunology*, Vol. 36, 2006, pp. 2544-2555.

[113] Pham W, Kobukai S, Hotta C, Gore JC. "Dendritic cells; therapy and imaging", *Expert Opinion in Biology and Therapy*, Vol. 9, no. 5, 2009, pp. 539-564.

[114] Kraitchman DL, Tatsumi M, Gilson WD, Ishimori T, Kedziorek D, Walczak P, Segars WP, Chen HH, Fritzges D, Izbudak I, Young RG, Marcelino M, Pittenger MF, Solaiyappan M, Boston RC, Tsui BM, Wahl RL, Bulte JW, "Dynamic imaging of allogeneic mesenchymal stem cells trafficking to myocardial infarction", *Circulation*, Vol. 112, no. 6, 2005, pp. 1451–1461.

[115] Kraitchman DL, Heldman AW, Atalar E, Amado LC, Martin BJ, Pittenger MF, Hare JM, Bulte JW, "*In vivo* magnetic resonance imaging of mesenchymal stem cells in myocardial infarction", *Circulation*, Vol. 107, 2003, pp. 2290–2293.

[116] Hoshino K, Ly HQ, Frangioni JV, Hajjar RJ, "*In vivo* Tracking in Cardiac Stem Cell-Based Therapy" *Progress in Cardiovascular Diseases*, Vol. 49, no. 6, 2007, pp. 414-420.

[117] Jendelova P, Herynek V, Urdzikova L, Glogarova K, Kroupova J, Andersson B, Bryja V, Burian M, Hajek M, and Sykova E, "Magnetic resonance tracking of transplanted bone marrow and embryonic stem cells labeled by iron oxide nanoparticles in rat brain and spinal cord", *J Neurosci Res,* Vol. 76, 2004, pp. 232–243.

[118] Lee IH, Bulte JW, Schweinhardt P, Douglas T, Trifunovski A, Hofstetter C, Olson L, and Spenger C, "In vivo magnetic resonance tracking of olfactory ensheathing glia grafted into the rat spinal cord", *Exp Neurol,* Vol. 187, 2004, pp. 509–516.

[119] Pirko I, Johnson A, Ciric B, Gamez J, Macura SI, Pease LR, and Rodriguez M, "In vivo magnetic resonance imaging of immune cells in the central nervous system with superparamagnetic antibodies", *FASEB J,* Vol.18, 2004, pp. 179–182.

[120] Chin BB, Nakamoto Y, Bulte JW, Pittenger MF, Wahl R, Kraitchman DL, "111In oxine labelled mesenchymal stem cell SPECT after intravenous administration in myocardial infarction", *Nuclear Medicine Communications*, Vol. 24, 2003, pp. 1149 –1154.

[121] Barbash IM, Chouraqui P, Baron J, Feinberg MS, Etzion S, Tessone A, Miller L, Guetta E, Zipori D, Kedes LH, Kloner RA, Leor J, "Systemic delivery of bone marrow-derived mesenchymal stem cells to the infarcted myocardium: feasibility, cell migration, and body distribution", *Circulation*, Vol. 108, 2003, pp. 863–8.

[122] Aicher A, Brenner W, Zuhayra M, Badorff C, Massoudi S, Assmus B, Eckey T, Henze E, Zeiher AM, Dimmeler S, "Assessment of the tissue distribution of transplanted human endothelial progenitor cells by radioactive labelling", *Circulation*, Vol. 107, 2003, pp. 2134 –2139.

[123] Lappalainen RS, Narkilahti S, Huhtala T, Liimatainen T, Suuronen T, N¨arv¨anen A, Suuronen R, Hovatta O, Jolkkonen J, " The SPECT imaging shows the accumulation of neural progenitor cells into internal organs after systemic administration in middle cerebral artery occlusion rats", *Neuroscience Letters,* Vol. 440, 2008, pp. 246–250.

[124] Contag CH and Bachmann MH, " Advances in *in vivo* bioluminescence imaging of gene expression", *Annu Rev Biomed Eng,* Vol. 4, 2002, pp. 235–260.

[125] De A, Lewis XZ and Gambhir SS "Noninvasive imaging of lentiviral-mediated reporter gene expression in living mice", *Mol Ther, Vol.* 7, 2003, pp. 681–691.

[126] Bai Y, Soda Y, Izawa K, Tanabe T, Kang X, Tojo A, Hoshino H, Miyoshi H,Asano S and Tani K, "Effective transduction and stable transgene expression in human blood cells by a third-generation lentiviral vector", *Gene Ther,* Vol. 10, 2003, pp. 1446–1457.

[127] Wu JC, Chen IY, Sundaresan G, Min JJ, De A, Qiao JH, Fishbein MC, Gambhir SS, "Molecular imaging of cardiac cell transplantation in living animals using optical bioluminescence and positron emission tomography", *Circulation*, Vol. 108, 2003, pp. 1302 -13058.

[128] Hwang DW, Kang JH, Jeong JM, Chung JK, Lee MC, Kim S, Lee DS. "Noninvasive *in vivo* monitoring of neuronal differentiation using reporter driven by a neuronal promoter", *Eur J Nucl Med Mol Imaging*, Vol. 35, 2008, pp.135–145.

[129] Boutry S, Brunin S, Mahieu I, Laurent S, Vander Elst L and Muller RN, "Magnetic labeling of non-phagocytic adherent cells with iron oxide nanoparticles: a comprehensive study", *Contrast Media & Moleculr Imaging*, Vol. 3, 2008, pp. 223-232.

[130] Dull T, Zufferey R, Kelly M, Mandel RJ, Nguyen M, Trono D, and Naldini L, "A Third-Generation Lentivirus Vector with a Conditional Packaging System", *Journal Of Virology*, Vol. 72, no. 11, 1998, pp. 8463–8471.

[131] Heid CA, Stevens J, Livak KJ And Williams PM, " Real time quantitative PCR", *Genome Res*, Vol. 6, 1996, pp. 986–994.

RINGRAZIAMENTI

Innanzitutto, vorrei ringraziare il Prof. Giovanni Lucignani e la Dott.ssa Luisa Ottobrini per avermi accolto nel loro gruppo di ricerca e per avermi fatto da guida durante lo svolgimento del mio dottorato.

Rivolgo un ringraziamento speciale alla mia famiglia per avermi supportata in tutti questi anni di studio, per avermi sempre incoraggiata ed essermi stata vicina anche nei momenti di crisi.
Ringrazio, inoltre, i miei zii Memi e Piero per il loro importante contributo nella revisione linguistica della tesi.

Un particolare ringraziamento va ad una persona speciale, William, per esser stato sempre paziente, comprensivo e presente e per aver sacrificato insieme a me i suoi week end ed il suo tempo libero senza mai lamentarsi.

Ringrazio le mie colleghe Ilaria e Cristina per la loro disponibilità, per i loro consigli lavorativi e per aver condiviso con me le loro conoscenze e Stefania per essere stata il mio "braccio destro" in questi ultimi mesi.

Infine rivolgo un grazie anche alle mie amiche per aver sempre creduto in me, per essere sempre state a mio fianco anche quando lontane.